UCRL-11150
c.2

University of California

Ernest O. Lawrence Radiation Laboratory

TWO-WEEK LOAN COPY

This is a Library Circulating Copy which may be borrowed for two weeks. For a personal retention copy, call Tech. Info. Division, Ext. 5545

A MEASUREMENT OF THE FORWARD DIFFERENTIAL CROSS SECTION FOR π^--p ELASTIC CHARGE-EXCHANGE SCATTERING AT 1.03 BeV/c USING THE 72-INCH HYDROGEN BUBBLE CHAMBER AS A NEUTRON DETECTOR

Berkeley, California

UCRL-11150
c.2

DISCLAIMER

This document was prepared as an account of work sponsored by the United States Government. While this document is believed to contain correct information, neither the United States Government nor any agency thereof, nor the Regents of the University of California, nor any of their employees, makes any warranty, express or implied, or assumes any legal responsibility for the accuracy, completeness, or usefulness of any information, apparatus, product, or process disclosed, or represents that its use would not infringe privately owned rights. Reference herein to any specific commercial product, process, or service by its trade name, trademark, manufacturer, or otherwise, does not necessarily constitute or imply its endorsement, recommendation, or favoring by the United States Government or any agency thereof, or the Regents of the University of California. The views and opinions of authors expressed herein do not necessarily state or reflect those of the United States Government or any agency thereof or the Regents of the University of California.

UCRL-11150
UC-34 Physics
TID-4500 (24th Ed.)

Research and Development

UNIVERSITY OF CALIFORNIA

Lawrence Radiation Laboratory
Berkeley, California

AEC Contract No. W-7405-eng-48

A MEASUREMENT OF THE FORWARD DIFFERENTIAL CROSS SECTION FOR π^--p ELASTIC CHARGE-EXCHANGE SCATTERING AT 1.03 BeV/c USING THE 72-INCH HYDROGEN BUBBLE CHAMBER AS A NEUTRON DETECTOR

Alan Natapoff

(Ph. D. Thesis)

December 1963

Printed in USA. Price $2.25. Available from the
Office of Technical Services
U. S. Department of Commerce
Washington 25, D.C.

A MEASUREMENT OF THE FORWARD DIFFERENTIAL CROSS SECTION FOR π^--p ELASTIC CHARGE-EXCHANGE SCATTERING AT 1.03 BeV/c USING THE 72-INCH HYDROGEN BUBBLE CHAMBER AS A NEUTRON DETECTOR

Contents

Abstract v

Introduction 1

General Description of Method and Results. 6

Conclusion 17

Appendix

A. Scanning Procedure 18

B. Some Details of the Measuring and Fitting Procedures . . 25

C. Choice of Selection Criteria for Valid Events 38

D. Detailed Discussion of a Valid Forward Event Having an Associated Electron Pair 45

E. A Boolean Algebraic Method of Analysis Applied to the Problem of Discovering the Essential Physical Combinations of Variables 56

F. Estimation of Background Due to Spurious Short Proton Tracks 68

The Use of the FAKE Program to Generate Events in the Laboratory System 68

G. Anomalous Events and Borderline Interpretations . . . 74

1. Events whose χ^2 value reproduced unreliably on successive measurements 74

2. Events on which the sign curvature decided the validity of the event 76

H. Length of Beam Track. 78

I. Kinematics of the Reaction $\pi^- + p \rightarrow \pi^0 + n$ 80

J. Escape or Geometric Correction and Detection Efficiency . 89

K. Computation of the Average Visibility of Protons Recoiling From a Neutron of Given Momentum and Direction . . 94

FORTRAN Routine PROFIL 94

L. Scanning-Table Measurements 97

M. Scanning Efficiency 101

N. Imperfect Measurements and Their Reproducibility . . . 106

Acknowledgments 113

References 114

A MEASUREMENT OF THE FORWARD DIFFERENTIAL CROSS SECTION FOR π^-- p ELASTIC CHARGE-EXCHANGE SCATTERING AT 1.03 BeV/c USING THE 72-INCH HYDROGEN BUBBLE CHAMBER AS A NEUTRON DETECTOR

Alan Natapoff

Lawrence Radiation Laboratory
University of California
Berkeley, California

December 1963

ABSTRACT

From the principle of microscopic causality and the optical theorem certain important dispersion relations are deducible. These permit the calculation of the real parts of the forward amplitudes for π^--p and π^+-p scattering at a fixed energy if the corresponding total cross sections are known as a function of energy. If charge independence is assumed, the forward differential cross section, $d\sigma^{ce}(0)/d\Omega$, for charge-exchange ($\pi^- + p \rightarrow \pi^0 + n$) can also be calculated. Experimental values for the latter, therefore, can help to determine the validity of the principle of microscopic causality.

The paper describes a low statistics measurement of $d\sigma^{ce}(0)/d\Omega$ at 1.03 BeV/c in the 72-inch hydrogen bubble chamber. The π^- beam comes from the Bevatron, and the secondary neutrons are detected when subsequent elastic scatters $n + p \rightarrow n + p$ yield visible stopping protons. The real events were separated from the spurious by a Boolean algebraic method that reduced the set of all events to a sum of a small number of physically significant sets. The residual background fraction was estimated at 10% by a computer simulation technique using the known beam distribution and a pure sample of background events. The bubble chamber, so used, detects about 5% of the secondary neutrons emitted in the charge-exchange reaction.

There were 12 experimental events in three intervals lying the the range $0.84 \leq \cos\theta^{c.m.}_{\pi^0} \leq 0.96$. A zero-constraint, least-squares fit of the distribution yielded the estimate $d\sigma^{ce}(0)/d\Omega = (3.65 \pm 1.93)$mb/sr. This result is consistent with the predictions based on the dispersion relations.

INTRODUCTION

The Berkeley 72-inch hydrogen bubble chamber has been used to detect (or to infer directly) the orbits of particles of three main classes: First, the class of charged particles, both stable (as the proton) and unstable (as the Σ^-); second, that of uncharged particles that decay rapidly, through strong or electromagnetic reactions, into charged particles (e.g., η meson); and third, the class of uncharged particles that decay through weak interactions into charged particles, and do so--on the average--in a time short enough that this decay may occur, with reasonable likelihood, before the particle has left the chamber. Of the particles of the original strongly interacting families (pion, kaon, nucleon, lambda, sigma, and xi), there are only four that do not fall into one of the three classes above. They are the π^0, n, Σ^0, and Ξ^0. The orbits of all the others can be directly detected or inferred from a reasonably popular decay mode into charged particles. Even though they do not fall into any of the classes above, the Σ^0 and Ξ^0 are successfully detected by the bubble chamber because their decay ultimately produces particles of the efficiently detectable classes. The π^0 and n, on the other hand, are not easily detected, and when they occur--as they often do--their essential quantities are inferred indirectly through the use of conservation laws. We discuss the detection of secondary neutrons in the 72-inch hydrogen bubble chamber by direct inference, using the reasonably likely n-p elastic-scattering reaction to trace the orbit of the neutron. We use the technique to detect neutrons formed in the reaction $\pi^- + p \rightarrow \pi^0 + n$ at 1.03 BeV/c and obtain, first, a low-statistics determination of the forward-differential-scattering cross section for this charge-exchange reaction and, second, an index of the efficiency of the bubble chamber as a slow-neutron detector relative to its efficiency in its usual role of detector of charged particles. We have chosen to examine the charge-exchange reaction because it is relevant to the verification of pion-nucleon dispersion relations.

Starting from the assumption of microscopic causality, Goldberger and others have derived an integral relation that permits, in principle, the calculation of the real part of the forward-scattering amplitude for $\pi^{\pm}$-p elastic scattering at a fixed energy E, if the total $\pi^{\pm}$-p cross section is known as a function of energy.[1] That is, Re f_0^+ (E) = D^+(E) can be calculated

if we know $\sigma_T^+(E')$ for all E', and $\mathrm{Re}\, f_0^-(E')$ can be calculated if we know $\sigma_T^-(E')$ for all E', where $\sigma_T^+(E')$ is the total cross section for π^+-p scattering at energy E'. Such calculations have been performed in the past for π^--p and π^+-p scattering separately, and their results have been compared with experimental values for $D^+(E)$ and $D^-(E)$. Unfortunately, $D^+(E)$ and $D^-(E)$ are not very rapidly varying functions of E (Fig. 1). This makes it easier for Goldberger's integral relation (usually called a dispersion relation) to reproduce the experimental results. If, for example, $D^+(E)$ had jagged peaks or rapid jumps, the dispersion relation would have a severe test to meet. As it is, there are some adjustable parameters to help improve the fit to experimental data. There is also some uncertainty as to the form of $\sigma_T(E)$ for very high energies, which contributes further to the uncertainty in the predictions of the dispersion relation when it is applied to π^+-p and π^--p scattering separately. In short, a test of the dispersion relation using π^--p and π^+-p data separately is handicapped by the stolid, slowly varying nature of the functions $D^+(E)$ and $D^-(E)$. Had they more character, a theory predicting that character would be more unambiguously verified, or contradicted, by experiment. This suggests that we seek a function whose behavior is predicted by the dispersion relation, but whose character is stormier than that of either $D^+(E)$ or $D^-(E)$. Such a function, as has been suggested for example by Cool et al.,[2] is the forward-scattering amplitude, f_0^{ce}, for charge-exchange scattering ($\pi^- + p \rightarrow \pi^0 + n$). It is related to f^+ and f^-, assuming charge independence, by

$$f^{ce} = (1/\sqrt{2})\,(f^+ - f^-)\,.$$

This relation holds for all angles, and so it holds in particular at zero degrees. Calling D the dispersive (real) part, and A the absorptive (imaginary) part of each amplitude at zero degrees, we have

$$f_0^{ce}(E) = (1/\sqrt{2})\,[\,D^+(E) - D^-(E)] + (i/\sqrt{2})\,[\,A^+(E) - A^-(E)]\,,$$

where "ce" refers to charge-exchange scattering and +, - refer to (π^+-p, π^--p) elastic scattering, respectively.

Now, by the optical theorem, we have

$$A^+(E) = \frac{k}{4\pi}\,\sigma_T^+(E)$$

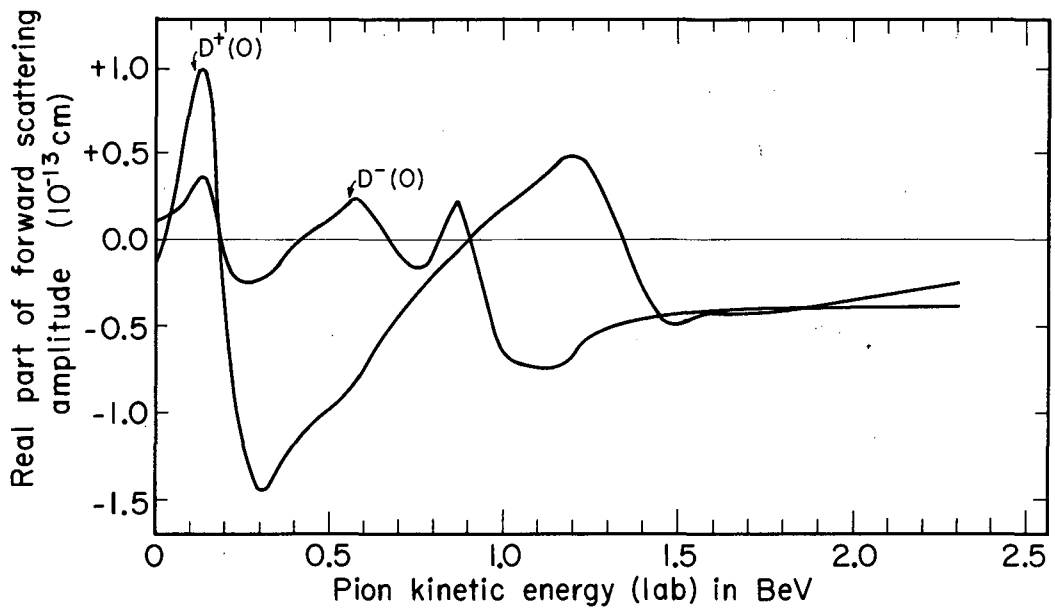

MU-32907

Fig. 1. Plot of $D^+(E)$, $D^-(E)$ as a function of E (after Cronin[9]).

and

$$A^-(E) = \frac{k}{4\pi}\ \sigma_T^-(E);$$

hence,

$$f_0^{ce}(E) = (1/\sqrt{2})[\,D^+(E)-D^-(E)] + (i/\sqrt{2})\,\frac{k}{4\pi}\,[\,\sigma_T^+(E)-\sigma_T^-(E)]\ .$$

But $|f_0^{ce}(E)|^2$ can be inferred experimentally from examining charge-exchange scatterings at small angles, and $\sigma_T^+(E)$ and $\sigma_T^-(E)$ are well known at many energies. This gives an experimental determination of $[\,D^+(E) - D^-(E)]^2$. Since $D^+(E)$ and $D^-(E)$ are predicted separately by the dispersion relation, their difference is also predicted by it. A measurement of $|f_0^{ce}(E)|^2$ is therefore an interesting physical quantity relevant to the experimental verification of the dispersion relation. Further, $D^+(E)-D^-(E)$ is often a more rapidly varying function of E than either $D^+(E)$ or $D^-(E)$ and so can be expected to provide interesting information as to the validity of the dispersion relation that predicts its character.

Having established that the variation of $f_0^{ce}(E)$ with energy (E) will provide a test of the dispersion relation, we should choose our energies carefully to give the maximum information. Specifically, it is the variation of $\mathrm{Re}\,f_0^{ce}(E) = D^{ce}(E)$ that we seek, and it is $|f_0^{ce}(E)|^2$ that we measure experimentally. But since $|f_0^{ce}(E)|^2 = D^{ce}(E)^2 + A^{ce}(E)^2$, we should choose for our first measurement an energy such that $A^{ce}(E)$ is small. The optical theorem and charge independence imply

$$A^{ce}(E) = \frac{1}{\sqrt{2}}\,\frac{k}{4\pi}\,[\,\sigma^+(E) - \sigma^-(E)]\ ,$$

so that the ideal energy is one for which $\sigma^+(E)$ and $\sigma^-(E)$ are nearly equal (e.g., $p(\pi^-) = 1.24$ BeV/c). The momentum we have used, 1.03 BeV/c, is one for which $\sigma^+(E) - \sigma^-(E)$ is nearly as large as possible, contrary to the reasoning above. This choice was made to insure that the resulting sample of events would be as large as possible. Since the experimental technique of analyzing zero-prong and recoil combinations has not been used extensively, it is important to be sure that it works. Specifically, we must be certain that the "real" events can be distinguished from background by the analysis programs. By "background" we mean combinations of

zero-prong and proton recoil that appear to result from our reaction, although they do not. Because the chamber is not perfectly shielded, many neutrons originating in the Bevatron pass through it and cause recoil-proton tracks. In the vicinity of a given zero-prong event, one or more such spurious recoils may occur. The expected influence of such background is discovered by use of FORTRAN program FAKE that simulates background of this kind. The results are discussed in Appendix F. A further contribution to background can be expected from the reaction

$$\pi^- p \rightarrow \pi^0 \pi^0 n, \quad \text{then} \quad n + p \rightarrow n + p \, .$$

This, too, is analyzed with the help of the FAKE program. To enhance our discrimination of real events from background, we chose the energy that would give us the largest possible number of real events. If we found ourselves unable to distinguish signal from background at such an energy, we could discard the method conclusively. In short, it is desirable to test this new experimental technique first on such a problem as will give the greatest likelihood of success. This consideration determined our choice of energy.

The interest in the pion-nucleon dispersion relation motivated our choice of reaction, but our numerical result--because of the meager statistics on which it is based--is not the ripest fruit of the experiment. Other experiments,[2,3] completed and current, in counters and in bubble and spark chambers, provide the basis for much stronger statements with respect to the validity of the dispersion relations. Rather, we have treated the problem as a pilot problem. We sought to find the limitations of our instrument and to discover the conditions under which its performance is best. The copiousness of neutrons in high-energy reactions, the desirability of their detection as an auxiliary to the study of these reactions, and the great store of information about such reactions recorded and to be recorded on hydrogen bubble chamber film, were thought to justify this study.

GENERAL DESCRIPTION OF METHOD AND RESULTS

The vehicle for this measurement of $|f_0^{ce}(E)|^2$ (for a single energy E) is the 72-inch hydrogen Berkeley bubble chamber used in conjunction with the Berkeley Bevatron. A beam of π^- mesons is led from the Bevatron target into the chamber, and the bubble trails of charged particles are photographed from above through the glass top of the chamber. The film is later reprojected on scanning tables, where the bubble trails are examined for configurations that may yield interesting information. The film we have analyzed was exposed during the Associated Production Experiment run under the direction of Professor Frank S. Crawford.[4] When interesting configurations are found, they are recorded and later traced out on the digitized measuring projector, Franckenstein. These configurations can be reconstructed in space, by the computer program PANG,[5] from the information punched on paper tape by the Franckenstein. Other computer programs then extract and analyze the information residing in the configurations.

Our "interesting" configurations are those that would enable us to deduce that a charge-exchange scattering has occurred. The reaction $\pi^- + p \rightarrow \pi^0 + n$ leaves a characteristic pattern of tracks. The incident π^- particle leaves a continuous trail of bubbles that is abruptly terminated when it collides with the stationary proton target. The final-state particles, because they are uncharged, leave no bubble trails. The sudden termination of a beam track within the chamber is called a "zero prong" and is characteristic of our reaction (Fig. 2). There are other reactions, though, that can give the same characteristic zero-prong track pattern:

$$\pi^- + p \rightarrow \begin{cases} \pi^0 \pi^0 n \\ \Lambda^0 K^0 \\ \Sigma^0 K^0 \end{cases} .$$

In order to distinguish our reaction from these, we must have further information. No information can be gotten in our chamber unless one of the product particles (π^0, n) undergoes a detectable reaction in the chamber.

The π^0 decays immediately into two γ rays. The likelihood of their conversion into electron pairs is small because the radiation length for liquid hydrogen is 990 cm,[6] whereas the average thickness of target traversed by one of the γ rays is roughly 1/20 as large (the chamber's useful dimensions are approximately 150 by 35 by 35 cm).

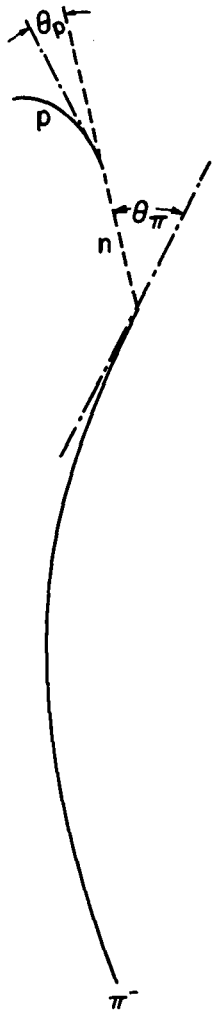

MU-32908

Fig. 2. Schematic diagram of a typical zero-prong with recoil.

Much more likely is the event that the neutron will collide with a second proton target before leaving the chamber. The cross section for n-p scattering is approximately $10/T_n$ at our energies, so that a neutron of 5 MeV kinetic energy will have a cross section of 2 b for an n-p collision. The detailed calculations of detection efficiency are described in Appendix J. If such an n-p collision occurs, and if the momentum transferred is great enough, the recoil proton will be visible and the path of the neutron can be inferred. This information is enough to allow the reconstruction of the original scattering. Further, using conservation laws, there is enough information to decide reliably whether a given zero-prong and a nearby stopping proton track (see Fig. 2) form the skeleton of a real event ($\pi^- p \rightarrow \pi^0 n$). This is done by the IBM 709-7090 program KICK.[7]

Occasionally, both a conversion pair and a recoil proton seem to be associated with a given zero-prong. This gives additional information for use in determining whether or not the apparent event is a real one. Since there are many stray, short proton tracks seen in the chamber, some of these may appear to be associated with a zero-prong. The fitting program KICK, we have concluded, discriminates reliably between spurious and real events of our type. The additional information bestowed by the conversion pair is enormously useful. An event having a conversion pair (or a Dalitz pair) can immediately and decisively be hailed as valid or stigmatized as void. Without such a pair, it will appear, the course of the analysis of individual events is often tortuous.

Unfortunately, events with associated pairs occur very seldom. Of the dozen certified events of our sample, only one has as associated conversion pair. This, in approximately 100 kilometers of pion beam track. Of course, there are many more conversion pairs in all, but only one occurs with a valid recoil. That event (502-353) is treated in detail in Appendix D.

The accompanying table (Table I) lists all the events accepted, with identification and a set of the interesting physical parameters.

A most important piece of information can be gained from a casual glance at the table. Our experiment should detect, with varying efficiency, events on which $0.65 \leq \cos\theta^{c.m.}(\pi^0) \leq 0.96$. Yet, the range for the experimental events is $0.8574 \leq \cos\theta^{c.m.}(\pi^0) \leq 0.9570$. We must modify, therefore, the estimates made in other sections, of background and casualty, for

Table I. Final list of valid events and events failing because of high missing-mass error.

Serial	Ord.	Sig.	$\cos\theta^{c.m.}$	χ^2	$\delta\lambda$ (deg)	L_p (cm)	$\cos\theta_{gl}$	δMM (MeV/c^2)	RD(MM)*
501-501	71	0	0.9380	1.007	0.7900	3.751	0.2035	9.446	-0.9758
502-353	141	0	0.8574	1.482	0.7078	6.188	0.4010	13.31	1.296
504-162	255	0	0.9410	0.3521	1.216	1.935	-0.5352	9.957	-0.5853
504-467	308	0	0.9530	0.6154	1.806	1.541	-0.2713	13.14	0.8167
505-155	375	0	0.9281	0.1615	1.297	1.062	0.7900	12.62	0.4092
507-057	572	0	0.8896	0.3621	0.3245	3.118	0.7892	8.144	0.6076
507-294	776	0	0.8793	0.4032	0.7413	4.534	0.5601	8.829	0.6476
509-020		0	0.9138	0.0003	0.78			5.936	
514-435	1661	0	0.9570	0.5637	2.476	0.7356	0.6132	12.32	-0.6952
519-429	1897	0	0.9505	0.7157	2.031	0.7419	0.6946	15.74	-0.7883
519-497	1935	0	0.9314	0.0098	1.737	1.368	0.4518	10.42	-0.0344
565-430		0	0.9433	1.477	2.04			10.90	
501-005	19	32	0.8831	0.0056	0.5267	3.027	-0.8626	36.92	0.2432
508-506	1169	32	0.7735	0.0068	1.721	1.121	0.6175	91.17	0.3023
553-357	2270	32	0.8394	1.538	0.6396	15.50	0.5651	29.47	-1.079
565-355	2754	32	0.8039	1.851	0.4832	13.21	0.5140	27.33	-1.202

*RD(MM) means "the deviation of the missing mass from its ideal value relative to experimental error in its determination". RD(MM) = [MM-m(π^0)/ δMM].

the full spectrum. Our full-spectrum estimate of the background is 0.49±0.24 events based on 4 spurious events in 10 passes. With the list of accepted experimental events, there is the corresponding list of FAKE-simulated events that passed the corresponding criteria (Table II). We note, on the latter list, that of the four originally acceptable simulated events, three were simulated on the basis of the single event 553-082. Further, these simulated events agree closely in their values of $\cos\theta^{c.m.}$. The latter circumstance is to be expected. It is not to be expected that a given set of tracks would fit our hypothesis well for a wide range of π^0 emission angles. That the same event should give several different simulated fits on different passes indicates that a zero-prong that would fit it, would occur in a neighborhood of the chamber where the beam is dense. Since we simulate events in proportion to beam density, it is not surprising that certain events give several successful simulations. In such cases, the values of $\cos\theta^{c.m.}$ varied by no more than 0.01, which may be considered to define the accuracy of determination of $\cos\theta^{c.m.}$ on any single measurement.

We must now formalize the limits of our subspectrum. We wish to accept all the experimental data. We have enough events to justify, at most, three histogram intervals, whereas an ideal histogram should have intervals over which the occupancy is not rapidly varying. Since (from experimental data from other experiments) we expect our occupancy to vary rapidly, we choose histogram intervals as small as possible. Therefore, we use $0.84 \leq \cos\theta^{c.m.} \leq 0.96$ as our subspectrum--the smallest subspectrum containing our experimental range that also divides into three intervals of convenient size.

Now, all our former full-spectrum background lies in the new subspectrum, and our background estimate thus remains unchanged. The same is not true, however, of the casualties.

Of our four original casualties, only one lies inside the subspectrum. One other lay near its border, but it was moved farther away by a remeasurement made later. This circumstance permits us to reject the event with an easy mind. Of 16 original simulated events having signature 32, only 4 lay in the subspectrum, and these had values of $\cos\theta^{c.m.}$ (0.8709, 0.8891, 0.8909, 0.8900) near the value of our single casualty (0.8831); this supports our hope that the casualty was really a background event. (The clustering

Table II. Events simulated by FAKE (F10.0) that passed all criteria or failed only because of high missing-mass error.

Serial	Ord.	Sig.	$\cos\theta^{c.m.}$	χ^2	$\delta\lambda$ (deg)	L_p (cm)	$\cos\theta_{gl}$	δMM (MeV/c^2)	RD(MM)
505-564	530	0	0.8806	1.683	1.615	2.436	0.0020	14.95	1.512
553-082	605	0	0.9485	1.970	1.118	1.563	-0.7862	6.894	1.462
553-082	857	0	0.9491	0.1426	1.118	1.563	-0.7862	7.280	0.3781
553-082	986	0	0.9487	1.136	1.118	1.563	-0.7862	7.014	1.098
547-202	88	32	0.8234	0.4957	2.150	1.424	0.4209	39.74	0.2349
547-429	96	32	0.8365	1.760	1.573	1.892	0.4998	21.54	1.600
565-435	380	32	0.8709	0.1108	1.184	3.832	0.1016	19.46	-0.3226
505-564	403	32	0.8891	0.0493	1.615	2.436	0.0020	18.53	-0.2169
508-138	548	32	0.7121	1.062	1.268	3.236	-0.2504	132.1	-0.5817
507-080	660	32	0.7679	0.3487	1.520	2.464	0.2813	40.66	0.6767
547-429	730	32	0.8436	0.1570	1.573	1.892	0.4998	26.49	0.4210
505-564	782	32	0.8909	0.3628	1.615	2.436	0.0020	19.71	-0.5585
508-560	808	32	0.8457	1.705	0.8159	7.574	0.5155	33.98	-1.108
509-392	823	32	0.7626	0.0000	0.8165	10.87	0.2641	25.09	-0.0006
547-202	849	32	0.8211	0.8777	2.150	1.424	0.4209	30.95	1.147
502-366	1024	32	0.8108	1.109	1.302	2.520	-0.4569	69.41	-0.7474
547-429	1112	32	0.8365	1.781	1.573	1.892	0.4998	21.51	1.611
505-564	1164	32	0.8900	1.654	1.615	2.436	0.0020	19.08	-0.3871
508-560	1190	32	0.8442	0.8822	0.8159	7.574	0.5155	30.32	-0.8519
547-202	1231	32	0.8394	0.8569	2.150	1.424	0.4209	77.19	-0.6534

of the four values is striking but illusory. As a glance at the table shows, three of the four are derived from a single physical event.) We therefore estimate that $(0.4\pm0.2)\ F_c = (0.49\pm0.24)$ spurious events of signature 32 will occur in our experimental sample, whereas 1±1 event actually did occur. We therefore estimate that $0.51^{+1.03}_{-0.51}$ valid events were thrown out with the bathwater.

It is important, too, to notice that although we scanned for all recoils that had at least 0.1-in. projection on the scan table (about 0.38-cm spatial projection), there were no valid events with spatial projections below 0.7 cm, and the accepted events tend to be even longer. This is probably due to increase of scanning efficiency for longer recoils (not corrected for--we assumed all events to be equally likely of detection). This result strongly suggests the adoption of a higher scanning cutoff on acceptable proton length, for exhaustive scanning of our type. The higher cutoff would also accelerate the scanning rate.

Now we analyze the results and collect the various correction factors derived in separate appendices. We had 12 acceptable events. Our background was estimated at 0.49±0.24 events. The casualties of otherwise acceptable events to our acceptance criteria are 10% to the missing-mass-deviation criterion of 1.65 standard deviations and to the missing-mass error criterion, the 0.51 valid events, derived above.

We have estimated, elsewhere, the overall scanning efficiency for finding whole events at 0.758±0.007, and we can therefore compile a set of multiplicative factors to be applied to the observed distribution to discover the actual distribution. These are given below.

Source of Factor	Magnitude	Error
Scanning efficiency	1.32	0.12
Imposition of missing-mass criterion (1.65 standard deviations = 90% level)	1.11	---
Background	0.959	0.020
Totality of the effects above	1.41	0.13

The factors above are applied to the whole distribution as a unit, but there remain the effects of geometric and escape corrections. The latter, because it depends on angle, is applied separately to each part of the angular distribution. The correction, tabulated in a separate section, is numerically integrated over the histogram intervals and applied to the corrected experimental distribution. Also, we are going to take seriously the crude angular distribution of the estimated 0.51 events we have lost to the missing-mass-error criterion. We apply the resulting correction to the single histogram interval in which all the simulated events fall rather than to the distribution as a whole. (See Table III.)

Now we must integrate the detection probabilities, given in the section on escape and geometric corrections, over each of the histogram intervals (0.84, 0.88), (0.88, 0.92), (0.92, 0.96) in $\cos\theta^{c.m.}$.

Using the probabilities calculated and tabulated in the section on geometric and escape correction, we find the estimated average probability for detecting a neutron.

$\cos\theta_n^{c.m.}$	Average probability in interval	Average correction factor
-0.84		
	0.09557 35578	10.46
-0.88		
	0.11397 85687	8.774
-0.92		
	0.11749 57194	8.511
-0.96		

(A "detectable" neutron, in the sense above, is one that has scattered from a proton in such a way that the proton track, first, projects more than 0.7 cm on the plane of the top glass and, second, makes an angle, at its beginning, of less than 60 deg with the plane of the top glass.)

From the estimate of the length of beam track in our experiment, $(1.09\pm0.03)\times10^7$ cm, we deduce the cross section to be $2.55\pm0.07\,\mu b$ for each event observed.

Table III. Distribution of experimental events with successive corrections.

$\cos\theta^{c.m.}$	N	N'	N''	N'''	Partial cross section (μb)
0.84					
	$2\pm\sqrt{2}$	$2.51^{+1.75}_{-1.50}$	$3.54^{+1.75}_{-1.52}$	$37.018^{+26.0}_{-22.6}$	$94.4^{+66.4}_{-64.4}$
0.88					
	$2\pm\sqrt{2}$	$2\pm\sqrt{2}$	2.82 ± 1.41	24.743 ± 17.8	63.1 ± 45.4
0.92					
	$8\pm\sqrt{8}$	$8\pm\sqrt{8}$	11.3 ± 2.82	96.004 ± 36.2	244.8 ± 92.5
0.96					

N number of experimental events in the interval;

N' = N corrected for causalities to low missing-mass-error criterion;

N'' = N' corrected for background, scanning efficiency, and causalities to the missing-mass-deviation criterion;

N''' = N'' corrected for geometric, visibility, and escape probabilities; and

N''' = estimated number of actual events, detected and undetected, that occurred in our experiment in the given histogram interval.

Using the data above, we extract three experimental points on the differential cross-section curve (see Fig. 3):

$$(\cos\theta\ ,\ d\sigma/d\Omega\,[\,\mathrm{mb/sr}])$$
$$(0.94,\ 0.974\pm0.3680),$$
$$(0.90,\ 0.2510\pm0.1806),$$

and

$$(0.86,\ 0.3756\pm0.2602).$$

The best we can do with these three experimental points is to derive a suitable curve with three parameters that passes through them. The suitable curve is the second-order-polynomial curve expanded about the point $\cos\theta=1$, namely:

$$d\sigma/d\Omega\ (\mathrm{mb/sr}) = b_0+b_1(\cos\theta-1)+b_2(\cos\theta-1)^2.$$

The parameter b_0 gives our estimate of the forward differential cross section we are seeking.

From a least-squares fit, we obtain the result

$$b_0 = 3.65\pm1.93\ \mathrm{mb/sr},$$
$$b_1 = 60.5\pm38.0\ \mathrm{mb/sr},$$

and

$$b_2 = 265.0\pm181\ \mathrm{mb/sr}.$$

Our estimate of 3.65±1.93 mb/sr at 1.03 BeV/c (900 MeV KE) compares to current theoretical calculations that range from about 2-1/2 to 3-3/4 mb/sr, and no violation of the dispersion relation is indicated. Even more interesting, however, the various theoretical estimates agree in the prediction of a rapid fall of this parameter with increase in the incident energy of the π^-.[8,9] The paper of Weinberg, Brenner, and Strauch[3] describing a bubble-chamber measurement at 960 MeV gives a value of (1.34±0.39)mb/sr, which is consistent with the predicted fall in this region.

The integrated partial cross section in the region $0.84 \leq \cos\theta^{c.m.} \leq 0.96$ is estimated at (0.40±0.12)mb.

There were no valid events that indicated a reaction $\pi^- + p = n + X$, where X is a known single particle--as for example, the η. We are below threshold for ω production.

Detection of neutrons by this method has an efficiency of about 0.04 to 0.08, relative to the corresponding efficiency for the detection of a charged secondary particle of reasonable length. For faster neutrons the index of efficiency falls to about one-fourth of this value.

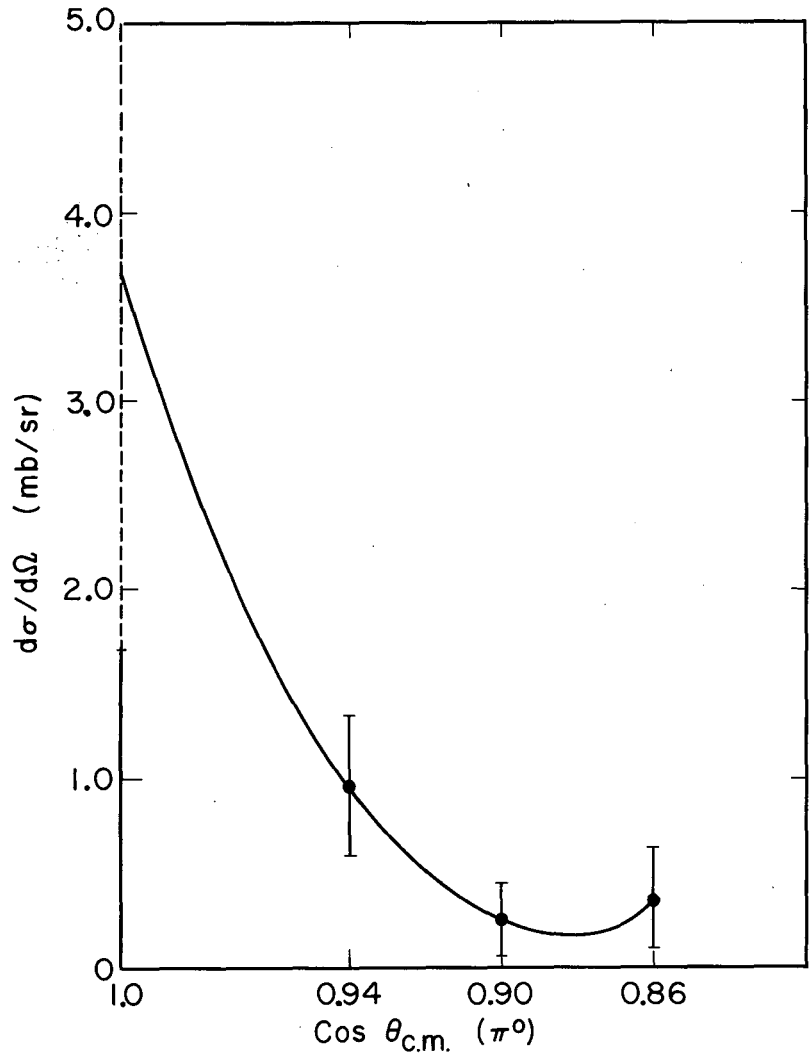

Fig. 3. Differential cross section for reaction ($\pi^- + p \rightarrow \pi^0 + n$) showing uncertainty in extrapolated forward value under least-squares fit.

CONCLUSION

We have sought to show that neutrons can be detected reliably in the 72-inch hydrogen bubble chamber, that the background fraction can be reduced to about one part in ten, and that this fraction can be plausibly estimated by a computer technique using rejected events. We sought to achieve consistency in our results by using a plausible scheme that employs Boolean algebraic methods. The results were not physically unreasonable.

Apart from the detection of neutrons in the bubble chamber, we wished to achieve a result that could be compared with the predictions of the pion-nucleon dispersion relation. We obtained a low-statistics result that did agree within broad experimental limits. Other more efficient methods, based on the detection of π^0's rather than of neutrons, have given or promise to give more detailed information about the elastic charge-exchange process. Nevertheless, it was felt that the additional experimental effort was justified in the study of what Professor Mandelstam has called the "Hydrogen Atom Problem of Strong-Coupling Physics."[10]

APPENDICES

A. Scanning Procedure

The reaction $\pi^- p \rightarrow \pi^0 n$, occurring in the H_2 bubble chamber, causes the π^- beam track to disappear. In scanning we seek, therefore, all beam tracks that suddenly terminate inside the chamber. Any beam track that does terminate inside the chamber is called a valid zero-prong. The adjective "valid" is applied to distinguish such tracks from

(a) tracks that only appear to terminate inside the chamber (they may actually leave through the top or bottom of the chamber and appear to stop inside), or

(b) tracks that only appear to be beam tracks (on closer examination, they may be found to differ from the beam in ionization or in direction).

Since we are measuring the quantity $D^{ce}(E)$ for a fixed E, we want all our events to come from a beam of the same E, and because we are applying various geometric corrections based on the beam distribution, we exclude nonbeam tracks from our sample, no matter what their energy is.

When a valid zero-prong is seen, the vicinity is searched for a recoil proton that might be associated with the neutron assumed to have been emitted at the zero-prong. The acceptance criteria for a recoil follow.

(a) The recoil proton must have scattered forward with respect to the assumed path of the neutron.

(b) The first point of the recoil must lie spatially outside a 60-deg cone whose axis is the beam track. This simplifies scanning enormously and limits our sample of neutrons to those that will be useful in our extrapolation.

(c) The recoil proton must not scatter.

(d) The recoil proton must be at least 0.1 in. long in the two stereo views, as measured on the scanning table.

(e) The recoil must stop inside the chamber.

(f) The recoil must be clearly visible, and measurable without undue distortion.

All valid recoil candidates seen near valid zero-prongs are marked for measurement on the Franckenstein (digitized projector and measuring engine). There is one exception to this rule. When a Vee (decay of a neutral

strange particle) occurs near the zero-prong and downstream from it, we assume that an associated production took place and therefore do not measure recoil candidates that would otherwise be valid. The set of such candidates is useful in determining background because we can safely assume that any recoils nearby form a pure background sample.

Each piece of information is entered on a scan sheet arranged in key-punch format. The scan sheets are designed so that they may be used conveniently for direct measurements on the scanning table. The details of the scanning-table measurements are discussed in Appendix L. Figure 4 shows the form of the scan sheet. The meaning of each of the field names is

(1) Flag: An indicator code -- specified in the next paragraph.

(2 to 6) Roll: Number of roll.

(7 to 10) Frame: Number of frame.

(11 to 12) Zero-prong No. -- When several zero-prong events appear in a single zone, they are numbered from the left to make identification easier.

(13 to 14) Zero-prong Zone--The number of the zone in which the track referred to appears to stop, as seen in the view specified in field View Sk view sketched).

(15 to 16) Recoil No. } When more than one recoil is found, such that

(17 to 18) Recoil Zone } each satisfies conditions (a) to (d) above and is associated with a zero prong in a given zone, all such are numbered counterclockwise. Specifically, an imaginary radius is drawn from zero-prong No. 1 to the initial point of each candidate recoil. Starting from the reversed beam direction and proceeding counterclockwise, each such recoil candidate is numbered consecutively. The recoils themselves do not need to lie in the same zone as the associated zero-prongs. Further, a recoil may possibly

FLAG = 0 If no recoil is seen
= 1 If recoil is seen & is measured on table
= 2 If recoil is seen & is to be measured on Franckenstein

	ROLL	FRAME	ZERO-PRONG		RECOIL		PAR	VIEW		$\phi_{n\pi}$	Δ_n	S_n	Δ_f	ϕ_{np}	Δ_p	S_p	SCAN		DATE	CODE	REMARKS
			No.	Zone	No.	Zone		SK.	BEST								NO.	BY			
1	2 3 4 5 6	7 8 9 10	11 12	13 14	15 16	17 18	19	20	21 22	23 24 25 26 27 28	29 30 31 32 33	34 35 36 37 38	39 40 41 42 43	44 45 46 47 48 49	50 51 52 53 54	55 56 57 58 59	60 61	62 63	64 65 66 67 68	69 70 71 72	73 74 75 76 77 78 79 80

MUB-2288

Fig. 4. Scan sheet for recoil protons from charge-exchange neutrons [experiment number 4 (APE), event types 52 and 54].

be associated with zero-prongs in two different zones. In that case the same physical track will have two different recoil numbers, each of which corresponds to its appearance in association with zero-prongs from two separate zones.

In the schematic diagram of Fig. 5, eight possible candidate combinations present themselves. They would appear on the data sheet as

Zero-Prong		Recoil	
No.	Zone	No.	Zone
1	7	1	7
1	7	2	8
1	7	3	7
2	7	1	7
2	7	2	8
2	7	3	7
0	8	1	8
0	8	2	7

Note that since Zone 8 contains only one zero-prong, it is not numbered. Further, recoils B and C are called numbers 2 and 3 with reference to the prongs in Zone 7, but are called 1 and 2 when they are considered with the prong in Zone 8. The basic goal of the numbering system is the unambiguous association of a pair of numbers (Zero-prong number, Recoil number) to every event originating in a zero-prong located in any zone. This pair of numbers is entered as a two-digit "beam-track number" on the Franckenstein and serves as a permanent label for bookkeeping purposes.

(19) Pair: A code word indicating the presence of Dalitz or non-Dalitz pairs.

$$\text{Pair} = 3 \times (\text{number of non-Dalitz pairs}) + (\text{number of Dalitz pairs})$$

Those cases in which an electron pair appears are treated distinctly from cases in which none appears. Events showing an e^+-e^- pair are called event-type 54. Those without an e^+-e^- pair are called event-type 52.

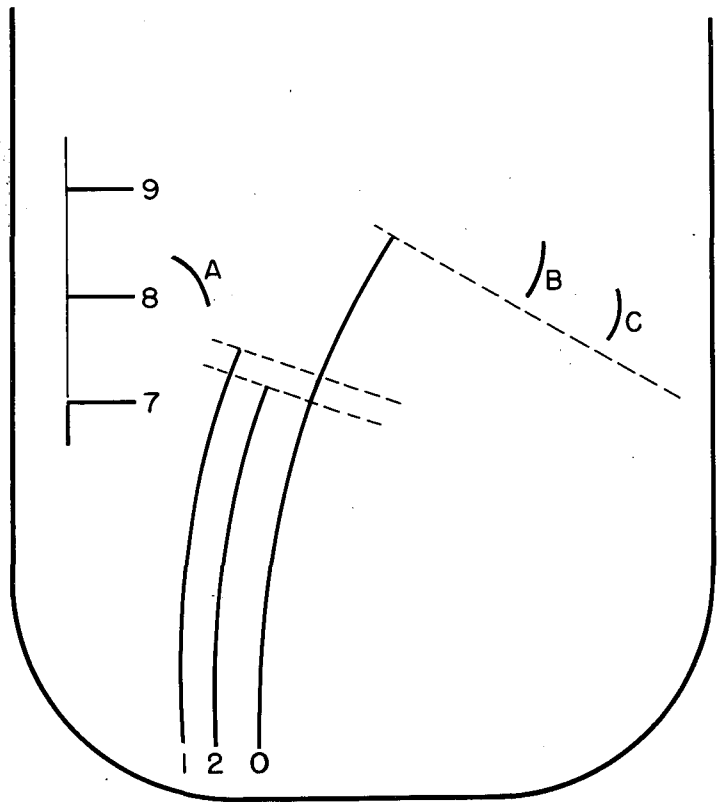

MU-32910

Fig. 5. Schematic diagram of typical zero-prongs with possibly associated recoils.

(20) View-sketched: The number of the view (1, 2, 3--there are three cameras taking pictures of the chamber) in which the sketch was prepared. The zone in which the zero-prong appears and the angle $\phi_{N\pi}$ (see below) will vary with the view chosen. Normally, view 1 is chosen as the reference view.

(21 to 22) View-best: Not used.

(23 to 28) $\phi_{N\pi}$: The angle made between the reverse beam direction and the radius from the zero-prong to the initial point of the recoil, (as measured in degrees on the scanning table in the view specified in View-sketched. All angles are measured from the reverse beam direction.

(29 to 59) Scanning-table quantities that are used when measurements are made entirely on the scanning table, as opposed to those made on the Franckenstein. The use of such measurements is discussed in Appendix L.

Scan No.: The number of scan [i.e., first (1), second (2), ··· .] .

Scan by: The number of the scanner performing the scan.

Date: Month, day, and year on which current roll was begun (e.g., July 4, 1961 = 07041).

Code: Additional identifying number whose use is described below.

Remarks: Eight BCD characters that may provide additional information.

Flag	Code	Means
0	0	Frame is O. K. Valid zero-prong found. No valid recoil candidates.
	1	Frame was not scanned. Too many beam tracks.
	2	Frame was not scanned. Film or track quality (or both) was poor.
	3	Frame O. K. Invalid prong (leaves top or bottom).
	4	Frame O. K. Invalid prong (on a nonbeam track).
	5	Frame O. K. Valid prong. Nearby Vee.
	6	Frame O. K. Valid prong. Cadidate recoil is unmeasurable.
	7	Frame O. K. Valid prong. Nearby double Vee.
	8	Frame O. K. Valid prong. Indistinct or unmeasurable beam track.
	9	Frame O. K. Valid prong. Spurious (but perhaps misleading) recoil.
1		Event was measured on the scanning table.
2		Event is to be Franckensteined (Code = No. of remeasurement).
3		Event has been measured on the Franckenstein.
4		Event had a file reject.
5		Event failed in KICK.
6		Event passed KICK and EXAMIN.
9	2	This frame is the first of a series of scanned frames.
	3	This frame is the last of a series of scanned frames.
	9	This card contains only a comment.

B. Some Details of the Measuring and Fitting Procedures

The fitting of events to our hypothesis is done by the PACKAGE computer program to which a special subprogram (called an event-type program) is added that specializes PACKAGE to the needs of our experiment. This event-type program dictates, for each measured event, which fits are to be attempted by the main program. We describe below the character of these fits and the reason for performing them.

Of the several thousand measured events, all but a few dozen have neither a Dalitz pair nor a conversion pair resulting from the decay of the π^0. There are cases in which a Dalitz or a conversion pair appears without accompanying recoil. In such cases, no measurement is made because the pair alone is not enough to permit reconstruction of the event. We deduce this by counting the unknown quantities. If the pair is a Dalitz pair, the momentum and direction of the γ ray from the π^0 decay are entirely unknown (Dalitz decay of π^0: $\pi^0 \rightarrow e^- + e^+ + \gamma$), as are those for the π^0 itself. There are, then, six unknown quantities and only four constraints imposed by conservation principles. This precludes the reconstruction of the decay of the π^0 and dictates our insistence on more tracks. When the π^0 decays into four electrons, we have only three unknowns and four constraints and we could perform a 1-c fit of the decay that would not only provide the momentum and direction of the π^0, but would also give a χ^2 parameter that could be compared with an expected value of 1.0 and a known distribution to find whether the four electron tracks did in fact result from the decay postulated. Four-electron decays of the π^0 occur rarely, and we did not find any.

Instead, we can detect secondary scattering of the neutron. This provides us with the course, and hence the direction, of the neutron. Detecting the recoil proton from the scattering gives us the direction and momentum of the proton, which leaves us with seven unknown quantities: the direction of the π^0 (=2), the momentum of the π^0 (=1), the momentum of the neutron before the secondary scattering (=1), the direction of the neutron (=2), and the momentum of the neutron after the secondary scattering (=1). These seven parameters are subject to the eight constraints imposed by the four-dimensional conservation laws at the two vertices. Thus we can extract a one-constraint (1-c) fit from our information that will enable us to

decide if the information is consistent with our hypothesis. This can be done in two ways that are not precisely equivalent.

First, fit the seven quantities for both vertices at once, subject to the constraints. This is the ideal way, and we use it.

Second, fit the two vertices separately. First, fit the scattering of the neutron. In that fit, there are four unknowns and four constraints. This provides the missing quantities, but does not provide a check on the validity of the hypothesis. We then use the fitted neutron momentum at the production vertex; three parameters are now missing, so we can perform a 1-c fit.

The advantage of the second procedure is that it does not assume the identity of the particle or particles produced with the neutron in the production reaction until the end; its disadvantage is its incorrect assumption that the neutron and recoil proton are perfectly measured. The information from the 0-c fit can then be used to see if the event actually arose from a different production process from the one assumed. Specifically, we insert the fitted neutron momentum in the production vertex and calculate the missing mass at that vertex. With large statistics, good measurements, and low background, it would be theoretically possible to discover new particles this way. Any particle that could be produced with a neutron from a $\pi^- p$ collision would have its missing mass represented in a histogram of the missing masses calculated, event by event, as described above. Unfortunately, all three conditions are violated in this experiment, and such particles as the η meson would be smeared thinly over a heavy background and hence would not appear as a peak on the histogram of missing masses. In any case, we perform both the 0-c fit and the 1-c, two-vertex fit on every event. A comparison then shows how much the fitting procedure moved the measured parameters of the charge-exchange neutron.

We measure together all recoils that seem to be associated with any one zero-prong. Because PACKAGE handles measurements of no more than fourteen tracks at a time, we measure no more than six neutron-proton combinations with any single zero-prong when no Dalitz or conversion pair accompanies the event. When there is a pair, the maximum falls to three. When we say that a track is "measured" we mean that the digitizing spot is run over the length of the track, as projected on the screen of the Franckenstein measuring projector. At appropriate intervals the coordinates

of the digitizing point are caused by the measurer to be punched onto paper tape. For the neutron, only the beginning point (which is the end point of the zero-prong) and the end point (the first point of the recoil proton) are measured. On the proton, the number of points measured increases with the length of proton track, because points closer together than a certain minimum are considered the same point. On the event discussed in detail elsewhere, 11 points were measured on a 6.69-cm proton track, and 5 points were measured on a recoil proton track of 0.64 cm. These numbers are representative, and show that for short tracks the density of measured points is greater. The absolute number is about six and is not very sensitive to the length of track for reasonably long tracks.

The event-type program attempts, for each event (composed of a measured beam track and one or more measured neutron-proton combinations) a succession of fits. A fit is the procedure by which the physical parameters corresponding to the set of particles participating in the fit are varied from their measured values; this fit must be within limits prescribed by measurement errors until the constraints of the conservation laws are satisfied and the χ^2 parameter, which measures the total squared deviation of the independent parameters, is least.

Each fit attempted by the event-type program is numbered with an index called the check-point mark (CPM). If the tracks that a fit requires have not been provided, the fit is simply ignored. We distinguish between two kinds of events, those without and those with a Dalitz or conversion pair in addition to the recoil. They are called event types 52 and 54, respectively, and the event-type program treats them differently.

We list below the significance of the track numbers and fit numbers for each event type.

Track number	Particle for event type	
	52	54
1	π^- beam track	π^- beam track
2, 4, 6	neutron	neutron
3, 5, 7	proton	proton
8, 10, 12	neutron	-----
9, 11, 13	proton	-----
9, 12	-----	e^- from Dalitz or conversion pair
10, 13	-----	e^+ from Dalitz or conversion pair
11, 14	-----	γ ray from conversion pair

Thus if a pair appears, its e^-, e^+ is measured as tracks 12, 13. If it is a conversion pair, the γ ray is measured as track 14. If there is a second pair, its electrons are measured as tracks 9 and 10, respectively, whereas the γ ray--if any--is measured as track 11. This scheme provides for all possible combinations of Dalitz and non-Dalitz pairs. Although cases in which more than one pair appeared did not occur in our experiment, they were provided for in the event-type program and are included, for the sake of completeness, in the inventory below.

Check-point mark: Reaction(s) being fitted	Description
1, 3, 5 $n+p \rightarrow n+p$	0-c fit of the secondary elastic n-p scattering for each of the measured n-p combinations (2, 3), (4, 5), and (6, 7), respectively.
2, 4, 6, $\pi^- + p \rightarrow \pi^0 + n$; then $n+p \rightarrow n+p$	1-c, two-vertex fit of charge-exchange and n-p scattering, for each of the n-p combinations, respectively.
7, 8, 9, $\pi^0 \rightarrow e^- + e^+ + \gamma$	1-c fit of Dalitz decay of the π^0 fit in CPM (2, 4, 6) into the electron pair composed of tracks (13, 14).

10, 11, 12	Same as CPM(7, 8, 9) except that the Dalitz pair is composed of tracks (9, 10).
13, 14, 15 $\pi^0 \rightarrow e^- + e^+ + e^- + e^+$	Double Dalitz decay. 4-c fit of the decay of the π^0 from CPM (2, 4, 6), respectively, into the four e's, tracks (9, 10, 12, 13).
16, 17, 18 $\pi^0 \rightarrow \gamma + \gamma$ $\gamma + p \rightarrow e^+ + e^- + p$	Single conversion pair. 1-c, two-vertex fit of decay of the π^0 fit in CPM (2, 4, 6), respectively, into two γ's, and the subsequent conversion of one of them (track 14) into the e pair composed of tracks (12, 13).
19, 20. 21	Same as CPM (16, 17, 18) except that the conversion pair is composed of tracks (9, 10), and the converting γ ray is track 11.
22, 23, 24 $\pi^0 \rightarrow \gamma + e^- + e^+$ $\gamma + p \rightarrow e^- + e^+ + p$	Dalitz decay followed by conversion. 1-c, two-vertex fit of Dalitz decay of the π^0 fit in CPM (2, 4, 6), respectively, into the Dalitz pair, tracks (9, 10), followed by the conversion of the γ ray, track 14, into the conversion pair (12, 13).
25, 26, 27	Same as CPM (22, 23, 24) except that the Dalitz pair is (12, 13), the converting γ is (11), and the conversion pair is (9, 10).
28 $\gamma + p \rightarrow e^- + e^+ + p$	Conversion of γ ray. 0-c fit of conversion of γ ray (track 14) into e pair composed of tracks (12, 13).
29	Same as CPM 28 except that the converting γ ray is track 11 and the pair is (9, 10).

30, 31, 32 $\pi^0 \rightarrow \gamma + \gamma$	Decay of π^0 into two γ's, both converting into e pairs. 4-c fit of decay of the π^0 fitted in CPM (2, 4, 6), into the two γ rays. The γ rays have both converted into e pairs and the conversions have been fitted in CPM 28 and 29.
33, 34, 35 $\pi^0 \rightarrow \gamma + e^- + e^+$	Dalitz decay of π^0 followed by conversion of γ ray into e pair. 4-c fit of the decay of the π^0 fitted in CPM (2, 4, 6) into an e pair composed of tracks (9, 10) and a γ ray (track 14) that has been previously fitted in CPM 28.
36, 37, 38	Same as CPM (33, 34, 35) except that the Dalitz pair is composed of tracks (12, 13) and the converting γ ray is track 11, fitted previously in CPM 29.

We can think of the experiment as a filter of several stages whose purpose is the extraction, from an initially given mixture of sand and diamonds (noise and signal), of a pure diamond yield. At each stage of filtration, some diamonds are accidently lost, and some new impurities are introduced. We now follow the experiment through to discuss, for each stage of analysis, what fraction of the diamonds passes through and what fraction of spurious substances is introduced.

We are presented originally with a set of pictures of the bubble chamber taken just after the passage of a set of beam tracks (π^- mesons at 1.03 BeV/c). The diamonds we wish to extract are the evidences that the following sequence of reactions took place: $\pi^- + p \rightarrow \pi^0 + n$ followed by $n + p \rightarrow n + p$, which resulted in a π^0 emitted nearly forward in the center-of-mass system (i.e., $0.7 \leq \cos\theta^{c.m.} \leq 1.0$). When we have gathered these "diamonds," we examine their distribution and deduce the forward partial cross section for charge-exchange scattering. We now describe the various stages of the extraction process, some of which we perform; other, nature performs.

First, of the pictures we are given, some contain pictures of beam tracks that have been involved in the interesting sequence of reactions described. Such beam tracks all end at the point where the reaction took place (the products of the reaction are neutral, and only charged particles leave tracks in the chamber). Thus, no interesting events are lost in considering only those having a terminating beam track (or "zero-prong"). Some spurious events are introduced because the interesting reaction is not the only one producing zero-prongs.

Given that our event has appeared as a zero-prong (the first half of the reaction sequence), we accept only those events for which the neutron produced in the first reaction scatter from a proton before leaving the chamber. We insist further that this reaction produce a secondary recoil proton that is visible in the cameras. These stages of analysis are performed by "Nature." The efficiency with which she "turns" a secondary neutron into a visible recoil proton depends on the momentum and direction of the neutron, the size and geometry of the chamber, and the nature of the n-p elastic scattering. The correction for this efficiency is discussed in Appendix J.

At this stage we have interesting events that have left zero-prongs and visible recoil protons. The remaining stages of analysis are devoted to finding and identifying these. The film is scanned twice, independently, to find all zero-prongs, and when a zero-prong is found, the region about it is searched for appropriate stopping protons. These processes are neither totally efficient nor totally discriminating. Not all the events leaving visible recoils are found by the scanners, and in those zero-prong—stopping-proton pairs found by the scanners, there are many that did not result from the sequence of events described. The efficiency of scanning is broken down into independent efficiencies for finding zero-prongs and recoils, and is discussed in Appendix M. The failure to discriminate means that our sample contains, at this stage, a large fraction of noise. We seek to remove it at a later stage.

The events are then traced out on the Franckenstein scanning projector, and the orbits of the measured tracks are punched out on paper tape. The paper tape is converted to magnetic tape, and the latter is run through the editing program PANAL,[6] which prepares it for analysis by the computer.

We assume that no noise is introduced by these operations. Some events could be lost, however, by minor carelessness in measurement (substantial carelessness would be detected by the computer and a remeasurement ordered). Some events, too, might be lost because the measurer interchanged the beginning and end of the recoil proton in cases where the proton track is short, and where the direction of its curvature is hard to distinguish. These effects are discussed in Appendix N.

When the events have been measured, they are reconstructed and fitted by the computer program PACKAGE. We expect no new noise to be introduced here, and we expect all the good events that have reached this stage to pass through. Much of the noise introduced in the earlier stages, however, remains. More specifically, PACKAGE seeks to fit the measured tracks to the hypothesis that they arose from the sequence of reactions ($\pi^- + p \rightarrow \pi^0 + n$; $n + p \rightarrow n + p$) that interests us. It performs a χ^2 fit, based on the errors inherent in the measurements of the tracks and provides the χ^2 value if and when a fit is achieved. A low χ^2 value implies a good fit and implies also that the orbits of the tracks measured are consistent, within measurement errors, with the hypothesis that the tracks arose from the interesting sequence of reactions. Some of the noise introduced in earlier stages will not be filtered out by the fitting process, but will persist in the sample of events that has fitted the hypothesis with a low χ^2 value. The most important contribution to this persistent noise comes from short proton tracks scattered throughout the chamber and not arising from interactions of the beam tracks with the chamber fluid. The effect of such short spurious protons and the estimation of its magnitude by use of the FAKE program is duscussed in Appendix F.

The sample could also contain events that fit the hypothesis but arise from other zero-prong-producing reactions. The events of this type fall into two categories. First, events in which the recoil is caused by a neutron, which implies that the other final-state particles are nonstrange; second, events in which the recoil is caused by some other neutral. In the first case, we expect the fitting routine to be able to distinguish a missing mass of a single π^0 from one of more than two π^0's or of an η (we are below threshold for ω production). In the second case, the particle causing the recoil would have to be a π^0, K^0, Λ, or Σ^0. The π^0 has a decay length of the order of 10^{-5} cm in the chamber, which excludes its "faking" an

n-p collision. In any reaction involving a strange particle, the likelihood of at least one decay (because at least two strange particles will always be present in the final state arising from a $\pi^- p$ collision) reduces the already small possibility of such a successful masquerade. Further, of the zero-prong-producing reactions at this energy, elastic charge exchange has a high cross section approximated only by inelastic charge exchange producing an additional π^0; the lower basic cross section for the others added to the improbability of their producing a convincing masquerade enables us to neglect their effect. For the multipion charge exchange, the effect is small compared with that of spurious short, randomly distributed recoils.

Output from the processing stage	Description of the processing	Processing done by	Efficiency	Noise introduced
Elastic charge-exchange events occurring on valid beam tracks in the prescribed portion of the chamber in which the π^0 is emitted at an angle $\theta^{c.m.}$ in the c.m., such that $\cos\theta^{c.m.} \geq 0.7$...	Essential production reaction	Nature	1.0	None
... and on which zero prongs have formed	Zero-prong formation	Nature	1.0	None
... and on which recoils have arisen from secondary scatterings of the neutron formed in the essential-production reaction	Recoil formation by secondary-neutron scattering	Nature	Given by escape-correction calculation (1)	None

Output from the processing stage	Description of the processing	Processing done by	Efficiency	Noise introduced
... and on which the recoil projects more than a certain minimum length on the plane of the film	Selection of recoils theoretically visible to scanners examining the film	Nature	Given by visibility of profile-correction calculation (2)	None
... and whose zero-prongs have been found by a scanner	Scanning film for zero-prongs	Scanner	Zero-prong scanning efficiency (3)	Zero-prongs not arising from elastic charge exchanges
... and on which the associated recoil has been found	Scanning the vicinity of zero-prong for possibly associated stopping-proton recoil	Scanner	Recoil scanning efficiency (3)	Recoils not associated with the zero-prong through the essential production reaction

Output from the processing stage	Description of the processing	Processing done by	Efficiency	Noise introduced
				followed by elastic n-p scattering (5)
... and have been successfully measured on the Franckenstein	Tracing the orbits of the particles on the digitized measuring projector	Measurer	Given by fraction of imperfect or anomalous measurements (4)	Assume none
... and have been successfully converted to magnetic tape and put in appropriate format by the PANAL program	Paper-to-magnetic-tape conversion; processing by editing program	Tape converter and computer	Assume equal to 1.0	Assume none

Output from the processing stage	Description of the processing	Processing done by	Efficiency	Noise introduced
... and have been successfully reconstructed and fitted by the PACKAGE program	Computer reconstruction of measured tracks and fitting of these to the hypothesis that they arose from the essential reaction	Computer	0.90 (Based on χ^2 cutoff equal to 2.706)	Assume none

References to Appendices discussing the effects above. See Appendix discussing

(1) Escape Correction (Appendix J)

(2) Visibility or Profile Correction (Appendix K)

(3) Scanning Efficiencies (Appendix M)

(4) Reproducibility and Fluctuations in Measurement (Appendix N)

(5) The Estimation of Background Due to Spurious Short Proton Tracks (Appendix F)

C. Choice of Criteria for the Selection of Valid Events

Our objective in choosing selection criteria is the achievement of a final sample of valid events that is relatively insensitive to the known fluctuations in measuring and scanning, and contains the best possible compromise of high statistics and low admixture of background. To achieve reproducibility of measurements, we insist that recoils rise no more steeply than 60 deg relative to the top glass. Many small spurious recoils inhabit the chamber, so we scan for recoils that project more than 0.1 in. on the scan table in the two stereo views. This translates to a projection of about 0.38 cm in space. Our detection efficiency is so low for recoils of such lengths, however, that we insist on a projection exceeding 0.7 cm on the top glass. The accompanying histograms show our loss to be small and our increase in discrimination from the rain of short spurious recoils to be considerable. If we tightened this restriction further, we would begin to lose reasonable numbers of otherwise acceptable events. We therefore choose 0.7 cm as the limit of acceptance.

The 60-deg and 0.7-cm criteria are essentially direct reflections of the reproducibility of scanning and measuring techniques. Earlier, we rejected events on beam tracks that were not within acceptable limits with respect to azimuth, dip, and coordinates at entry. We have distinguished reliably detectable events from all others. How do we distinguish valid from invalid events among these?

Four criteria relate to this problem. The first is the traditional one. Does the χ^2 value for the fit of the event to the hypothesis render the hypothesis likely? Our hypothesis has one more measured quantity than is necessary for calculation of all quantities for the event (1-c); hence, ideally, 90% of all real events will have χ^2 values below 2.706. That is the acceptance level we adopt.

The χ^2 value above, however, is computed relative to the errors in the measured quantities. Thus, a poorly measured event may give a spuriously good fit to the hypothesis, simply because the large deviations of the measured quantities from the values acceptable to the hypothesis are examined on the scale of very large inherent measurement errors. Clearly we don't wish to contaminate our sample with events included merely because they are poorly measured. The solution is to find a good index of the quality of measurement and eliminate all poorly measured events. Of course, some

wheat will be discarded with the chaff of poorly measured events. We must estimate this loss and correct for it.

We have found one reasonably good index of good measurement, the error in dip of the recoil. We must remember that the effects we are discussing do not arise from mistakes in measurement, but from the limitations of our instruments and programs. Certain short tracks are simply difficult to measure accurately, and large errors are inevitable. These tracks may indeed have arisen from the hypothesized series of reactions, but our limitation persists and we are bound to discard the event nonetheless. By comparing histograms of real and "FAKE" events, we conclude that 2.50 deg is as large an error in recoil dip as we should accept. We are aided in this decision by the presence of one absolutely ironclad valid event, which is discussed in detail in a separate section. Its legitimacy is guaranteed not only by its satisfaction of our criteria but by the presence of a conversion pair that fits the hypothesis. This bellwether event has a recoil dip error of about 0.8 deg, so that a limit three times as great may not seem too small.

The χ^2 dip-error pair provide a measure both of the degree of constraint of the event (how well its validity is determined) and its validity relative to that degree of constraint. This scheme has weaknesses, however, as the dip error of the recoil is not the only factor in determining the actual degree of constraint. There are cases, in fact, in which even a large error in recoil dip will contribute little to the uncertainty in the validity of the event as a whole. The primary variables in every case are the space angles between π and n and between n and p, and the momenta. Because the π and n are long tracks, the angle between them will be determined with low error. The latter angle, θ_{np}, however, will be poorly determined if the direction of the proton is. If the neutron and proton are both flat, however, the space angle, θ_{np}, will be relatively insensitive to variations in proton dip, even within reasonably large limits. In this case, the event might be well constrained by the physical measurements despite a large dip error. (The dip error was our first guess as index because the cameras are approximately parallel to the xy plane, and components of vectors normal to the camera planes must be stereo reconstructed. Further, this is hardest for short tracks.)

The imperfections in the χ^2 and dip-error index pair lead us to

seek an alternate set of indices, and we have adopted the missing mass and its error. These quantities are calculated directly from unfitted data and contain no prejudices as to the masses we expect. As we chose the 90% confidence limit (2.706) in our χ^2 cutoff, so do we choose a 90% limit in examining missing masses. We consider an event to be consistent with our hypothesis if the missing mass computed from it lies within 1.65×error in its determination. If we assume measurements of missing masses to be normally distributed about the "true" missing-mass value for the tracks being measured, with a width equal to the missing-mass error, then 1.65 times the latter gives the 90% confidence limit.

We seek now the analogue to the dip-error maximum of 2.5 deg in the maximum permitted missing-mass error. The accompanying histogram shows a gap in the distribution after 16.0 MeV/c^2, and we adopt this as our index of constraint. Our ironclad event has an error of 13 MeV/c^2, which enables us to identify the group of events with errors below 16.0 with the set of valid events. The gap in distribution beyond 16.0 causes us to regard those with higher errors as background. This guess is supported by the relatively higher density of spurious events in the region above 16.0 MeV/c^2, as estimated by the FAKE program. This increase in density is used in detail elsewhere to estimate the loss of valid events because of the restriction on mass error. It is useful to note that the missing-mass deviation is reproduced better on successive measurements than is χ^2.

We should now decide whether the two sets of criteria are equivalent, and if not, which is to be preferred. Since the χ^2 criterion is the most widely used, let us examine it relative to the others. Our first question should be: How many events of low χ^2 fail the other criteria, and how many of high χ^2 satisfy them?

The histogram of signatures (Fig. 6) answers these questions, and we consider only events with positive measured proton curvature. We assume, further, that only forward events having flat recoils with acceptably long projections are to be considered. The Boolean signatures of the events under discussion will have, therefore $X_0 = 0$ (forward), $X_3 = 0$ (long projection), $X_4 = 0$ (flat recoil trajectory), and $X_7 = 0$ (positive recoil curvature). (The notation and its applications are discussed in the section on the method of Boolean signatures.) There are sixteen possible combinations of the four remaining variables, and the number of events occurring with each

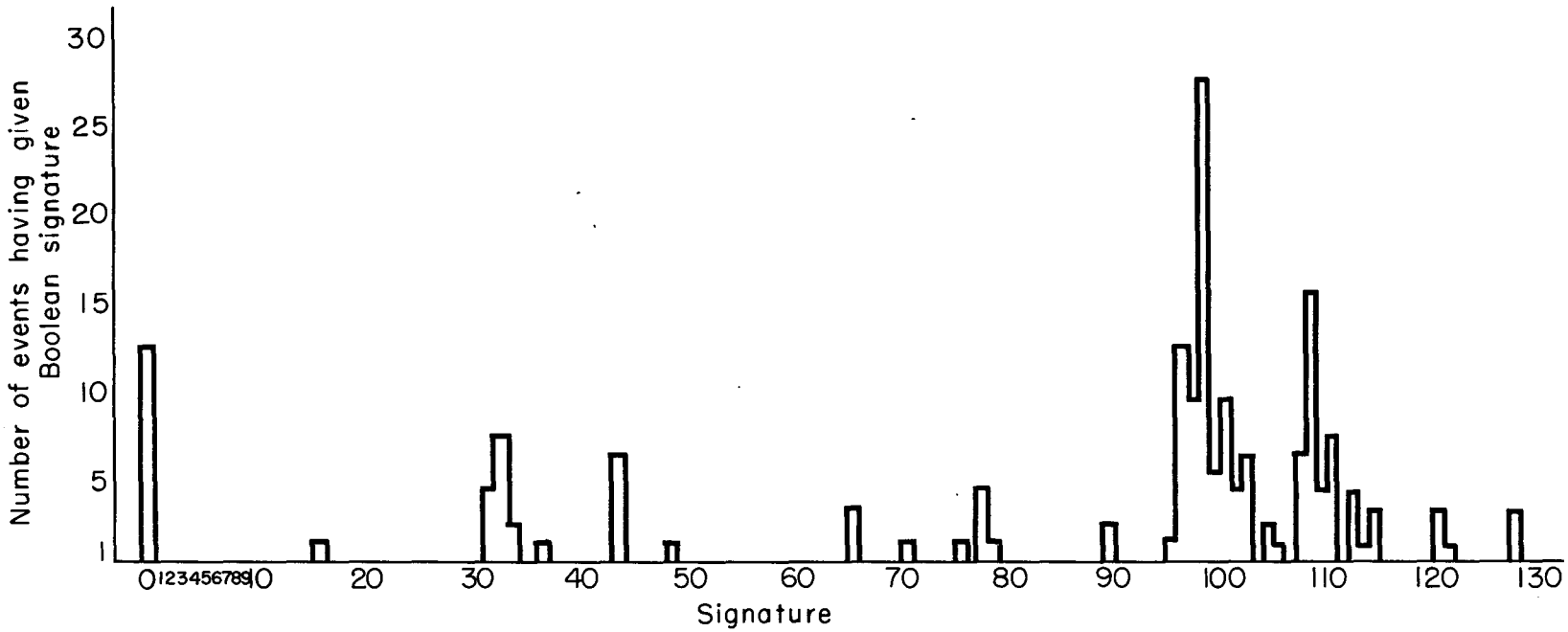

MUB-2289

Fig. 6. Distribution of the experiment events among the $2^7 = 128$ possible Boolean signatures.

combination is given in the table below.

Signature	Number of events	MM consistent with $M(\pi^0)$	δMM	Dip error	χ^2
0	11	Yes	Low	Low	Low
2	0	Yes	Low	Low	High
4	0	Yes	Low	High	Low
6	0	Yes	Low	High	High
32	4	Yes	High	Low	Low
34	2	Yes	High	Low	High
36	0	Yes	High	High	Low
38	0	Yes	High	High	High
64	0	No	Low	Low	Low
66	3	No	Low	Low	High
68	0	No	Low	High	Low
70	0	No	Low	High	High
96	1	No	High	Low	Low
98	9	No	High	Low	High
100	5	No	High	High	Low
102	4	No	High	High	High

We conclude that there are no events having high χ^2, independent of dip error, that also have missing masses consistent with $M(\pi^0)$ to within $1.65\times$ an error less than 16.0 MeV/c^2 (there are no events with signatures 2 or 4). Thus, a good, well-constrained missing mass implies a low χ^2 value. We note, too, that there are events with high χ^2 and low dip error that have good but poorly constrained missing masses (two events of signature 34) and events with well-constrained but poor values of missing mass (three events with signature 66). There are, however, no events with high χ^2 and high dip error (signatures 38 and 70) that have either well-constrained or good values of missing mass. Thus, if any event satisfies at least one missing-mass criterion, its dip error must be low; if both, its χ^2 value must also be low. This implies that the missing-mass criteria are at least as stringent as the χ^2 dip-error pair.

To complete the analysis, we should determine how much more stringent are the missing-mass criteria. The table shows that there is a single event that satisfies the χ^2 dip-error criteria but fails the missing-mass set (1 event of signature 96), which places an upper bound on the possible difference introduced by changing the criteria. Of the other events failing both missing-mass criteria, nine have high χ^2 and low dip error (signature 98), five have low χ^2 and high dip error (signature 100), and four have high values of χ^2 and of dip error (signature 102).

We conclude that there is a high degree of agreement between the two sets of criteria. The obvious coherence between the two parts of the missing-mass-criterion set and the greater relative reproducibility of the missing-mass-index quantities leads us to choose them as final judges of the validity.

It is now appropriate to give a few numbers relating to the reproducibility of the missing masses and their errors. On three successive measurements of our ironclad event (502-353), the χ^2 values were 1.482, 0.04136, and 1.01, and there are instances of much worse variation. The dip errors were 0.7078, 0.7277, and 0.7087; the missing masses were 152.2, 137.9, and 149.0; and the missing-mass errors were 13.31, 14.31, and 13.20. These values are typical of those found on good events; χ^2 reproducibility is discussed elsewhere in some detail. The spread of determinations of the missing mass is of the same order as the quoted errors, so that restriction to low missing-mass errors is essentially a restriction to reproducible events; this is an extension of our earlier policy of adoption of criteria that will ensure reproducible measurements. (Note above that the χ^2 value varied by a factor of 30 on successive measurements of a single event.) Borderline events are discussed in Appendix G.

Where a separate discussion has assured us of adequate reliability of χ^2 values, the discussion above sought to show that missing-mass quantities were even more reliable. Further, we were fortunate to find that our missing-mass criteria were always stronger than the χ^2 criterion (even with the addition of the dip-error maximum), which simplifies our analysis considerably. There is no assurance, in general, of such a circumstance. Last, in this discussion of our criteria, we need to estimate the number of valid events sacrificed to the expedient of adopting our missing-mass criteria. We compare the numbers of events having missing-mass

error above 16.0 with the number of such background events estimated to be present by the FAKE[11] program. The former number of "real + background" events is reduced by the latter estimate to give our estimate of lost valid events. This estimate is made in the section on the estimate of background from short, spurious recoils.

Before we may estimate our casualties to the orthodoxy of our criteria, we must anticipate an objection to our use of the missing mass as an essential variable. The square of the missing mass is physically a more fundamental quantity than is the missing mass itself and would be distributed more normally. This is important, because we use the result that 90% of all events in a normal distribution will lie within 1.65 standard deviations of the mean of the distribution. Further, since no missing mass can be negative, the distribution is clearly not normal.

The salvation of our procedure lies in the use of the distribution only near its mean, where it is approximately normal. In fact, with the appropriate choice (5000 MeV^2) of a maximum permitted error in the square of the missing mass, MMSQ, we get precisely the same results as we had by using the missing mass as our prime variable. Further, the condition $[MM - M(\pi^0)]/(1.65 \times \delta MM) = R \leq 1.0$ is not very different from the condition $[MMSQ - M^2(\pi^0)]/(1.65 \times \delta MMSQ) = RQ \leq 1.0$. The latter condition may be rewritten as

$$\frac{[MM - m(\pi^0)]}{1.65\,\delta MM}\,\frac{[MM + m(\pi^0)]}{2 \times MM} = RQ \leq 1$$

$$R \times \left\{[1 + m(\pi^0)]/MM\right\}/2 = RQ \leq 1,$$

which is equivalent to $R \leq 1$, if $m(\pi^0) = MM$. More precisely, the conditions become the same as the missing mass approaches the ideal. Because we accept only those events whose missing masses are close to ideal, we may expect close agreement between the two criteria. Specifically, we permit δMM as large as 16 MeV/c^2 and $MM - m(\pi^0)$ as large as $1.65 \times \delta MM$, which equals, in the extreme case, about 26 MeV/c^2. Thus, compared to the best criterion $RQ \leq 1$, we would impose in the worst case a criterion that differed from that one by 10% (i.e., $0.9\,RQ \leq 1$ or $1.1\,RQ \leq 1$). In fact, all our events either pass or fail these two criteria jointly. Thus, we may continue to talk in the convenient physical units of

missing mass that we have been using throughout, although our results remain valid relative to the preferred standard.

D. Detailed Discussion of a Valid Forward Event Having an Associated Electron Pair

The event we chose (see Fig. 7) occurred on roll 502, frame 353 of the Associated-Production-Experiment run and is chosen to illustrate each of the following points mentioned in the main discussion:

(a) How more than one recoil may appear on a given zero-prong.

(b) How configurations of tracks arising from the sequence of events $\pi^- + p \rightarrow \pi^0 + n$, then $n + p \rightarrow n + p$ are distinguished from those that do not.

(c) How a γ ray may convert into an electron pair.

(d) How a random proton recoil in the chamber may "impersonate" one that arises from the reactions in which we are interested.

(e) How the criterion of well-measured dip removes background events.

(f) The problem of reproducibility of measurements. (Two separate measurements of the same event are given to indicate the reliability of single measurements.)

The accompanying photograph is an enlargement of the original 45-mm photograph of about a fifth of the bubble chamber; it includes nearly the whole width. The numbers on the left are etched onto the steel teeth of a fiducial rake that is immersed in the chamber fluid. The common separation of teeth is about 4 inches.

At point P we see the termination of a beam track in the chamber. We assume that the production reaction $\pi^- + p \rightarrow \pi^0 + n$ has occurred there. In the neighborhood of P, we find a long proton recoil whose initial point is R and a shorter recoil at S that proves to be spurious. The streak at f is not a stopping proton, but rather a fiducial mark on the glass boundary of the chamber.

At point C we have what we suppose to be a conversion electron pair arising from the conversion of one of the γ rays of the π^0 decay. At D the e^- of the conversion pair scatters from an atomic electron, and makes a low-energy electron track or δ ray. We should point out that

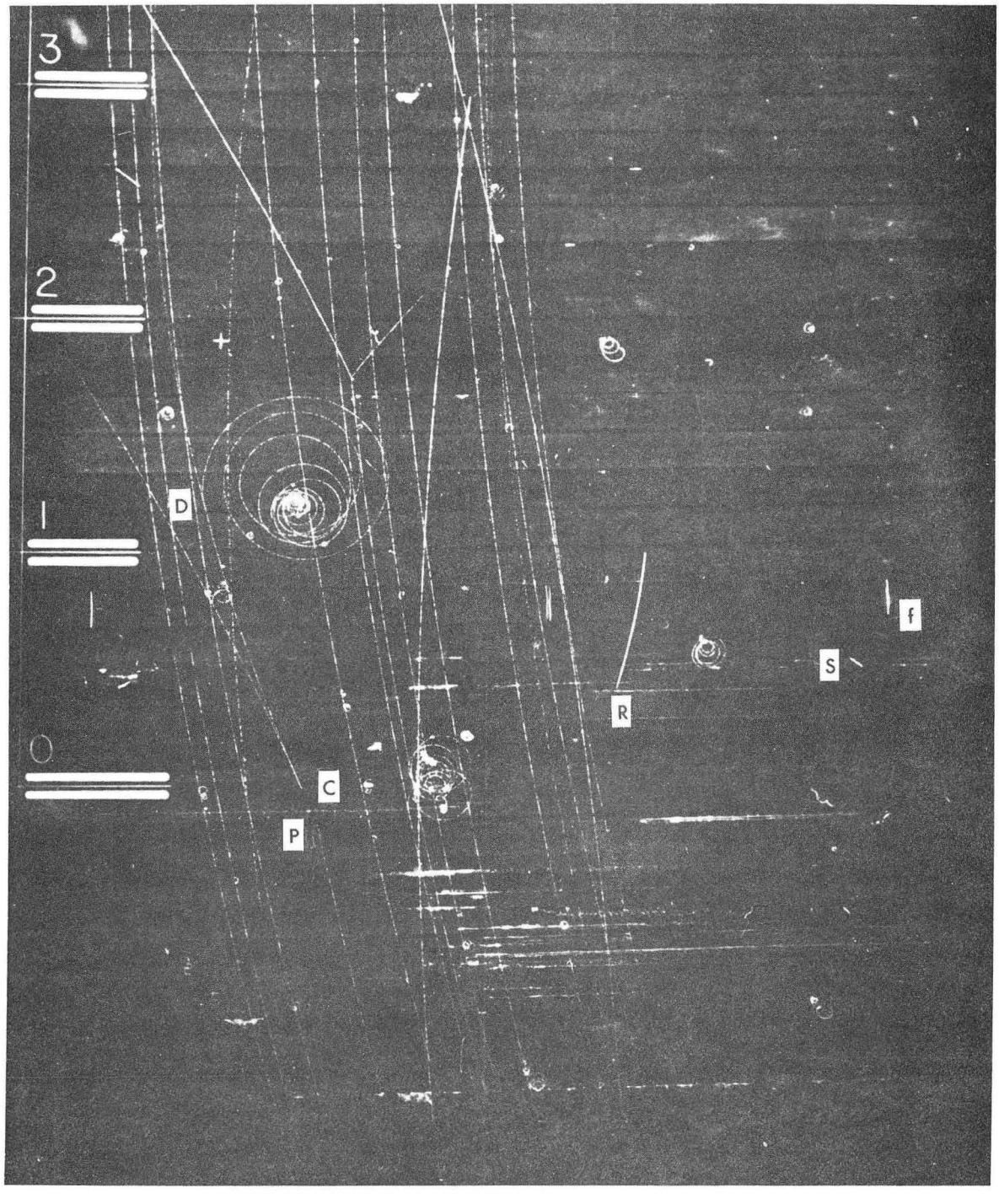

ZN-4084

Fig. 7. Reproduction of a photograph of an experimental event showing zero-prong, recoil, and associated conversion pair.

this picture is more ideal than typical. The long recoil, the easily visible pair, and the large δ ray (which reinforces our certainty that the track is an electron) appear relatively infrequently.

The reactions we postulate are:

At point	Reaction description	Reaction
P	Charge-exchange	$\pi^- + p \rightarrow \pi^0 + n$
R, S	Elastic scattering of neutron	$n + p \rightarrow n + p$
C	Conversion of γ ray from π^0 decay	$\gamma + p \rightarrow e^+ + e^- + p$ (after $\pi^0 \rightarrow \gamma + \gamma$)
D	Electron-electron scattering forms a δ ray	$e^+ + e^- \rightarrow e^- + e^-$

The figures following contain the results of two distinct measurements of the two recoils in the frame. First, recoil R is measured alone with the conversion pair, then recoil S is measured alone without the pair; and finally both are measured on a single measurement with the pair. These figures are reproductions of the output of the EPC program,[8] which digests the information on the tapes presented by PACKAGE and writes a summary of the more commonly used parameters on a tape that may be printed. The figures are samples of the summary presented by EPC.

Nearly all the headings are self explanatory. The heading LSZ referers to a track code (1, 2, and 3), which designates the track to which the number refers, as a leaving, stopping, or zero-length track. Any measured track that is not assumed to come to rest in the chamber is called "leaving", and a track is assumed to be "stopping" only if so specified at the time of measurement. In that case, the value of the momentum of the track is taken from a range-momentum table for the measured length of track. For leaving tracks, the momentum is computed (with a lesser accuracy) from the curvature of the track, by using the known value of the magnetic field in the chamber. The term "zero length" is applied to an unmeasured track of a

SUMMARY OF A GOOD, FORWARD EVENT HAVING AN ASSOCIATED ELECTRON PAIR.

EXP	ROLL	FRAME	TYPE	PU	MEAS	OPER	MEASURED	PANGED	KICKED	SKELMID	PGM ID	EXP ID	PAGE	1
4	0502	353 01	52	0	0	91	610725	630829	08/29/1963	000000	A38-00	RECOIL	ORD=	109

PANG DATA — MASS INDEPENDENT INFORMATION

TRACK	LSZ	FTN	PHT	VIEWS	POINTS	LENGTH	DL	X(BEG)	Y(BEG)	Z(BEG)	X(END)	Y(END)	Z(END)
1	1	0	0	1 2	9 10	14.05	0.02	-6.00	-87.50	15.26	-9.35	-73.85	15.69
2	1	0	0	2 3	2 2	17.41	0.09	-9.30	-73.76	16.08	1.53	-66.05	27.33
3	2	0	0	1 2	12 11	6.75	0.01	1.50	-66.09	27.10	2.18	-60.03	30.07

MASS DEPENDENT INFORMATION

TRK	MASS	P(BEG)	P(END)	DP/P	P(L)	DPL	KPTEST	PHI(B)	PHI(E)	ERROR	DIP(B)	DIP(E)	ERROR	C/R	S(XY)	S(Z)
1	-139.6	-1226.3	-1223.0	0.09	75.3	0.7		105.36	102.22	0.16	1.46	1.60	0.31	0.2	.0131	.0813
B		1060.3		0.014			-1.76									
2	939.5	1.0	1.0	10.00	1.0	10.0	-0.10	35.43	35.43	0.10	40.25	40.25	0.24	0.	.	.
3	938.2	216.6	-20.5	0.14	239.2	0.8	-1.64	78.98	89.21	0.56	25.29	25.43	0.71	2.8	.0043	.0297

CPM	CHI SQ	LC	STP	CUT	DMN							TARGET	IH1	IH2	IH3	IH4	IH5	IH6	IH7	IH8
1	0.	0	0	0	-1							938.2	0	0	0	0	0	0	0	0
	0.000			0.			0.			0.		0.		0.			0.			0.
TRK	MASS	LSZ		MOMENTUM			AZIMUTH			DIP		KKTEST	PCM		CMCOS		XI(PHI)	XI(S)		XI(K)
-2	939.5	1		312.2		3.0	35.27	0.19	40.28	0.24		0.	153.9		1.000		0.	0.		0.
3	938.2	2		239.2		0.8	78.98	0.56	25.29	0.71		0.	153.9		0.188		0.	0.		0.
31	939.5	3		197.4		4.3	333.98	0.67	30.32	0.88		0.	153.9		-0.188		0.	0.		0.

CPM	CHI SQ	LC	STP	CUT	DMN		TWO VERTEX FIT.				TARGET1	TARGET2	IH1	IH2	IH3	IH4	IH5	IH6	IH7	IH8
2	1.48	1	2	0	-1						938.2	938.2	0	0	0	0	0	0	0	0
	13.518			0.			0.			0.		0.		0.			0.			0.
TRK	MASS	LSZ		MOMENTUM			AZIMUTH			DIP		KKTEST	PCM		CMCOS		XI(PHI)	XI(S)		XI(K)
-18	-139.6	1		1051.1		13.8	102.28	0.15	1.38	0.26		0.	580.2		1.000		1.22	-1.22		1.22
3	938.2	2		239.3		0.8	79.18	0.53	25.04	0.68		0.	383.6		-0.942		1.22	-1.22		-1.22
2	939.5	1		314.2		2.5	35.15	0.17	40.34	0.23		0.	580.1		-0.857		-1.22	1.22		0.
31	939.5	3		200.3		3.7	334.18	0.65	30.65	0.84		0.	736.3		-0.973		0.	0.		0.
30	135.0	3		998.8		13.7	115.26	0.23	-10.27	0.23		0.	580.1		0.857		0.	0.		0.

REPORT TYPE 6

-0.21267	-0.97711	0.00514	0.97683	-0.21273	-0.02361	0.02417	0.	0.99971	0.
0.	0.	0.	0.	1051.09987	0.	-0.00000	1060.33369	201.82168	-85.06882
96.45526	968.25406	97.97860	-220.68063	201.11658	990.66599	-103.84309	-135.61180	104.66131	960.62450
953.12129	220.68070	-201.11657	1007.88089	0.	0.	0.	0.	0.	0.
0.	0.	0.	0.	0.	0.	0.	0.	0.	0.
0.	0.	0.	0.	0.	0.	0.	0.	0.	0.
0.	0.	0.	0.	0.	0.	0.	0.	0.	0.
0.	0.	22.00000	22.00000	22.00000	22.00000	22.00000	22.00000	22.00000	22.00000
22.00000	22.00000	0.	0.	0.	0.	0.	0.	0.	0.
0.	0.	0.	0.	0.	0.	0.	0.	0.	0.
0.	0.	0.	0.	0.	0.	0.	0.	0.	0.
0.	0.	0.	0.	0.	0.	0.	0.	0.	0.
0.	0.	0.	0.	0.	0.	0.	0.	0.	0.
0.	0.	0.	0.	0.	0.	0.	0.	0.	0.

SUMMARY OF A GOOD, FORWARD EVENT HAVING AN ASSOCIATED ELECTRON PAIR.

EXP	ROLL	FRAME	TYPE	PU	MEAS	OPER	MEASURED	PANGED	KICKED	SKELMID	PGM ID	EXP ID	PAGE	2
4	0502	353 01	54	0	3	0	660803	630829	08/29/1963	000000	A38-00	RECOIL	ORD=	110

PANG DATA — MASS INDEPENDENT INFORMATION

TRACK	LSZ	FTN	PHT	VIEWS	POINTS	LENGTH	DL	X(BEG)	Y(BEG)	Z(BEG)	X(END)	Y(END)	Z(END)
1	1	0	0	1 2	14 14	14.09	0.03	-5.94	-87.51	15.52	-9.33	-73.84	15.79
2	1	0	0	2 3	2 2	17.42	0.09	-9.29	-73.82	16.01	1.51	-66.06	27.24
3	2	0	0	1 2	7 7	6.72	0.01	1.49	-66.06	27.26	2.18	-60.01	30.14
12	1	0	0	1 2	10 11	20.85	0.00	-9.97	-72.39	15.35	-15.50	-52.82	11.12
13	1	0	0	1 2	11 10	17.09	0.03	-9.97	-72.40	15.28	-17.58	-57.64	11.94
14	1	0	0	1 2	2 2	1.64	0.03	-9.33	-73.84	15.77	-9.96	-72.40	15.33

MASS DEPENDENT INFORMATION

TRK	MASS	P(BEG)	P(END)	DP/P	P(L)	DPL	KPTEST	PHI(B)	PHI(E)	ERROR	DIP(B)	DIP(E)	ERROR	C/R	S(XY)	S(Z)
1	-139.6	-1150.3	-1147.0	0.07	75.4	0.7		105.63	102.28	0.14	0.62	0.77	0.29	0.3	.0062	.0448
8		1059.6		0.014			-1.25									
2	939.5	1.0	1.0	10.00	1.0	10.0	-0.10	35.66	35.66	0.10	40.18	40.18	0.24	0.	.	.
3	938.2	217.0	-19.7	0.14	238.8	0.8	-1.52	79.01	89.14	0.58	25.06	25.19	0.73	2.3	.0018	.0140
12	-0.5	-396.0	-391.1	0.02	5.6	2.5	99.99	113.08	98.42	0.14	-12.17	-11.21	0.29	1.3	.0079	.0517
13	0.5	588.6	584.6	0.04	4.8	2.0	99.99	113.35	121.36	0.16	-11.22	-11.75	0.30	0.5	.0084	.0337
14	0.	1.0	1.0	10.00	1.0	10.0	-0.10	113.71	113.71	0.55	-15.62	-15.62	2.29	0.	.	.

CPM	CHI SQ	LC	STP	CUT	DMN	TARGET	IH1	IH2	IH3	IH4	IH5	IH6	IH7	IH8
1	0.	0	0	0	-1	938.2	0	0	0	0	0	0	0	0
	0.000		0.			0.	0.			0.		0.		0.

TRK	MASS	LSZ	MOMENTUM		AZIMUTH		DIP		KKTEST	PCM	CMCOS	XI(PHI)	XI(S)	XI(K)
-2	939.5	1	311.5	3.0	35.51	0.19	40.21	0.24	0.	153.6	1.000	0.	0.	0.
3	938.2	2	238.8	0.8	79.01	0.58	25.05	0.73	0.	153.6	0.189	0.	0.	0.
31	939.5	3	196.8	4.4	334.04	0.69	30.54	0.91	0.	153.6	-0.189	0.	0.	0.

CPM	CHI SQ	LC	STP	CUT	DMN	TWO VERTEX FIT.	TARGET1	TARGET2	IH1	IH2	IH3	IH4	IH5	IH6	IH7	IH8
2	0.04	1	2	0	-1		938.2	938.2	0	0	0	0	0	0	0	0
	14.959		0.			0.	0.		0.			0.			0.	

TRK	MASS	LSZ	MOMENTUM		AZIMUTH		DIP		KKTEST	PCM	CMCOS	XI(PHI)	XI(S)	XI(K)
-18	-139.6	1	1055.4	13.8	102.29	0.13	0.74	0.25	0.	581.7	1.000	0.20	-0.20	0.20
3	938.2	2	238.8	0.8	79.04	0.55	25.01	0.70	0.	387.3	-0.942	0.20	-0.20	-0.20
2	939.5	1	311.9	2.5	35.49	0.16	40.23	0.23	0.	581.7	-0.860	-0.20	0.20	0.
31	939.5	3	197.3	3.7	334.08	0.67	30.60	0.86	0.	736.7	-0.974	0.	0.	0.
30	135.0	3	1003.8	13.6	115.11	0.22	-10.79	0.22	0.	581.7	0.860	0.	0.	0.

CPM	CHI SQ	LC	STP	CUT	DMN	TARGET	IH1	IH2	IH3	IH4	IH5	IH6	IH7	IH8
7	1.67	1	4	0	-1	-0.	0	0	0	0	0	0	0	0
	13.333		0.			0.	0.			0.		0.		0.

TRK	MASS	LSZ	MOMENTUM		AZIMUTH		DIP		KKTEST	PCM	CMCOS	XI(PHI)	XI(S)	XI(K)
12	-0.5	1	394.1	7.5	113.09	0.14	-12.13	0.29	2.26	28.4	0.841	1.29	1.29	1.29
13	0.5	1	569.8	15.7	113.38	0.16	-11.17	0.30	2.34	39.4	0.918	1.29	1.29	1.29
-15	135.0	3	1013.7	11.6	114.94	0.17	-10.82	0.22	0.	0.0	1.000	-1.29	-1.29	-1.29
30	0.	3	58.7	11.8	143.01	4.36	2.85	3.91	0.	67.3	-0.892	0.	0.	0.

SUMMARY OF A GOOD, FORWARD EVENT HAVING AN ASSOCIATED ELECTRON PAIR.

EXP	ROLL	FRAME	TYPE	PU	MEAS	OPER	MEASURED	PANGED	KICKED	SKELMID	PGM ID	EXP ID	PAGE
4	0502	353 01	54	0	3	0	660803	630829	08/29/1963	000000	A38-00	RECOIL	3
													ORD= 110

CPM	CHI SQ	LC	STP	CUT	DMN	TWO VERTEX FIT.				TARGET1	TARGET2	IH1	IH2	IH3	IH4	IH5	IH6	IH7	IH8
16	3.09	1	3	0	-1					-0.	938.2	0	0	0	0	0	0	0	0
	11.912			0.		0.		0.		0.		0.			0.			0.	
TRK	MASS	LSZ		MOMENTUM		AZIMUTH		DIP		KKTEST		PCM	CMCOS		XI(PHI)		XI(S)	XI(K)	
-15	135.0	3	1008.3		13.5	115.03	0.21	-10.81	0.22	0.		0.0	1.000		-1.76		-1.76	-1.76	
12	-0.5	1	395.4		7.8	113.08	0.14	-12.17	0.29	2.26		28.8	0.827		1.76		1.76	1.76	
13	0.5	1	577.9		20.7	113.34	0.16	-11.22	0.30	2.34		40.4	0.905		1.76		1.76	1.76	
14	0.	1	973.3		21.9	113.94	0.54	-11.93	1.02	0.		67.5	0.921		1.76		1.76	0.	
31	938.2	3	12.9		13.6	208.42	16.43	-24.55	63.30	0.		7003.5	-1.000		0.		0.	0.	
30	0.	3	44.1		25.8	140.45	21.06	15.91	14.10	0.		68.1	-0.922		0.		0.	0.	

CPM	CHI SQ	LC	STP	CUT	DMN	TARGET	IH1	IH2	IH3	IH4	IH5	IH6	IH7	IH8
28	0.	0	0	0	-1	938.2	0	0	0	0	0	0	0	0
	0.000			0.		0.	0.			0.			0.	
TRK	MASS	LSZ		MOMENTUM		AZIMUTH	DIP	KKTEST		PCM	CMCOS		XI(PHI)	XI(S)	XI(K)
12	-0.5	1	396.7		7.9	113.08 0.14 -12.17 0.29	2.26			225.6	0.994		0.	0.	0.
13	0.5	1	588.0		22.2	113.34 0.16 -11.22 0.30	2.34			334.8	0.991		0.	0.	0.
-14	0.	1	987.3		23.8	113.71 0.55 -15.62 2.29	0.			560.3	1.000		0.	0.	0.
31	938.2	3	69.5		39.5	263.63 33.32 -76.86 4.01	0.			560.3	-0.992		0.	0.	0.

REPORT TYPE 6

-0.38725	-0.91560	-0.10824	0.88181	-0.40209	0.24647	-0.26918	0.	0.96309	0.
0.	0.	0.	0.	395.94188	-4.26834	23.82014	396.68105	586.28486	-3.65078
45.03116	588.02326	987.27439	-0.	-0.	987.27443	5.04765	7.91913	-68.85131	940.78281
0.32321	11.71208	-5.39408	938.30164	35.32302	18.18231	19.03859	44.05429	0.	0.
0.	0.	0.	0.	0.	0.	0.	0.	0.	0.
0.	0.	0.	0.	0.	0.	0.	0.	0.	0.
0.	0.	0.	0.	0.	0.	0.	0.	0.	0.
0.	0.	22.00000	22.00000	22.00000	22.00000	0.	0.	0.	22.00000
0.	0.	22.00000	0.	0.	0.	0.	0.	22.00000	0.
0.	22.00000	0.	0.	22.00000	0.	0.	0.	22.00000	0.
0.	0.	22.00000	0.	0.	0.	0.	0.	0.	0.
0.	0.	0.	0.	0.	0.	0.	0.	0.	0.
0.	0.	0.	0.	0.	0.	0.	0.	0.	0.
0.	0.	0.	0.	0.	0.	0.	0.	0.	0.

SUMMARY OF A GOOD, FORWARD EVENT HAVING AN ASSOCIATED ELECTRON PAIR.

EXP	ROLL	FRAME	TYPE	PU	MEAS	OPER	MEASURED	PANGED	KICKED	SKELMID	PGM ID	EXP ID	PAGE	4
4	0502	353 01	54	0	5	0	660421	630829	08/29/1963	000000	A38-00	RECOIL	ORD=	111

PANG DATA — MASS INDEPENDENT INFORMATION

TRACK	LSZ	FTN	PHT	VIEWS	POINTS	LENGTH	DL	X(BEG)	Y(BEG)	Z(BEG)	X(END)	Y(END)	Z(END)
1	1	0	0	1 2	18 18	13.95	0.03	-6.00	-87.48	15.29	-9.34	-73.89	15.64
2	1	0	0	2 3	2 2	17.37	0.09	-9.32	-73.80	16.03	1.49	-66.09	27.21
3	2	0	0	1 2	11 11	6.69	0.01	1.49	-66.11	27.07	2.17	-60.06	29.92
4	1	0	0	2 3	2 2	25.10	0.04	-9.32	-73.78	16.04	10.64	-64.74	28.26
5	2	0	0	2 3	5 5	0.64	0.03	10.65	-64.70	28.39	11.13	-65.10	28.34
12	1	0	0	1 2	16 12	13.14	0.01	-9.97	-72.43	15.26	-14.02	-60.29	12.67
13	1	0	0	1 2	12 15	16.84	0.03	-9.98	-72.43	15.24	-17.50	-57.81	11.88
14	1	0	0	1 2	2 2	1.64	0.03	-9.34	-73.90	15.61	-9.97	-72.43	15.27

MASS DEPENDENT INFORMATION

TRK	MASS	P(BEG)	P(END)	DP/P	P(L)	DPL	KPTEST	PHI(B)	PHI(E)	ERROR	DIP(B)	DIP(E)	ERROR	C/R	S(XY)	S(Z)
1	-139.6	-1372.2	-1369.0	0.08	75.2	0.7		105.15	102.36	0.13	1.30	1.43	0.29	0.2	.0075	.0476
B		1067.6		0.014			-3.60									
2	939.5	1.0	1.0	10.00	1.0	10.0	-0.10	35.49	35.49	0.10	40.10	40.10	0.24	0.	.	.
3	938.2	220.4	-16.7	0.14	238.6	0.8	-1.20	79.09	88.97	0.55	24.91	25.04	0.71	2.8	.0025	.0173
4	939.5	1.0	1.0	10.00	1.0	10.0	-0.10	24.38	24.38	0.08	29.14	29.14	0.23	0.	.	.
5	938.2	-103.7	3.1	1.07	125.1	1.7	-0.86	322.43	315.75	7.06	-6.70	-6.62	5.49	0.1	.0201	.0606
12	-0.5	-382.4	-379.3	0.04	3.8	1.6	99.99	113.16	103.69	0.18	-11.68	-11.09	0.32	0.7	.0042	.0255
13	0.5	565.0	561.1	0.04	4.7	2.0	99.99	113.14	121.43	0.16	-11.57	-12.11	0.30	0.6	.0070	.0457
14	0.	1.0	1.0	10.00	1.0	10.0	-0.10	113.18	113.18	0.54	-12.01	-12.01	2.32	0.	.	.

CPM	CHI SQ	LC	STP	CUT	DMN	TARGET	IH1	IH2	IH3	IH4	IH5	IH6	IH7	IH8
1	0.	0	0	0	-1	938.2	0	0	0	0	0	0	0	0

	0.000		0.		0.		0.		0.		0.		0.		0.
TRK	MASS	LSZ	MOMENTUM		AZIMUTH		DIP		KKTEST		PCM	CMCOS	XI(PHI)	XI(S)	XI(K)
-2	939.5	1	312.5	3.0	35.33	0.19	40.13	0.24	0.		154.1	1.000	0.	0.	0.
3	938.2	2	238.6	0.8	79.09	0.55	24.91	0.71	0.		154.1	0.180	0.	0.	0.
31	939.5	3	198.5	4.3	334.23	0.66	30.55	0.88	0.		154.1	-0.180	0.	0.	0.

CPM	CHI SQ	LC	STP	CUT	DMN	TWO VERTEX FIT.	TARGET1	TARGET2	IH1	IH2	IH3	IH4	IH5	IH6	IH7	IH8
2	1.01	1	2	0	-1		938.2	938.2	0	0	0	0	0	0	0	0

	13.990		0.		0.		0.		0.		0.		0.		0.
TRK	MASS	LSZ	MOMENTUM		AZIMUTH		DIP		KKTEST		PCM	CMCOS	XI(PHI)	XI(S)	XI(K)
-1B	-139.6	1	1059.3	13.9	102.40	0.13	1.27	0.24	0.		583.1	1.000	1.00	-1.00	1.00
3	938.2	2	238.7	0.8	79.26	0.53	24.70	0.68	0.		386.1	-0.944	1.00	-1.00	-1.00
2	939.5	1	314.2	2.5	35.23	0.16	40.19	0.23	0.		583.1	-0.859	-1.00	1.00	0.
31	939.5	3	201.0	3.6	334.40	0.64	30.83	0.83	0.		739.8	-0.973	0.	0.	0.
30	135.0	3	1007.0	13.7	115.30	0.21	-10.26	0.22	0.		583.1	0.859	0.	0.	0.

CPM	CHI SQ	LC	STP	CUT	DMN	TARGET	IH1	IH2	IH3	IH4	IH5	IH6	IH7	IH8
3	0.	0	0	0	-1	938.2	0	0	0	0	0	0	0	0

	0.000		0.		0.		0.		0.		0.		0.		0.
TRK	MASS	LSZ	MOMENTUM		AZIMUTH		DIP		KKTEST		PCM	CMCOS	XI(PHI)	XI(S)	XI(K)
-4	939.5	1	366.6	119.7	24.28	0.13	29.14	0.23	0.		179.9	1.000	0.	0.	0.
5	938.2	2	125.1	1.6	322.43	7.06	-6.70	5.49	0.		179.9	-0.759	0.	0.	0.
31	939.5	3	343.1	126.9	47.00	8.04	34.26	2.61	0.		179.9	0.759	0.	0.	0.

SUMMARY OF A GOOD, FORWARD EVENT HAVING AN ASSOCIATED ELECTRON PAIR.

EXP	ROLL	FRAME	TYPE	PU	MEAS	OPER	MEASURED	PANGED	KICKED	SKELMID	PGM ID	EXP ID	PAGE
4	0502	353 01	54	0	5	0	660421	630829	08/29/1963	000000	A38-00	RECOIL	5
													ORD= 111

CPM	CHI SQ	LC	STP	CUT	DMN	TWO VERTEX FIT.						TARGET1	TARGET2	IH1	IH2	IH3	IH4	IH5	IH6	IH7	IH8
4	10.45	1	5	0	-1							938.2	938.2	0	0	0	0	0	0	0	0
	4.551		0.			0.			0.			0.		0.			0.			0.	
TRK	MASS	LSZ	MOMENTUM			AZIMUTH			DIP			KKTEST		PCM	CMCOS		XI(PHI)		XI(S)	XI(K)	
-18	-139.6	1	1067.0		15.0	102.32	0.13		1.52	0.29		0.		585.9	1.000		-3.23		3.23	-3.23	
5	938.2	2	125.8		2.3	342.36	3.44		1.31	4.97		0.		674.0	-0.987		3.23		3.23	-3.23	
4	939.5	1	191.6		4.0	24.31	0.13		29.12	0.23		0.		585.9	-0.947		3.23		-3.23	0.	
31	939.5	3	143.8		5.7	73.01	1.74		38.93	5.17		0.		486.9	-0.977		0.		0.	0.	
30	135.0	3	1046.8		14.7	111.34	0.18		-3.55	0.24		0.		585.9	0.947		0.		0.	0.	

CPM	CHI SQ	LC	STP	CUT	DMN	TARGET	IH1	IH2	IH3	IH4	IH5	IH6	IH7	IH8
7	0.96	1	3	0	-1	-0.	0	0	0	0	0	0	0	0
	14.044		0.			0.	0.			0.			0.	
TRK	MASS	LSZ	MOMENTUM			AZIMUTH			DIP			KKTEST	PCM	CMCOS	XI(PHI)	XI(S)	XI(K)
12	-0.5	1	377.5		12.2	113.18	0.17		-11.63	0.31		2.44	27.5	0.823	0.98	0.98	0.98
13	0.5	1	553.0		15.9	113.17	0.16		-11.51	0.29		2.34	40.1	0.831	0.98	0.98	0.98
-15	135.0	3	1013.3		12.2	115.17	0.17		-10.30	0.22		0.	0.0	1.000	-0.98	-0.98	-0.98
30	0.	3	91.7		14.5	135.52	2.92		3.28	2.16		0.	67.5	-0.828	0.	0.	0.

CPM	CHI SQ	LC	STP	CUT	DMN	TWO VERTEX FIT.						TARGET1	TARGET2	IH1	IH2	IH3	IH4	IH5	IH6	IH7	IH8
16	0.14	1	4	5	1							-0.	938.2	0	0	0	0	0	0	0	0
	14.861		0.			0.			0.			0.		0.			0.			0.	
TRK	MASS	LSZ	MOMENTUM			AZIMUTH			DIP			KKTEST		PCM	CMCOS		XI(PHI)		XI(S)	XI(K)	
-15	135.0	3	1007.9		13.7	115.28	0.21		-10.26	0.22		0.		0.0	1.000		-217.88		-277.86	-209.14	
12	-0.5	1	379.6		11.2	113.16	0.18		-11.68	0.32		2.44		28.0	0.804		0.		0.20	0.43	
13	0.5	1	558.6		11.2	113.14	0.16		-11.57	0.30		2.34		41.1	0.811		62.71		0.20	0.35	
14	0.	1	938.1		0.2	113.25	0.54		-11.33	2.33		0.		68.0	0.839		220.51		266.01	0.	
31	938.2	3	4.9		36.1	177.15	243.79		67.46	157.99		0.		7002.4	-1.000		0.		0.	0.	
30	0.	3	79.7		15.2	139.42	8.54		3.41	26.68		0.		73.2	-0.863		0.		0.	0.	

CPM	CHI SQ	LC	STP	CUT	DMN	TWO VERTEX FIT.						TARGET1	TARGET2	IH1	IH2	IH3	IH4	IH5	IH6	IH7	IH8
17	7.91	1	7	7	-1							-0.	938.2	0	0	0	0	0	0	0	0
	7.092		0.			0.			0.			0.		0.			0.			0.	
TRK	MASS	LSZ	MOMENTUM			AZIMUTH			DIP			KKTEST		PCM	CMCOS		XI(PHI)		XI(S)	XI(K)	
-15	135.0	3	1048.3		14.7	111.33	0.18		-3.60	0.24		0.		0.0	1.000		-2.95		-2.82	-2.98	
12	-0.5	1	379.8		13.4	113.16	0.18		-11.68	0.32		2.44		55.1	-0.120		-2.91		2.49	2.31	
13	0.5	1	557.9		19.8	113.14	0.16		-11.56	0.30		2.34		79.7	-0.107		-2.76		2.49	2.31	
14	0.	1	943.9		22.3	112.91	0.53		-5.58	0.63		0.		67.7	0.788		-2.80		2.82	0.	
31	938.2	3	99.3		9.4	102.43	33.50		77.63	26.47		0.		7207.8	-1.000		0.		0.	0.	
30	0.	3	113.2		23.5	97.73	5.83		13.28	7.83		0.		69.0	-0.797		0.		0.	0.	

CPM	CHI SQ	LC	STP	CUT	DMN	TARGET	IH1	IH2	IH3	IH4	IH5	IH6	IH7	IH8
28	0.	0	0	0	-1	938.2	0	0	0	0	0	0	0	0
	0.000		0.			0.	0.			0.			0.	
TRK	MASS	LSZ	MOMENTUM			AZIMUTH			DIP			KKTEST	PCM	CMCOS	XI(PHI)	XI(S)	XI(K)
12	-0.5	1	382.8		13.7	113.16	0.18		-11.68	0.32		2.44	220.3	1.000	0.	0.	0.
13	0.5	1	564.5		20.4	113.14	0.16		-11.57	0.30		2.34	324.9	1.000	0.	0.	0.
-14	0.	1	947.3		24.6	113.18	0.54		-12.01	2.32		0.	545.2	1.000	0.	0.	0.
31	938.2	3	6.5		38.4	271.70	362.19		-77.58	29.61		0.	545.2	-1.000	0.	0.	0.

REPORT TYPE 6

-0.38502	-0.91927	-0.08188	0.89916	-0.39363	0.19122	-0.20801	0.	0.97813	0.
0.	0.	0.	0.	382.80709	-0.13986	2.18323	382.81370	564.43895	-0.37295
4.30880	564.45576	947.29395	-0.	0.00000	947.29400	0.04793	0.51282	-6.49201	938.23559
14.89059	-3.28854	98.07848	943.44875	105.25118	-25.90985	32.67032	113.20990	0.	0.
0.	0.	0.	0.	0.	0.	0.	0.	0.	0.
0.	0.	0.	0.	0.	0.	0.	0.	0.	0.
0.	0.	0.	0.	0.	0.	0.	0.	0.	0.

SUMMARY OF A GOOD, FORWARD EVENT HAVING AN ASSOCIATED ELECTRON PAIR.

EXP	ROLL	FRAME	TYPE	PU	MEAS	OPER	MEASURED	PANGED	KICKED	SKELMID	PGM ID	EXP ID	PAGE	6
4	0502	353 02	52	0	0	91	610725	630829	08/29/1963	000000	A38-00	RECOIL	ORD=	112

PANG DATA — MASS INDEPENDENT INFORMATION

TRACK	LSZ	FTN	PHT	VIEWS	POINTS	LENGTH	DL	X(BEG)	Y(BEG)	Z(BEG)	X(END)	Y(END)	Z(END)
1	1	0	0	1 2	12 11	14.03	0.03	-6.01	-87.51	15.22	-9.35	-73.88	15.60
2	1	0	0	2 3	2 2	25.10	0.04	-9.30	-73.77	16.04	10.67	-64.75	28.23
3	2	0	0	2 3	5 5	0.61	0.02	10.66	-64.80	28.03	11.15	-65.16	28.09

MASS DEPENDENT INFORMATION

TRK	MASS	P(BEG)	P(END)	DP/P	P(L)	DPL	KPTEST	PHI(B)	PHI(E)	ERROR	DIP(B)	DIP(E)	ERROR	C/R	S(XY)	S(Z)
1	-139.6	-1145.1	-1141.8	0.08	75.3	0.7		105.43	102.07	0.15	1.23	1.38	0.30	0.3	.0058	.0618
B		1058.8		0.014			-1.08									
2	939.5	1.0	1.0	10.00	1.0	10.0	-0.10	24.31	24.31	0.08	29.09	29.09	0.23	0.	.	.
3	938.2	-102.7	3.0	0.63	123.9	1.3	-1.49	328.42	320.29	7.93	10.12	10.19	5.68	0.2	.0243	.0767

CPM	CHI SQ	LC	STP	CUT	DMN	TARGET	IH1	IH2	IH3	IH4	IH5	IH6	IH7	IH8
1	0.	0	0	0	-1	938.2	0	0	0	0	0	0	0	0

	0.000		0.		0.		0.		0.		0.		0.	
TRK	MASS	LSZ	MOMENTUM		AZIMUTH		DIP		KKTEST	PCM	CMCOS	XI(PHI)	XI(S)	XI(K)
-2	939.5	1	219.8	42.1	24.21	0.13	29.09	0.23	0.	109.1	1.000	0.	0.	0.
3	938.2	2	123.9	1.3	328.41	7.93	10.12	5.68	0.	109.1	-0.358	0.	0.	0.
31	939.5	3	180.8	50.7	63.44	8.60	28.09	4.07	0.	109.1	0.358	0.	0.	0.

CPM	CHI SQ	LC	STP	CUT	DMN	TWO VERTEX FIT.	TARGET1	TARGET2	IH1	IH2	IH3	IH4	IH5	IH6	IH7	IH8
2	0.63	1	3	0	-1		938.2	938.2	0	0	0	0	0	0	0	0

	14.371		0.		0.		0.		0.		0.		0.	
TRK	MASS	LSZ	MOMENTUM		AZIMUTH		DIP		KKTEST	PCM	CMCOS	XI(PHI)	XI(S)	XI(K)
-1B	-139.6	1	1056.1	14.7	102.06	0.15	1.40	0.30	0.	582.0	1.000	-0.79	0.79	-0.79
3	938.2	2	123.9	1.4	334.24	3.00	11.67	5.28	0.	681.1	-0.989	0.79	0.79	0.79
2	939.5	1	192.2	4.2	24.21	0.13	29.09	0.23	0.	581.9	-0.946	0.79	-0.79	0.
31	939.5	3	146.3	5.6	70.13	1.75	27.88	4.93	0.	468.4	-0.979	0.	0.	0.
30	135.0	3	1035.8	14.5	111.20	0.18	-3.75	0.25	0.	581.9	0.946	0.	0.	0.

REPORT TYPE 6

-0.20892	-0.97792	0.00509	0.97763	-0.20898	-0.02384	0.02438	0.	0.99970	0.
0.	0.	0.	0.	1056.08276	0.	-0.00000	1065.27339	-73.74869	-95.81573
26.85873	946.35327	37.61993	-164.19284	92.55315	958.96408	111.36862	-68.37711	65.69441	950.82366
1018.46281	164.19290	-92.55315	1044.52275	0.	0.	0.	0.	0.	0.
0.	0.	0.	0.	0.	0.	0.	0.	0.	0.
0.	0.	0.	0.	0.	0.	0.	0.	0.	0.
0.	0.	0.	0.	0.	0.	0.	0.	0.	0.
0.	0.	22.00000	22.00000	22.00000	22.00000	22.00000	22.00000	22.00000	22.00000
22.00000	22.00000	0.	0.	0.	0.	0.	0.	0.	0.
0.	0.	0.	0.	0.	0.	0.	0.	0.	0.
0.	0.	0.	0.	0.	0.	0.	0.	0.	0.
0.	0.	0.	0.	0.	0.	0.	0.	0.	0.
0.	0.	0.	0.	0.	0.	0.	0.	0.	0.
0.	0.	0.	0.	0.	0.	0.	0.	0.	0.

particle that is assumed to have taken part in a reaction that is being fitted.

We illustrate these types of tracks in the lines in the third block of the figure beneath the device CPM I. As we discuss in the section describing the kinematics fits in detail, the fit in CPM I is of the reaction $n+p \rightarrow n+p$. Track 2 (the neutron, whose index is negative because it is incident on the vertex) hits a proton target. Track 2 is a measured, non-stopping track, whose LSZ is, therefore, equal to one. One assumes that the proton stops (track 3, LSZ = 2), and the final-state neutron is unmeasured (track 31, LSZ = 3). Notice (in the section containing Mass-Dependent Information) that the dip of the measured proton (at its beginning) with respect to the plane of the top glass is less than 60 deg. (Its dip in the chamber is 25.05 deg, and the top glass dips at 7.5 deg with respect to the chamber coordinate system). Notice, too, that the error in the dip of the proton is less than 2.5 deg (=0.29 deg), and that its projection on the plane of the top glass exceeds 0.7 cm. (The length of the proton equals 6.75 cm and its dip with respect to the top glass cannot be more than 32.55 deg). These are the three criteria applied to every acceptable event. The bias introduced by the steepness and projection criteria are calculated and rectified in Appendix K. The bias due to the dip-error cutoff is treated in Appendix F.

The fit of the tracks, without the electron tracks of the converted γ ray, to the hypothesis is done in Check-Point Mark (CPM) 2 and gives a χ^2 value of 0.21, a very good fit. Further, the π^0 is emitted at an angle in the c.m. whose cosine is 0.861, which makes it a forward event. In CPM (7;8) the π^0 fit in CPM 2 is used to fit the hypothesis that the π^0 decayed into ($\cdot\cdot$ $e^+ + e^- + \gamma$ via Dalitz decay; $\cdot\cdot$ $\gamma+\gamma$ followed by conversion $\gamma + p \rightarrow e^+ + e^- + p$). We know that the former reaction did not occur because we can see a substantial gap between the zero-prong and the electron pair. The hypothesis is fitted--as we can see--by comparison with CPM 16, because the momenta assigned to the various tracks differ from the true values by an amount not large compared with the errors in their determination.

It is important to remember that we are nearly positive that the electron pair is associated with the zero-prong. The fitting of the electron pair really is done to verify that the recoil is also associated with the zero-prong, and that through the elastic charge-exchange reaction. The accidental fit of the electron pair to that false hypothesis indicates that first, the true and false hypotheses are not far apart kinematically, and second, the recoil

has kinematic parameters approximately consistent with the hypothesis of elastic charge exchange.

In CPM 16, the conversion process is fitted with a χ^2 of 3.16, about as well as 5 to 10% of good events of 1-c class would ideally fit. Note that the two decay γ rays had widely differing laboratory momenta, 973.0±21.9 MeV/c for the γ that converted, and 43.3±25.8 for the "other" γ. Suppressing the information that the "conversion" γ came from a π^0 decay, we fitted, in CPM 28, the conversion process itself. Comparison of momentum values from this fit with those in CPM 16 gives the distortion introduced by the fitting process to achieve energy-momentum conservation. The small distortion required explains the low χ^2 value.

Turning to the spurious recoil S, we see that it fits the hypothesis with $\chi^2 = 0.58$ and involves a π^0 emitted forward ($\cos\theta^{c.m.} = 0.946$). This would be a spurious fit if it were not for two factors. First, the error in its measured dip is larger than can be permitted (5.68 deg) and second, a subsequent remeasurement with the electron pair included shows that it is recoil R and not recoil S that is associated with the zero-prong. On the remeasurement, recoil S fitted the hypothesis with a χ^2 of 10.19 and the conversion with a χ^2 of 8.05. This, relative to the weaker restrictions placed on it by its large dip error, must be compared with the strongly restricted fits of recoil R that gave χ^2 values of 1.60 and 0.212. The table below summarizes these results and gives the appropriate confidence levels (CL) for each χ^2 value.

Recoil	Measurement	χ^2 recoil	CL	χ^2 conversion	CL	Proton dip error	$\cos\theta^{c.m.}$
R	1	0.21	0.65	3.16	0.08	0.73	0.861
	2	1.60	0.21	0.212	0.65	0.71	0.860
S	1	0.58	0.45	--	--	5.68	0.946
	2	10.19	0.0005	8.05	0.005	5.49	0.947

The confidence level quoted for a measurement of an event is the fraction of good events (based on an ideal distribution of 1-c fits) that would have χ^2 values greater than that given for the event.

The table above is consistent with the statements made in Appendix N as to the reliability of single measurements of the $\cos\theta^{c.m.}$ and dip error, and as to the relative variability of the values of χ^2 achieved.

E. A Boolean Algebraic Method of Analysis Applied to the Problem of Discovering the Essential Physical Combinations of Variables

We discuss, in this section, a method that can be applied whenever we are given a distribution of N events and a set of M binary criteria, such that each event lies in one of the two classes determined by each criterion. Further, we must have enough information to decide, for each event, relative to each criterion, to which class the event actually belongs. With such a set of events, criteria, and information, we can decompose the N events into families that partition the original N events as economically as possible. We will discuss the meaning of the word "economical" and some of the characteristics of the partition after we illustrate the method by applying it to our experiment.

In our case, we have N=212 events that have given fits with $\chi^2 < 15.0$ to our hypothesis and occurred in the twice-scanned frames on valid beam tracks. These events contain all those of any possible interest in the experiment. We expect a fraction of background in this sample, and we are not interested in events for which the π^0 is emitted relative to the beam at an angle in the center of mass whose cosine is less than 0.7. Further, we have discovered difficulties with events that project too short a length (less than 0.7 cm) on the top glass, with events that rise too steeply (60 deg or more) relative to the top glass irrespective of length, and with events whose dip error is too large > 2.5 deg).

To the four binary criteria mentioned, we add three more. The value of χ^2 for the fit of the entire event to our hypothesis must not exceed 2.706 (the 90% probability limit); the computed missing mass must differ from its ideal value M_{π^0} by no more than 1.65× the error in the missing mass, δ MM. Further, δ MM itself must not exceed 16.0 MeV/c^2.

The eighth and last criterion is simply that the measured curvatures of the proton recoil be positive.

The M(=8) binary criteria we have adopted may be tagged by the eight single phrases (forward, χ^2, dip error, projected length, dip,

missing mass, missing-mass error, curvature).

Let us define M(=8) variables X, each of which may take either of the two values (0, 1). These two values shall distinguish the two classes defined by the ith binary criterion. The table below gives the value prescribed for each X:

i	X_i relates to the phrase	X_i	= (0 , 1) if
0	Forward	$\cos\theta_{\pi^0}^{c.m.}$	is ($\geq$, $<$) 0.7
1	Chi square (χ^2)	χ^2	is ($\leq$, $>$) 2.706
2	Dip error ($\delta\lambda$)	$\delta\lambda$	is ($\leq$, $>$) 2.5 deg
3	Projected length (L_p)	L_p	is ($\geq$, $<$) 0.7 cm
4	Dip [relative to top glass] (λ)	$\lvert\lambda\rvert$	is ($\leq$, $>$) 60 deg
5	Missing mass error (δMM)	δMM	is ($\leq$, $>$) 16.0 MeV/c^2
6	Relative deviation of the missing mass [RD = MM-M (π^0)/ δMM]	RD	is ($\leq$, $\geq$) 1.65
7	Curvature (K)	K	is ($\geq$, $<$) 0 c/MeV

For example suppose an event with

$$\cos\theta_{\pi^0}^{c.m.} = 0.87;\ \chi^2 = 7.53;\ \delta\lambda = 1.17 \text{ deg};$$

$$L_p = 2.6 \text{ cm};\ \lambda = 54.7 \text{ deg};\ MM = 145.3 \text{ MeV}/c^2;\ \delta MM = 66.7 \text{ MeV}/c^2$$

and hence RD = 0.15; curvature, negative.

Its criterial variables, X_i, would have the following values:

$$X_0 = 0;\ X_1 = 1;\ X_2 = 0;\ X_3 = 0;\ X_4 = 0;$$
$$X_5 = 0;\ X_6 = 1,\ X_7 = 1.$$

We can condense this information into the single expression:

$\bar{X}_7\ \bar{X}_6\ X_5\ X_4\ X_3\ X_2\ \bar{X}_1\ X_0$; where a bar over X_i means $X_i = 1$ and the absence of the bar signifies $X_i = 0$. Writing these (0,1) values in the same order without the variables gives 11000010, which we can always interpret as a binary number, $(11000010)_2$ and condense by writing its decimal equivalent, $0 \times 2^0 + 1 \times 2^1 + 0 \times 2^2 + 0 \times 2^3 + 0 \times 2^4 + 0 \times 2^5 + 1 \times 2^6 + 1 \times 2^7 = (194)_{10}$. The signature for this event, then, is 194. The numerical signature for an arbitrary event having the value X_i for its ith criterial variable is simply $\sum_i X_i 2^i$.

Having established a unique numerical signature for each event, we then simply plot a histogram of the signatures of all the interesting events. (We may call these signatures "Boolean" signatures because they are based on binary or "Boolean" variables.)

Thus far we have done no Boolean algebra and no physics apart from choosing the criteria. We have only created a convenient number that characterizes each event relative to the criteria and plotted that number in a histogram of all of our events (Fig. 6). The next step is the only nonmechanical one in our procedure. We examine the histogram and extract a subset containing those intervals that we choose to consider to have similar populations. In our own case, we choose to consider that all histogram intervals having more than two events have similar populations, as do all those having two or fewer events. The division is not unreasonable when one considers that intervals with two or fewer events have populations nearly consistent with zero under Poisson statistics. If no such convenient division presented itself, we could try several and examine the results separately.

With this division, we have a set of signatures that have relatively many events and a set having relatively few events. The former class is the class of "events that occur often in our experiment," and the latter, its complementary class, the class of "events that do not abound in our experiment."

The procedure we shall follow, by using an approach initiated by Quine, will characterize either of these two classes economically with respect to our basic criteria.[12 to 18] A full discussion of the procedure, including references to the literature, is given in an earlier paper.[17] It also contains a description of the IBM 7090 program SALOME that exhibits all minimal coverings of an arbitrary Boolean truth function. In particular, SALOME performs the kind of calculations we are to perform below.

Without discussing the reduction procedure in detail, we give a simplified example to illustrate the method. Suppose that the following signatures were the only popular ones, S = (16, 17, 18, 20, 21, 22), and we wish to express this set in as economical a logical form as possible. Assume we have 8 variables X_0 through X_7. We express the fact that S includes the given signatures by S = (16) + (17) + (18) + (20) + (21) + (22):

$$(16) = X_7\, X_6\, X_5\, \overline{X}_4\, X_3\, X_2\, X_1\, X_0,$$
$$(17) = X_7\, X_6\, X_5\, \overline{X}_4\, X_3\, X_2\, X_1\, \overline{X}_0,$$
$$(18) = X_7\, X_6\, X_5\, \overline{X}_4\, X_3\, X_2\, \overline{X}_1\, X_0,$$
$$(20) = X_7\, X_6\, X_5\, \overline{X}_4\, X_3\, \overline{X}_2\, X_1\, X_0,$$
$$(21) = X_7\, X_6\, X_5\, \overline{X}_4\, X_3\, \overline{X}_2\, X_1\, \overline{X}_0,$$
$$(22) = X_7\, X_6\, X_5\, \overline{X}_4\, X_3\, \overline{X}_2\, \overline{X}_1\, X_0.$$

We notice immediately that $X_7\, X_6\, X_5\, \overline{X}_4\, X_3$ appears in each listed signature and that the only variables that do not remain fixed are $X_2\, X_1\, X_0$. Stated differently, our interesting signatures share the same values for variables X_3 through X_7, and we can therefore express S (the set of interesting signatures) as

$$S = X_7\, X_6\, X_5\, \overline{X}_4\, X_3\, (X_2\, X_1\, X_0 + X_2\, X_1\, \overline{X}_0 + X_2\, \overline{X}_1\, X_0 + \overline{X}_2\, X_1\, X_0 + \overline{X}_2\, X_1\, \overline{X}_0 + \overline{X}_2\, \overline{X}_1\, X_0),$$

where we have simply "factored out" the constant expression $X_7 X_6 X_5 \overline{X}_4 X_3$ from the sum $S = (16) + (17) + (18) + (20) + (21) + (22)$, which represents the set of signatures. [It is clear, of course, that we are performing these operations in a strange (Boolean) algebra, one that needs justification and further discussion. This outline is meant to make familiar the kind of notion that is involved. The references provide the substance.] We now work only with the parenthetic expression,

$$P = X_2 X_1 X_0 + X_2 X_1 \overline{X}_0 + X_2 \overline{X}_1 X_0 + \overline{X}_2 X_1 X_0 + \overline{X}_2 X_1 \overline{X}_0 + \overline{X}_2 \overline{X}_1 X_0 .$$

We now need two theorems that hold in this algebra, $X + \overline{X} = 1$ and $X + X = X$. The first theorem may be understood, as follows: Given any statement X and its complement $\overline{X}$ ($\overline{X} = 0$ if $X = 1$ and $X = 1$ if $\overline{X} = 0$), then at least one of them has the value 1. (In another context, "$\underline{X}$ is true, or <u>not X</u> is true.")

The second theorem states that any statement, when added to itself, gives itself "X or X = X". The latter permits us to duplicate terms in a sum without changing the value of the sum, and we do so now:

$$P = X_2 X_1 X_0 + X_2 \overline{X}_1 X_0 + \overline{X}_2 X_1 X_0 + \overline{X}_2 \overline{X}_1 X_0 + X_2 X_1 X_0 + X_2 X_1 \overline{X}_0 + \overline{X}_2 X_1 X_0 + \overline{X}_2 X_1 \overline{X}_0,$$

where the terms $X_2 X_1 X_0$ and $\overline{X}_2 X_1 X_0$ are duplicated. We "factor" P:

$$P = (X_2 X_1 + X_2 \overline{X}_1 + \overline{X}_2 X_1 + \overline{X}_2 \overline{X}_1) X_0 + (X_2 X_0 + X_2 \overline{X}_0 + \overline{X}_2 X_0 + \overline{X}_2 \overline{X}_0) X_1 ;$$

$$P = P_0 X_0 + P_1 X_1 ,$$

where

$$P_0 = X_2 X_1 + X_2 \overline{X}_1 + \overline{X}_2 X_1 + \overline{X}_2 \overline{X}_1 = X_2 (X_1 + \overline{X}_1) + \overline{X}_2 (X_1 + \overline{X}_1) = (X_2 + \overline{X}_2) (X_1 + \overline{X}_1),$$

and

$$P_1 = X_2 X_0 + X_2 \overline{X}_0 + \overline{X}_2 X_0 + \overline{X}_2 \overline{X}_0 = X_2(X_0 + \overline{X}_0) + \overline{X}_2(X_0 + \overline{X}_0) = (X_2 + \overline{X}_2) (X_0 + \overline{X}_0).$$

Thus, $P = P_0 X_0 + P_1 X_1 = (X_2 + \overline{X}_2) (X_1 + \overline{X}_1) X_0 + (X_2 + \overline{X}_2) (X_0 + \overline{X}_0) X_1 1$

By using Theorem 1, it follows that $X_2 + \overline{X}_2 = \overline{X}_1 + X_1 = X_0 + \overline{X}_0 = 1$;

$$P = X_0 + X_1 ,$$

and thus

$$\begin{aligned} S &= X_7 X_6 X_5 \overline{X}_4 X_3 (X_0 + X_1) = C(X_0 + X_1) \\ &= X_7 X_6 X_5 \overline{X}_4 X_3 X_0 + X_7 X_6 X_5 \overline{X}_4 X_3 X_1 \\ &= \qquad A \qquad + \qquad B . \end{aligned}$$

Thus we started with an expression for S that had six terms of eight factors each, and we end with an expression with two terms of six factors each. In fact, the expression we have is the most economical possible--although we don't prove this--in the form of a single sum of products of simple factors. Roughly speaking, economy is measured by the number of simple factors, where these are counted each time they appear. Our original expression had $6 \times 8 = 48$, and our final expression, $2 \times 6 = 12$. We could also express $S = A + X_7 X_6 X_5 \overline{X}_4 X_3 X_1 \overline{X}_0 = A + B'$, which we can show to be true, as follows:

$$S = A + B = C (X_0 + X_1) .$$

Now there is another theorem in this algebra, which states that $1 + X = 1$ (and incidentally $0 + X = X$). Therefore, $X_0 = X_0 (1 + X_1) = X_0 + X_0 + X_1$.

$$S = C (X_0 + X_0 X_1 + X_1) ,$$

but

$$X_0 X_1 + X_1 = X_1 (1 + X_0) = X_1$$

and

$$X_0 X_1 + \overline{X}_0 X_1 = (X_0 + \overline{X}_0) X_1 = X_1 ;$$

hence,

$$X_0 X_1 + X_1 = X_0 X_1 + \overline{X}_0 X_1 = X_1$$

and

$$\begin{aligned} A + B' &= C(X_0 + \overline{X}_0 X_1) = C(X_0 + X_0 X_1 + \overline{X}_0 X_1) \\ &= C(X_0 + X_1) = S . \qquad \text{QED} \end{aligned}$$

The above shows that $A + B'$ is also a covering of S, but since B' contains seven factors instead of the six contained in B, it is a less economical covering of S.

We now proceed to interpret the result $S = A + B$. By techniques like the one above, we can show that $A = (16) + (18) + (20) + (22)$; $B = (16) + (17) + (20) + (21)$. This makes clear why $S = A + B$, and it shows

that we have only separated S into subsets A and B. The signatures of each set agree precisely among themselves in a certain number of factors, and all possible configurations of the other factors are represented. In the case of B, the signatures all agree in arguments 1, 3, 4, 5, 6, and 7, and the four possible configurations of the other two arguments with these six arguments fixed make up the set of four signatures in B.

To advance the argument another step, we can say that we have discovered a set of signatures characterized by agreement in six variables and indifference to two variables. Further, we can say that there is no set that contains B and is indifferent to a larger number of variables. For example, B' = (17) + (21) used above, is obviously a subset of B whose elements are indifferent to only one variable. Hence, using B' in B's stead eliminates fewer redundant variables.

In general, then, our procedure insures the elimination of the largest possible number of redundant variables and leaves the relations holding among the remaining variables as clearly visible as possible. We now proceed to apply the technique to the actual experimental data.

The first set we wish to reduce is the set of all signatures having more than two representatives among all events with positive curvature ($X_7 = 0$). (We are reducing the signatures below 128.) That set is S = (0, 32, 33, 44, 66, 78, 97, 98, 99, 100, 101, 102, 103, 108, 109, 110, 111, 113, 115, 121). Following the calculational procedure given in UCRL-9227 (which is equivalent but not identical to the theoretical procedure sketched above), we may express S as follows:

$$\begin{aligned} S = {} & (0, 32) + (44, 108) + (66, 98) + (78, 110) \\ & + (100, 101, 102, 103, 108, 109, 110, 111) + (97, 99, 113, 115) \\ & + (121, 113) + ((33)) . \end{aligned}$$

The above decomposition of S is the most economical (or minimal) of the set S without the signature 33. It is also the <u>unique</u> minimal covering of that set. For a general set S, there is not a unique minimal covering, but there is a subportion that has a unique minimal covering. In the case above the subportion with a unique minimal covering is all of S except (33). The last signature must be covered separately and will, in general, have more than one possible covering. For the moment we ignore this complication and deal with the "set S with (33) removed" = S'.

$$S' = (0, 32) + (44, 108) + (66, 98) + (78, 110) + (100, 101, 102, 103, 108, 109, 110, 111) + (97, 99, 113, 115) + (121, 113),$$

where each set in parentheses contains 2^r signatures that agree in M-r factors. The set is itself indifferent to the variation of the remaining r factors through all possible values (that is, all possible combinations of the remaining r arguments lie inside the set). Further, there are no such sets of higher r that contain any of the sets above.

We now analyze this decomposition and interpret the meaning of each set:

$(0, 32) = X_6\ X_4\ X_3\ X_2\ X_1\ X_0$ (notice that X_5 is missing; $r = 1$, and there are $2^r = 2$ signatures in the set).

This is the set of signatures of all events having forward π^0's, low χ^2, low dip error, long profile, recoils with flat trajectories, and missing masses consistent with $M(\pi^0)$ to 1.65 $\times$ its error. The absence of X_5 means that with these attributes, the events were indifferent to the magnitude of the error in missing-mass determination.

This is the most important set of all because it contains all our "good" events. The presence of events having high missing-mass error implies that we are actually throwing out good events by rejecting such events. Because such events lie in the same logical class after reduction, we assume their physical source to be the same as that of the "good" events. We reject "high missing-mass error" events because they are easily simulated by background, and we have corrected for their loss.

There are 11 "good" and 4 "high missing-mass error" events in our sample. Of the latter, a fraction estimated elsewhere is likely to be spurious.

The most important point to note is the complete absence of any other events in the class containing our best ones. This means that the physics of the good events of our experiment is not indifferent to the variation of any parameters by missing-mass error. When other single properties are varied, we get unphysical combinations that are not represented by events in our sample. What we seek to do, of course, is to make a logical distinction between good and spurious events, and that is what we seem to have done.

There are two points to consider very carefully in this regard. First, the assemblage of properties we use to identify good events must really correlate with goodness. Second, the different properties must not be too strongly correlated, or a spurious logical distance will be introduced by the variation of a single parameter. Such correlations can be detected in other parts of the reduction, however, and offset by appropriate measures. We therefore continue the analysis.

The second group (44, 108) = $\overline{X}_5 X_4 \overline{X}_3 \overline{X}_2 X_1 X_0$ has X_6 as a redundant variable [relative deviation of missing mass from $M(\pi^0)$] . This group has 12 events in it.

For the group (66, 98) = $\overline{X}_6 X_4 X_3 X_2 \overline{X}_1 X_0$ we find argument 5 redundant (mass error). In this group, all criteria are satisfied except the X_1 (χ^2) and X_6 (relative-mass-deviation) criteria, irrespective of mass error. These events are not background (they do not have low χ^2 nor appropriate missing masses); they are simply a class of rejects. The existence of this class implies a correlation between the χ^2 value and missing-mass consistency, which we must examine more carefully later. There are 15 events having these signatures. The class containing signatures (78, 110) is again invariant under the changing of X_5 (missing-mass error). The expression for the class $\overline{X}_6 X_4 \overline{X}_3 \overline{X}_2 \overline{X}_1 X_0$ implies that it is only in flatness (X_4) and forwardness (X_0) that these events resemble good ones. They constitute a set of eight unambiguous reject events.

The next set (100, 101, 102, 103, 108, 109, 110, 111) = $\overline{X}_6 \overline{X}_5 X_4 X_2$ contains 56 events that are indifferent to variations in these variables (X_0: forwardness X_1: χ^2; and X_3: projection). They have low dip errors, flat recoils, and inconsistent masses with high errors. The last two attributes mark them as invalid events. The existence of such a large reject class of events that is not correlated with high χ^2 shows the desirability of using missing mass and its error instead of χ^2 to distinguish valid from invalid events, where one might have thought the two standards would give similar results; their distinction for this experiment is clearly exhibited by the behavior of the logical distribution of our events.

Another relatively large set is (97, 99, 113, 115) = $\overline{X}_6 \overline{X}_5 X_3 X_2 \overline{X}_0$, which contains only nonforward events with high missing-mass deviation and error, low dip error, and flat recoils. There were 50 such events.

The last set in S' is (113, 121) = $\overline{X}_6\ \overline{X}_5\ \overline{X}_4\ X_2\ X_1\ \overline{X}_0$, which also consists of nonforward events with inconsistent masses and high errors. In this case, the events are "steep," have good χ^2 values and low dip errors. They are indifferent to projection. These too are rejects. Here, high mass inconsistency and error are coupled with low χ^2, which shows at least some anomaly in χ^2 behavior (we would expect only events with consistent missing masses to give low χ^2 values). There were seven events of this type.

The possible coverings of signature (33) are (33, 97) = $\overline{X}_5\ X_4\ X_3\ X_2\ \overline{X}_1\ X_0$ (19 nonforward, high mass-error events), or (32, 33) = $X_6\ \overline{X}_5\ X_4\ X_3\ X_2\ X_1$ (11 high mass-error events, neither forward nor nonforward). They both have the properties $X_5\ X_4\ X_3\ X_2\ X_1$ (high mass error, flat recoil, long projection, and low χ^2) and so might be accepted if not for our stringency requirement of low mass error.

Table IV summarizes the decomposition of S = "the set of signatures with more than two representatives." Because the class we believe to contain the real events is logically isolated with respect to the criteria chosen, we can believe the number we quote as the number of real events. All rejected events fail to satisfy at least two of our criteria. It is convenient that rejected events exhibit a syndrome instead of only a single pathology, because this makes it easier to enforce their quarantine. Our logical technique facilities the diagnosis of such syndromes and, hence, the reliable segregation of the invalid from the valid.

To make our procedure clearer, we discuss briefly an analogous procedure in the nonBoolean realm. Suppose we wish to examine a well-behaved function $f(x_1, x_2, \cdots, x_M)$ in a given neighborhood. Suppose, too, that its partial derivative with respect to x_1 is small. We could approximate f in that neighborhood by $f(c_1, x_2, \cdots, x_M) = g_1(x_2, x_3, \cdots, x_M)$, where c_1 is an appropriate fixed value that we substitute for x_1. If the partial derivative of f with respect to x_2 were small, we could approximate f by $f(x_1, c_2, x_3, \cdots, x_M) = g_2(x_1, x_3, x_4, \cdots, x_M)$. We conclude that if any one partial derivative is small, we can approximate f, originally a function of M variables, by a function of M-1 variables and one fixed parameter.

Suppose, now, that the partial derivatives with respect to x_1 and x_2 separately were small. We could then approximate f well by a function of M-2 variables and two fixed parameters, provided the cross derivative with

Table IV. Summary of Boolean analysis of fitted events.

Class	Representation	Number of events	$\frac{MM-M(\pi^{\bullet})}{\delta MM}$	δMM	Dip of recoil	Projection of recoil	Dip error of recoil	χ^2	Forward π^0 ?
(0, 32)	X_6 () X_4 X_3 X_2 X_1 X_0	15	low	-	flat	long	low	low	yes
(44, 108)	() $\overline{X}_5 X_4$ X_3 $\overline{X}_2$ X_1 X_0	12	-	high	flat	long	high	low	yes
(66, 98)	$\overline{X}_6$ () X_4 X_3 X_2 $\overline{X}_1$ X_0	15	high	-	flat	long	low	high	yes
(78, 110)	$\overline{X}_6$ () X_4 $\overline{X}_3$ $\overline{X}_2$ $\overline{X}_1$ X_0	8	high	-	flat	short	high	high	yes
(100, 101, 102, 103, 108, 109, 110, 111)	$\overline{X}_6$ $\overline{X}_5 X_4$ () X_2 () ()	56	high	high	flat	-	low	-	-
(97, 99, 113, 115)	$\overline{X}_6$ $\overline{X}_5$() X_3 X_2 () $\overline{X}_0$	50	high	high	-	long	low	-	no
(113, 121)	$\overline{X}_6$ $\overline{X}_5 \overline{X}_4$ () X_2 X_1 $\overline{X}_0$	7	high	high	steep	-	low	low	no

respect to x_1 and x_2 was also small. More generally, we could approximate f by a function of M-r variables and r fixed parameters, if for r of the M variables X_i the partial derivative of f with respect to X_i were small, and if any cross derivative with respect to any subset of the r variables (differentiating with respect to each variable no more than once) were also small. Thus, there are $2^r - 1$ partial derivatives that must be small to remove r variables from f. If the r first partial derivatives vanish, but not all the cross derivatives do, it may be possible to find some subset of the r variables for which all the cross derivatives to vanish. Further, we may be able to find a set of such subsets, such that each of the r variables will appear in at least one of the subsets. Then we could write $f(x_1, x_2, \cdots, x_M) = \sum_i g_i$, where each g_i is a function of less than M variables, and where each of the r variables whose first partial derivatives vanish is missing from at least one of the g's. If we were to write such a decomposition of f, we would want the one that employed the fewest g's, and g's that had as few remaining variables as possible. We could call such a decomposition of f into as few g_i's that have as few variables as possible a minimal decomposition. The essential object of the procedure is the search for sets of redundant variables in $f(x_1, x_2, \cdots, x_M)$, such that all possible combinations of them in cross derivatives give small results. In the Boolean case, we seek subsets of the M variables, such that all possible permutations of them generate signatures that are within the set of signatures we are reducing. To strengthen the analogy, we can define a Boolean function $f(x_1, x_2, \cdots, x_M) = (0, 1)$, according as the signature corresponding to $(x_1, x_2, \cdots, x_M)$ (is not, is) on the list of signatures to be reduced. We can continue and define a Boolean "derivative"

$$\partial/\partial x_i : f(x_1, x_2, \cdots, x_M) = (-1)^{x_i} [f(x_1, \cdots, x_{i+1}, 1, x_{i+1}, \cdots, x_M)$$

$$- f(x_1, \cdots, x_{i-1}, 0, x_{i+1}, \cdots, x_M)] .$$

This Boolean "derivative" evaluated in a neighborhood will be $(0, \pm 1)$ for a function that is (unchanged, changed) by a variation in x_i, where the other arguments are fixed.

We can also think of Boolean "partial derivatives"

$$\partial/\partial x_i \, \sigma x_j : f(x_1, x_2, \cdots, x_M) = (-1)^{x_i + x_j} [f(x_1, \cdots, x_{i-1}, 1, x_{i+1}, \cdots, x_{j+1}, \cdots x_M)$$

$$- f(x_1, \cdots, x_{i-1}, 0, x_{i+1}, x_{j-1}, 0, x_{j+1}, \cdots, x_M)] .$$

(Such Boolean "derivatives" are, of course, simple differences that we call "derivatives" to exhibit the formal analogy with those of ordinary calculus.)

Thus, a Boolean function $f(x_1, x_2, \cdots, x_M)$ is indifferent, in a neighborhood, to the variation of a subset of r of the M variables, if, in that neighborhood, all the $2^r - 1$ possible first-order cross "Boolean derivatives" vanish.

Just as in the case of ordinary calculus, the vanishing of the set of cross derivatives enables us to simplify the function. Our procedure, in the Boolean realm, simplifies the function as much as possible.

In many cases, the resulting most economical simplification--when interpreted properly--gives interesting information about the function f. In the case of our Boolean distributions, this knowledge can be translated into knowledge of the physics underlying the distribution that might be tedious to extract by other means.

F. Estimation of Background Due to Spurious Short Proton Tracks. The Use of the FAKE Program to Generate Events in the Laboratory System.

The unit of raw material on which this experiment depends is a charge-exchanging π^- beam track and a short proton track near it, but not connected to it. From among such combinations, we must extract those that are associated with the series of reactions

$$\underline{\pi^-} + p \rightarrow \pi^0 + n, \text{ then } n + p \rightarrow n + \underline{p} ,$$

where the last-named proton has a visible projection in the stereo views, and where the π^0 is emitted at an angle relative to the incident π^-, whose cosine is 0.7 or greater in the center-of-mass system. (The particles underlined are those giving the visible tracks.) There are, however, many spurious, short proton tracks everywhere inside the chamber caused by a "rain" of neutrons arising directly from the Bevatron, and not from secondary

reactions of our beam. This rain seems to depend primarily on the total Bevatron current and not on the number of tracks led into the bubble chamber. For this reason, our experiment used mainly film exposed on the least rainy days (i. e., when the Bevatron was not being shared with another experiment and, hence, was running at a low current.)

We must know how many of the protons originating from rain and lying near enough to a zero-prong to be written down by a scanner might be mistaken for protons arising from the reactions that interest us. We are asking, in other words, "What fraction of our final sample of events is accidentally derived from rain, and what fraction is derived from the sequence of reactions listed above?"

The only difference between the spurious protons and the charge-exchange protons is their source; the spurious protons arise from high-energy neutrons coming directly from the Bevatron (these may be scattered, however, before causing the spurious proton) and the charge-exchange protons, from secondary, low-energy neutrons. This distinction of energy suggests a way to discriminate against the former, so as to reduce the noise fraction we are trying to estimate. In Appendices J and K we discuss the dependence of detectability of a neutron on its slope and momentum. Among the steeply rising, the fast neutrons are much more likely to give visible recoils than are the slow ones. Further, the faster neutrons would tend to give longer recoils. If we restrict our sample to shallow protons (i. e., protons that dip less than 60 deg and more than -60 deg), we are reducing the fraction of rain-produced recoils. This is in addition to insisting that the projection of the proton exceed a certain length. The biases introduced by these restrictions are discussed in Appendix K.

We now restate our rain-estimation problem more fully. We are given a sample of zero-prongs with neighboring recoils, each of which satisfies all of the following criteria:

(i) The beam track entered the chamber through the approved part of the window and had a dip and azimuth within approved limits.

(ii) The roll and frame were of good quality for scanning; the frame was scanned twice and had fewer than a fixed maximum number of tracks.

(iii) The recoil was clearly visible and projected a length greater than a prescribed minimum in the two stereo views.

(iv) The initial point of the recoil lay downstream relative to the zero-prong, and in such a situation that it could not be concluded on the scanning table that the neutron scattered by an angle less than 60 deg with respect to the beam direction in the Laboratory system.

(v) The recoil did not point backward relative to the direction of the putative neutron.

(vi) The recoil dipped by more than -60 deg and less than 60 deg in the chamber, relative to the plane of the top glass.

(vii) The zero-prong-recoil combination fitted the hypothesis that they arose from the exchange-scattering sequence of reactions with a χ^2 value less than 2.706, and the π^0 was emitted at an angle in the c.m. whose cosine exceeded 0.7.

What fraction of this sample arose from interactions of stray rain neutrons?

We estimate this fraction first, by generating a large unbiased sample of combinations of real zero-prongs and rain-produced recoils that satisfy conditions i through vi above. Then we find the fraction of these that satisfy Condition vii and assume that the same fraction of rain contaminated our real experiment. This generation is by a Monte Carlo method involving the FAKE FORTRAN computer program.[11]

The general method is, as follows: We assume that the set of events satisfying conditions i through vi, but not vii, forms a pure background sample. We treat it as rain. If we leave the recoil of each such event unchanged, but generate a new beam track for each event (using the known beam distribution to achieve this without bias), we can attain an unbiased sample of events. To assure the satisfaction of condition vi, we create a new "faked" event that has the same distance downstream from the zero-prong to the initial point of the recoil as does the original event. In addition, we impose the condition that the putative neutron make an angle exceeding 60 deg in the laboratory system with the direction of the beam track. We assume the beam to point everywhere along the long axis of the chamber (an approximation), and then we need only translate our old beam track in the x direction to achieve a new unbiased event, all azimuths remaining fixed. The new x position is chosen by a Monte Carlo method by using the FORTRAN RANF random-number generator. (It employs the power-root method to

generate a random-number table having a period of 2^{33}.) The value of x is chosen for the faked event as it enters the chamber according to the known beam distribution there. The x coordinate at entry of the real beam track is then calculated, and the difference between these is the amount by which the real track is to be rigidly translated in the x direction. All the coordinates and momenta are preserved for the recoil, and only the x coordinate is changed for the beam track. The connecting neutron, however, is not the same at all. It must be constructed from the other two, and appropriate momenta supplied. When this is done, the FAKE main program transforms the information into a mock event record on magnetic tape that can be analyzed by the fitting program PACKAGE, just as the original data were analyzed. See Table V.

In short, we take the coordinates and momenta of the measured tracks derived from the analysis of our measured events, move the beam track in the x direction a suitable randomly generated distance, and then reconstruct a new event from it, using the unmoved recoil. The new events so generated are then run through the analysis programs again, and the fraction that fit gives the estimate of the fraction of background in our original sample.

In order to get a more reliable estimate of this background fraction, we ran several times through our set of original events, using each event of the original sample as the basis for generating ten new events, and using in each case a different part of the random-number table. This reduces by a factor of $(10)^{1/2}$ the uncertainty in the estimate of the background fraction.

This use of the FAKE program differs from the usual one in that our simulated events are manufactured according to a prescription specified in the laboratory system in terms of position coordinates, lengths, and angles. Usually, the prescription is given in the center-of-mass system in terms of angular distributions, cross sections, and similar physical parameters. This was achieved by a modification of FAKE that caused the main program to enter, for each track of each vertex, a subroutine, UMU, which had access to all the track areas. Within this subroutine, we generated the appropriate simulated tracks in three steps. First we read, when generating the first track of each event, a binary record containing--among other things--the PANG information relating to an original unfaked event. This binary record is read from a data-summary tape produced by our EXAMIN-type

Table V. Quantities used by FAKE program to simulate a track.

Quantity used	Dimension	Location in FAKE track bank	Prescribed for tracks	
			Beam	Nonbeam
Length	(cm)	3	Yes	
Curvature	(c/MeV)	5	Yes	
Curvature at beginning	(c/MeV)	7	Yes	
Curvature at end	(c/MeV)	9	Yes	
$\|K\|$ via arc	(c/MeV)	11	Yes	
$\delta\|K\|$ via arc	(c/MeV)	12	Yes	
Azimuth at beginning	(radian)	13	Yes	Yes
Azimuth at end	(radian)	14	Yes	
Slope at beginning	( )	16	Yes	Yes
Slope at end	( )	17	Yes	
Momentum at beginning	(MeV/c)	24	Yes	Yes
Momentum at end	(MeV/c)	25	Yes	
Momentum via arc	(MeV/c)	26	Yes	
Relative momentum error	( )	27	Yes	
Dip at beginning	(radian)	28	Yes	Yes
X at beginning	(cm)	29	Yes	Yes
Y at beginning	(cm)	30	Yes	Yes
Z at beginning	(cm)	31	Yes	Yes
X at end	(cm)	32	Yes	Yes
Y at end	(cm)	33	Yes	Yes
Z at end	(cm)	34	Yes	Yes
Beta = P/E	( )	38	Yes	Yes
Gamma = E/M	( )	39	Yes	Yes

program, TOYNBEE, which in turn uses the PACKAGE output from our measured events.[19] In short, we have, from earlier programs, a magnetic tape that contains a summary of all the data for each measured event on a single record. Having read that record, we decide whether to use it as the basis for a simulated event. Our decision is "yes", if an only if the event gave a fit to our hypothesis, but with $\chi^2 > 15$. The proton must dip less than 60 deg relative to the top glass (either up or down), and the putative neutron track must make an angle greater than 60 deg with the scan. (The repetition of "60 deg" in both criteria is of no significance. The first criterion results from the need to insure reproducibility of scanning, measuring, and fitting; the second is a purely geometric criterion imposed to narrow the field of scanning and reduce the number of spurious recoils.)

When an event is accepted as a base for a simulation, its beam track is translated in the x direction by an amount that is prescribed by a random-number generator working from a given beam distribution.

The third and last stage of simulation is the construction of the tracks for the simulated event. By "construction" we mean the specification of those parameters that the FAKE program requires and the insertion of these into the memory locations appropriate for the further processing by FAKE. The quantities needed for each track are listed in the accompanying table.

Our object in this procedure is the estimation of the fraction of background that we expect to masquerade as real events. As we have seen, not all the background is used. We use only events that give χ^2 values that exceed 15. The number of spurious events we expect in our whole sample will be larger than the average number occurring in our restricted sample, in the proportion that the whole of the background bears to the restricted portion we have chosen. We chose our restricted portion to achieve a "pure" background sample, and we consider the events that could not fit the hypothesis with χ^2 of 15 or less to comprise such a pure sample. There were ten successive samples of simulated events based on the pure background sample, each generated by use of a different portion of the random-number table. By scaling the number of successful masquerades by the factor specified above, we get a number of background events that can be compared with the number of real + background events obtained from analysis of our actual measured events.

In the section giving the results of the Boolean analysis of our data, we concluded that our real events can be expected to have Boolean signature 0 or 32. We decided, however, to discard all events having signature 32. We now estimate the number of spurious events having signature 0 (background) and the number of good events having signature 32 (casualties).

In the ten sets of pure background that we created, there were four events having signature 0, and 16 events having signature 32. These two numbers must be multiplied by the fraction, F_c, that the estimated whole background bears to the sample of pure background that we used. We estimate that the unused background is composed of all the events that satisfied the other criteria but had a χ^2 parameter between 2.706 (the highest acceptable value for a valid event and the 90% limit) and 15, the lowest value for a pure background event. This is a first-order approximation because that sample, in principle, contains 10% of all the real events, although it does not include the background that contaminates the events with χ^2 below 2.706. These two effects tend to cancel and are small in any case. We conclude, therefore, that $F_c = 1 + 29/135 = 1.215$. We assume Poisson statistics to hold. This is an approximation because we are using the same events ten times over to simulate our sample, and only the essential variables of the neutron are really varied by our procedure. Under Poisson statistics, the number of background events is $(4\pm2)\ F_c = 4.86\pm2.43$, and the number of events of signature 32 is $(16\pm4)\ F_c = 19.44 \pm 4.86$. The expected number in our experimental sample, is, of course, one tenth of each these values. These values are discussed further in the discussion of the main result.

G. Anomalous Events and Borderline Interpretations

1. Events whose χ^2 value reproduced unreliably on successive measurements

There were six different events (see Appendix N), whose χ^2 values on successive measurements were not similar. That is, given the partition of possible cases into the five segments (a) $\chi^2 \leq 2.706$; (b) $2.706 < \chi^2 \leq 8$; (c) $8 < \chi^2 \leq 15$; (d) fit was achieved only on the 0-c fitting of the elastic n-p scattering, (e) no fit, whatever, occurred, six events fell into separated segments on successive measurements. (Events having $\chi^2 > 15$ on the fit of the whole event are considered not to have fitted the whole event at all.) A list of these events follows:

Roll	Frame	Record number	χ^2	Comment
502	353	144	10.45	Projection = 0.62 cm
		145	0.628	Dip error = 5.68 deg
504	478	310	3.78	Projection = 0.62 cm;
		313		cos (angle with normal to glass)=0.8795
507	214	682	1.35	$\cos\theta_{\pi^0}^{c.m.} = 0.1687$
		686		
507	287	772	18.4	(see discussion below)
		774	6.10	
509	400	1425	0.264	$\cos\theta_{\pi^0}^{c.m.} = 0.1151$
		1428	10.5	
547	544	2172	6.77	$\cos\theta_{\pi^0}^{c.m.} = 0.6318$
		2174	18.1	

The recoil in the first of the events above has a projection on the film plane that is less than the minimum permitted, namely 0.7 cm. Further, its recoil dip error is 5.68 deg, much more than the 2.5 deg that is the standard for low dip error. This particular event is the spurious event that is discussed as an example in some detail in a separate section.

The second event has, likewise, a recoil projection that is too small (0.62 cm), but it also violates the steepness criterion, as the cosine of the angle between the momentum of the proton at its start and the normal to the plane of the top glass is 0.8795 (which exceeds cos 30 deg).

The third and fifth events have π^0's that are emitted in highly non-forward directions. The cosines of their angles of emission are 0.1687 and 0.1151, compared with the absolute lower bound of 0.6. We do not even scan for events below the latter value.

Events four and six, although they lie in separated parts of the spectrum, do so so narrowly that we may regard them as lying on the ragged edges of our arbitrarily drawn divisions. They each have χ^2 values of about 6 on one measurement, and about 18 on the other. Because the dividing lines are drawn at 8 and 15, and because χ^2 values are expected

to vary as the square of any errors, these events reinforce our feeling as to the approximate validity of our estimated limits. In any case, a χ^2 value even of six is well above the acceptable maximum, and we need fear no losses of events because of this slight deviation from our stated limits of reliability.

2. Events on which the sign curvature decided the validity of the event

The experimental technique we use does not give reliable values for the curvature of proton tracks, and we use ranges instead to deduce momentum values. There are cases, however, when an event passes all our criteria but has a recoil whose measured curvature is negative. In such cases, we first examine the error in curvature to see if the measurement is consistent to within one standard error with a positive value. It usually is. We then remeasure the event several times, assuming alternate ends of the recoil to be the actual physical beginning of the proton trajectory. If each of four or five measurements supports the conclusion that the recoil has negative curvature as originally measured, we discard the event. The number of events so discarded should be of the order of 0.3 for our whole experiment because that is the FAKE-estimated number of spurious fits to be expected from positive tracks on events that satisfy all our criteria. We might expect a similar number from "negative" tracks if we ignored the curvature information.

If, on the other hand, a subsequent measurement satisfies all our criteria with a positive curvature, we accept the event.

We find that most recoils (because they are stopping tracks) will give values of momentum at end (from curvature) of the order of only 10 MeV/c. When a recoil gives a much larger value--as many do--we suspect a poor measurement or a reversed recoil. (It must be said, too, that occasional recoils give the same sign of curvature when measured from either end.)

There are four events that required careful study in this connection, each giving negative curvatures with high error on first measurement.

Roll	Frame	Record	χ^2	P_{beg} (MeV/c)	P_{end} (MeV/c)	MM (MeV/c^2)	δMM (MeV/c^2)
519	429	1896	0.7157	121.2	-4.7	122.6	15.74
547	201	2068	0.0025	-117.0	4.3	133.2	11.65
556	90	--	0.0102	-309.8	-300.3	139.1	12.87
565	430	2792	0.5000	129.7	-5.4	150.0	10.90

Of the events above, we accepted the first and last and discarded the other two.

The first measurement of the first event gave a negative recoil curvature, but the remeasurement gave a believable positive value. The momentum at the beginning was 121.2 MeV/c, very close by the standards of this experiment to the far more reliable momentum value 142.9 MeV/c, deduced from range. The residual range was -4.7 MeV/c, a small value that is well within the normal range for well-measured stopping tracks. Note, however, that the missing-mass error is 15.74, close to the highest permitted value of 16.0. The gap between 16.0 and the next-highest-occurring missing-mass error is large enough, however, to support the conclusion that there is a real separation in this parameter between valid and invalid events. We take this separation to justify the inclusion of the marginal event.

The second event listed above, 547-201, gives a reliable negative value for the curvature with an initial momentum, -117.0, whose magnitude is close to that determined from range, 138.8 MeV/c. The final momentum, 4.3 MeV/c, is also consistent with our conclusion. On remeasurement, negative curvatures recurred, and no positive curvatures appeared, except when the track was reversed. Further, dip errors became larger on remeasurements, exceeding easily the maximum of 2.5 deg. We discarded the event.

Event three, 556-90, of the table, was rejected by both scanners but was given by the FAKE program in the recoil-end-exchanging option as a (the only) possible ignored event. With five measurements, we could not achieve a positive (nor reasonable) curvature on this event. We discarded it.

The last event of the four above (565-430) gave several believable values of negative curvatures, but also a believable positive value (that shown in the table above). For that measurement, all our criteria were satisfied, and we were, therefore, obliged to accept the event. With the acceptance, one rejected event remained that satisfied all our criteria with negative curvature. This is consistent with our estimate of a fraction of an event given by the FAKE program.

H. Length of Beam Track

The beam parameters used are those chosen in the analysis of so-called "Pre-Christmas" Associated Production Experiment (APE).[20] All beam tracks that are called "acceptable" satisfy a set of criteria imposed at their plane of entry into the chamber (y = - 102.6 cm in our PANG coordinate system). These are

Parameter	Lower limit	Upper limit
X PANG coordinate (cm)	-3.8	10.0
Z PANG coordinate (cm)	12.5	21.5
Aximuth relative to x axis (deg)	107.75	111.75
Dip relative to xy plane (deg)	-1.75	3.25

In addition to these, acceptable tracks must have, within limits, a radius of curvature and an ionization appropriate to π^- tracks of 1.035 BeV/c, as seen in the scanning table. Events are accepted on the APE criteria if the beam-track interaction occurs between y = - 70 cm and y = + 70 cm. We accept events occurring as early as y = - 80.0 cm (one bubble-chamber zone upstream from rake number zero), which lengthens our tracks by about 2% and decreases the beam attenuation by 2%. Further, we discard frames having more than 25 beam tracks, where as the standard APE cutoff is 30. This difference results in a decrease of about 2% in the estimated average number of tracks per frame. The calculation is given below.

Total path length = L_{total};

Average path length per beam track = $\overline{L}$;

Average number of entering beam tracks = $\overline{N}$;

Number of frames in the experiment is $F = 6501$;

Mean free path for beam-track scattering is $\lambda = 462.8$ cm., based on total cross section of 60 mb;

Length of path available between $y = -70$ and $y = +70$ cm is $\ell = 143.975$ cm;

Additional path available between $y = 80$ and $y = -70$ cm is $\delta\ell = 10.284$ cm.

Then

$L_{total} = \overline{L}\, F\, \overline{N} \exp(\delta L/\lambda)$;

$\overline{L} = \lambda \left\{1 - \exp\left[-(\ell + \delta\ell)/\lambda\right]\right\} = 131.19$ cm;

$F = 6501$ frames;

$\overline{N} = (13.48 \pm 0.25)$ beam tracks per frame based on standard APE count on frames with 25 or fewer tracks of (13.42 ± 0.30) on an unbiased set of frames, and (13.61 ± 0.42) on a set of linearly biased frames (the corresponding amalgamated average with 30-track cutoff was 13.84 ± 0.26 instead of 13.48 ± 0.25).

Accordingly, the total path length, L_{total}, for the experiment is $(1.175 \pm 0.022) \times 10^7$ cm.

The value L_{total} is the total length of beam track in our experiment, but this length includes contamination by μ mesons, electrons, and unacceptable beam tracks. The fraction of the whole represented by each (given by Leroy Price and Gerald Meisner of the APE experiment)[20] is

Effect	Contamination of the whole (%)	Estimate is based on a sample with contaminating events
μ meson	5.5 ± 1.8	10
electron	0.74 ± 0.18	22
dip and azimuth failure	3.8 ± 1.0	14

We assume the dip and azimuth distributions of the beam π^- and the contaminating particles to be the same. This gives a correction to L_{total} of 0.928±0.020.

The total length of accepted π^- beam track in our experiment, then, is $(1.09 \pm 0.03) \times 10^7$ cm.

I. Kinematics of the Reaction $\pi^- + p \rightarrow \pi^0 + n$

Tables V through VIII at the end of Section I give an illustrative set of kinematic quantities for the elastic charge-exchange reaction. Quantities are given for two beam momenta, 1.0 and 1.1 BeV/c. This permits interpolation for actual beam momenta (which vary in the vicinity of 1.035 BeV/c, the beam momentum near the middle of the chamber) and indicates the approximate range of kinematic values encountered in the experiment.

No event is sought by the scanner for which the neutron is emitted at an angle of less than 60 deg (with respect to the direction of the beam track). No event is included in our sample unless its neutron was emitted at an angle $\theta_n^{c.m.}$ such that $\cos \theta_n^{c.m.} \leq -0.7$. The quantities corresponding to these cases are given in the tables following. The remaining cases are conveniently spaced in values of the neutron momentum in the laboratory.

FORTRAN program KINE gave the results quoted above, but we needed a utility two - body kinematics program to perform event-by-event calculations. We used FORTRAN program ENTUM for this purpose. It is based on a simple formula that we derive below.

1. Derivation of the Formula

We derive a formula for reactions in which both the initial and final states contain two particles, and in which one of the initial-state particles is a fixed target. The formula applies when we are given

(a) the masses of all four particles,

(b) the cosine of the angle θ_{BC}, between the momentum of the incident particle B and the momentum of one of the exit particles, C, and

(c) the momentum of one of the particles, B or C.

The formula yields the momentum of the other particle.

We achieve our goal by formally symmetrizing the conservation laws with respect to the interchange of particles B and C. Specifically, the reaction is

$$\underset{\text{incident}}{(B)} + \underset{\text{target}}{(A)} \longrightarrow \underset{\text{exit particles}}{(C) + (D)} .$$

We write the conservation laws.

Conservation of momentum: $\overline{P}_D^{\,2} = (\overline{P}_B - \overline{P}_C)^2$,

Conservation of energy: $\overline{P}_D^{\,2} + m_D^{\,2} = (m_A + E_B - E_C)^2$;

then $(\overline{P}_B - \overline{P}_C)^2 = (m_A + E_B - E_C)^2 - m_D^{\,2}$.

The left-hand side of this equation remains invariant under the interchange of subscripts $B \longleftrightarrow C$, but the right-hand side does not. We achieve the desired invariance by introducing the parameters $f_B = +1$ and $f_C = -1$. The symmetrized equation is

$$(\overline{P}_B - \overline{P}_C)^2 = (m_A + f_B E_B + f_C E_C)^2 - m_D^{\,2} ,$$

and a solution of this equation for P_B in terms of P_C will also be a formal solution of P_C in terms of P_B.

Changing notation to exploit the formal symmetry between particles B and C, we let

(a) Particle O be the target particle A.

(b) Particle be the particle of known momentum, and particle 2 be that of unknown momentum.

(c) Particle 3 be the "other" exit particle D.

Then $(\overline{P}_1 - \overline{P}_2)^2 = (m_0^2 + f_1 E_1 + f_2 E_2)^2 - m_3^{\,2}$.

Note that the subscripts 1, 2 are only a permutation of the old subscripts B, C. This implies $f_1 f_2 = f_B f_C = (+1)(-1) = -1$ and $f_1^{\,2} = f_2^{\,2} = 1$, in turn implying $f_2 = -f_1$.

Using these values, we can reduce the combined conservation equation to simpler form:

$$p_1^{\,2} + p_2^{\,2} - 2p_1 p_2 \cos\theta_{12} = m_0^2 + 2m_0\,(f_1 E_1 + f_2 E_2) + f_1^2 E_1^2 + f_2^2 E_2^2 + 2f_1 f_2 E_1 E_2 - m_3^{\,2};$$

then

$$m_0^2+(f_1^2E_1^2-p_1^2)+(f_2^2E_2^2-p_2^2)-m_3^2+2p_1p_2\cos\theta_{12}+2m_0(f_1E_1+f_2E_2)+2f_1f_2E_1E_2 -m_3^2 = 0 ;$$

and

$$m_0^2+m_1^2+m_2^2-m_3^2+2p_1p_2\cos\theta_{12}+2m_0(f_1E_1-f_1E_2)-2E_1E_2-m_3^2 = 0;$$

which implies

$$-2f_1(m_0+f_1E_1)E_2+(2p_1\cos\theta_{12})p_2+m_0^2+m_1^2+m_2^2-m_3^2+2m_0f_1E_1 = 0. \quad (A.1)$$

Assuming $(m_0 + f_1E_1) \neq 0$, we can rewrite (A.1) as

$$-f_1E_2 + \frac{p_1\cos\theta_{12}}{m_0+f_1E_1}\, p_2 + \frac{m_0^2 + m_1^2 + m_2^2 - m_3^2 + 2m_0f_1E_1}{2(m_0 + f_1E_1)} = 0,$$

or

$$-f_1E_2 + \beta' p_2 + \alpha' = 0, \quad (A.2)$$

where

$$\beta' = \frac{p_1\cos\theta_{12}}{m_0+f_1E_1} \quad \text{and} \quad \alpha' = \frac{m_0^2 + m_1^2 + m_2^2 - m_3^2 + 2m_0f_1E_1}{2(m_0 + f_1E_1)}$$

with

$$f_1E_2 = \beta' p_2 + \alpha' \quad \text{and} \quad E_2^2 = \beta'^2 p_2^2 + \alpha'^2 + 2\alpha'\beta' p_2 .$$

Then we have $(\beta'^2 - 1)p_2^2 + (2\alpha'\beta')p_2 + (\alpha'^2 - m_2^2) = 0$, (A.3)

whose solutions are

<u>Case 0.0</u>. $p_2 \quad \dfrac{\alpha'\beta' \pm \left[\alpha'^2 + m_2^2(\beta'^2 - 1)\right]^{1/2}}{1 - \beta'^2}$, provided $\beta'^2 - 1 \neq 0$;

<u>Case 0.1.</u> $\alpha'^2 + m_2^2(\beta'^2 - 1) \leq 0$ (unphysical).

2. <u>Discussion of the Singular Cases</u>

In deriving Eq. (A.2) from Eq. (A.1), we assumed $m_0 + f_1E_1 \neq 0$. If not, we have

<u>Case 1.</u> $m_0 + f_1E_1 = 0$ for $f_1 = -1$;

$$2p_1 \cos\theta_{12} p_2 + m_0^2 + m_2^2 - m_3^2 + 2m_0 f_1 E_1 = 0, \tag{A.11}$$

$$2p_1 \cos\theta_{12} p_2 + m_1^2 - m_0^2 + m_2^2 - m_3^2 = 0 ; \tag{A.12}$$

Case 1.0. $p_1 \cos\theta_{12} \neq 0$,

$$p_2 = \frac{m_1^2 - m_0 + m_2^2 - m_3^2}{2p_1 \cos\theta_{12}} ;$$

Case 1.1. $p_1 \cos\theta_{12} = 0$;

Case 1.10. $p_1 = 0$, $\cos\theta_{12} \neq 0$;

Thus, since $E_1 = m_1$; $m_0 = m_1$, the target remains at rest.

Case 1.100. $m_2 = m_3$.

This case is physically realizable, but there is not enough information for a solution. No scatter occurred.

Case 1.101. $m_2 \neq m_3$ (unphysical).

Case 1.11. $\cos\theta_{12} = 0$ $(p_1 \neq 0)$;

Case 1.110. $m_1^2 + m_2^2 = m_0^2 + m_3^2$.

This case is physically realizable, but there is not enough information for a solution.

Case 1.111. $m_1^2 + m_2^2 \neq m_0^2 + m_3^2$ (unphysical);

Case 1.12. $\cos\theta_{12} = 0$, $p_1 = 0$;

Case 1.120. $m_0 = m_1$, $m_2 = m_3$.

The following cases are physically realizable, but there is not enough information for a solution.

Case 1.21. $m_0 \neq m_1$, or $m_2 \neq m_3$ (unphysical).

A second set of singularities arises when $m_0 + f_1 E_1 \neq 0$, but $\beta'^2 = 1$. In this case, (A.3) is valid but (A.4) does not hold. Then we have

Case 2. $m_0 + f_1 E_1 \neq 0$; $\beta'^2 = 1$.

This implies

$$2\alpha'\beta' p_2 + (\beta'^2 - m_2^2) = 0; \tag{A.31}$$

<u>Case 2.0.</u> $\alpha' \neq 0$, $p_2 = \dfrac{\beta'^2 - m_2^2}{2\alpha'\beta'}$;

<u>Case 2.1.</u> $\alpha' = 0$;

<u>Case 2.10.</u> $m_2 = 0$;

<u>Case 2.100.</u> $m_0 \neq 0$, $E_1 = \dfrac{m_3^2 - m_1^2 - m_0^2}{2m_0 f_1}$;

but there is not enough information for a solution in this case.

<u>Case 2.101.</u> $m_0 = 0$, then $m_1 = m_3$;

<u>Case 2.1010.</u> $m_1 = m_3 = 0$.

This case is physically realizable, but there is not enough information for a solution. (Photon decay into two photons is an example, kinematically, of such a reaction.)

<u>Case 2.1011.</u> $m_1 = m_3 \neq 0$ (unphysical),

<u>Case 2.11.</u> $m_2 \neq 0$ (unphysical).

The above formally embodies a symmetry in the conservation principles pointed out in Alvarez Group Memo 91 by Professor Bruce H. McCormick. The calculation is performed by Fortran Subroutine ENTUM, whose calling sequence is

CAL ENTUM (A, B, P, T, C, D, F, R, BETA, P2B0, TSTAR, IBREV, NIX), where

A = mass of target particle,

B = mass of particle of known momentum,

P = the known momentum,

T = $\cos\theta_{12}$,

C = mass of particle,

D = mass of fourth particle,

F = known flux (i.e., f_1 in the discussion above) = (+1, -1); if particle of known momentum is an incident particle,

R = root chosen +1 (or for exit, -1 in the solution of Eq. (A.3) above,

BETA = β, intermediate quantity sometimes useful as an output,

P2B0 = unknown momentum (p_2) solved for,

TSTAR = cosine of the space angle between the momenta of particles 1 and 2 as seen in the c.m. system,

IBREV = (abbreviation flag). If TSTAR is not needed, an abbreviated calculation is performed. IBREV = (0, 1) if an abbreviated calculation (is not, is) desired,

and

NIX = number indicating which singularity, if any, appeared in the calculation (see the summary of significant cases above).

Table VI. Summary of major cases.

NIX	Case	Conditions					Case is physical	Solution exists
0	0.0	No singularity	$\alpha'^2+m_2^2(\beta'^2-1)>0$				Yes	Yes
3	0.1		$\alpha'^2+m_2^2(\beta'^2-1)\leq 0$				No	No
	1	$m_0+f_1E_1=0$						
1	1.0		$p_1\cos\theta_{12}\neq 0$				Yes	Yes
	1.1		$p_1\cos\theta_{12}=0$					
	1.10			$p_1=0(\cos\theta_{12}\neq 0)$				
4	1.100				$m_2=m_3$		Yes	No
34	1.101				$m_2\neq m_3$		No	No
	1.11			$\cos\theta_{12}=0(p_1\neq 0)$				
14	1.110				$m_1^2+m_2^2=m_0^2+m_3^2$		Yes	No
44	1.111				$m_1^2+m_2^2\neq m_0^2+m_3^2$		No	No
	1.12			$p_1=\cos\theta_{12}=0$				
24	1.120				$m_2=m_3$		Yes	No
54	1.121				$m_2\neq m_3$		No	No
	2	$m_0+f_1E_1\neq 0;\ \beta'^2=1$						
2	2.0		$\alpha'\neq 0$				Yes	Yes
	2.1		$\alpha'=0$					
	2.10			$m_2=0$				
5	2.100				$m_0\neq 0$		Yes	No
	2.101				$m_0=0$			
35	2.1010					$m_1=0$	Yes	No
135	2.1011					$m_1\neq 0$	No	No
15	2.11			$m_2\neq 0$			No	No

Table VII. Samples of kinematic quantities for final-state particles of reaction $\pi^- + p \rightarrow \pi^0 + n$ (from FORTRAN Program KINE).

Beam Momentum = 1000.0 MeV/c					
θ_n^{lab} (deg)	P_n^{lab} (MeV/c)	$\theta_n^{c.m.}$ (deg)	$\cos\theta_n^{c.m.}$	$\theta_{\pi^0}^{lab}$ (deg)	$P_{\pi^0}^{lab}$ (MeV/c)
60.00	514.85	127.40	-0.60738	30.98	866.12
63.82	446.81	134.40	-0.69966	26.54	897.47
68.66	361.80	143.10	-0.79968	21.15	931.77
69.33	350.05	144.30	-0.81208	20.49	935.62
72.20	300.07	149.40	-0.86074	17.46	952.12
75.08	250.06	154.50	-0.90259	14.48	966.31
77.97	200.03	159.60	-0.93728	11.54	978.07
79.38	175.51	162.10	-0.95159	10.11	982.92
80.85	150.01	164.70	-0.96456	8.63	987.31
82.25	125.50	167.20	-0.97515	7.21	990.90
83.13	109.81	168.80	-0.98096	6.30	992.87

Table VIII. Samples of kinematic quantities for final-state particles of reaction $\pi^- + p \rightarrow \pi^0 + n$ (from FORTRAN Program KINE).

Beam momentum = 1100.0 MeV/c					
θ_n^{lab} (deg)	P_n^{lab} (MeV/c)	$\theta_n^{c.m.}$ (deg)	$\cos\theta_n^{c.m.}$	$\theta_{\pi^0}^{lab}$ (deg)	$P_{\pi^0}^{lab}$ (MeV/c)
60.00	542.42	128.20	-0.61841	29.54	952.67
63.43	477.53	134.40	-0.69966	25.73	983.92
68.32	386.25	143.10	-0.79968	20.55	1022.36
70.25	350.56	146.50	-0.83389	18.58	1035.49
72.99	300.19	151.30	-0.87715	15.83	1052.11
75.75	249.87	156.10	-0.91425	13.13	1066.36
78.51	199.60	160.90	-0.94495	10.45	1078.14
79.83	175.53	163.20	-0.95732	9.18	1082.89
81.20	150.43	165.60	-0.96858	7.86	1087.21
82.56	125.34	168.00	-0.97815	6.54	1090.88
83.40	109.67	169.50	-0.98325	5.72	1092.84

J. Escape or Geometric Correction and Detection Efficiency

In our experiment, we detect the secondary charge-exchange neutron by using the n-p elastic-scattering reaction. Because our chamber has finite dimensions, not all the neutrons produced scatter before leaving it. Further, of those that do scatter, a substantial fraction give undetectably short protons, or protons that make an angle of 60 deg or more with the top glass of the chamber (this violates our acceptance criterion). The incidence of proton tracks that are undetectable or steep is discussed in the section on the profile correction. The calculation involved, however, is incorporated into the overall detection efficiency. A complete discussion of the calculation is given in UCRL-9871.[21]

Now, we describe and give the results of the particular calculation performed for the current experiment.

To calculate the average detectability of emitted neutrons, we simulate on the computer a sample experiment consisting of (N_x+1) (N_z+1) tracks entering the chamber at the plane $y = 0$ and covering uniformly (at equal intervals $\Delta X, \Delta Z$ in X and Z) the rectangle whose area is $(N_x \Delta X\ x)$ $(N_z\ \Delta Z\ z)$. The momentum of all these tracks is the same (1035 MeV/c), their azimuth angle of entry is 1.9155 radians, and their dip angle is 0.0 deg. Along each track at intervals of ΔS, (N_s+1) points are chosen to simulate sites of charge exchanges. The magnetic field of -15.42 kG in the z direction determines the curvature of the beam track. Momentum losses of the beam track are ignored, as are the finite widths of azimuth and drip distributions at entry and the variation of the magnetic field through the chamber. The beam is assumed to be Gaussianly distributed at entry in the x and z directions. The beam density at x^E in the entry plane is proportional to $\exp[-(x^E-x^0)^2/2\sigma_x^2]$ with $x^0 = 6.9$ cm and $2\sigma_x^2 = 14.1224$ cm^2. The z distribution is similar with $z^0 = 17.5$ cm and $2\sigma_z^2 = 4.0132$ cm^2. The beam parameters used are the Standard Associated Production Experiment (Pre-Christmas) values, except for the effective Gaussian distribution widths, which are those determined by Dr. Norbert Schmitz.

In particular, $N_s = 4$, $N_z = 2$, $N_x = 4$ and $\Delta S = 30$ cm, $\Delta Z = 4.5$ cm, and $\Delta X = 3.45$ cm. The regions sampled in S, Z, and X are $40 \leq S \leq 160.0$ cm, $12.5 \leq Z \leq 21.5$ cm and $-3.8 \leq X \leq 10.0$ cm. For each point a weight is calculated that accounts for the beam density at entry (as

described above) and the attenuation of the beam since entry by a factor exp $(-S/S_A)$, where $S_A = 594.36$ cm.

The function that we average over the set of points and with the weights described above is the probability that a neutron emitted at an angle THETA with respect to the beam direction at the point of emission will react, before leaving the chamber, with a proton in such a way as to leave a detectable recoil that is not steeper than permitted by our acceptance criterion. We do this by performing, at each sample point, the calculation for neutrons emitted at eight different azimuths on the cone with opening angle THETA.

The first link in the determination for a single azimuth and fixed THETA is the computation of the distance the neutron will traverse before leaving the effective chamber boundaries. These boundaries are six planes based on boundaries given below.[22]

Their equations are

Left-hand plane	$-0.99368\,x + 0.00000y + 0.11229z - 24.1 = 0.0,$
Right-hand plane	$0.99228\,x + 0.00000y + 0.12404z - 26.1 = 0.0,$
Entrance plane	$0.00000\,x - 0.92848y + 0.37139z - 9.962048 = 0.0,$
Exit plane	$0.00000\,x + 0.92196y + 0.38722z - 179.593096 = 0.0,$
Bottom plane	$10^{-3} \times 4.0026x + 0.00000y - 0.999992z + 5.44963 = 0.0,$
Top plane	$-0.13086x + 0.00000y + 0.99140z - 36.0 = 0.0.$

The planes above are those in the note cited, with two qualifications. First, the bottom boundary of the note is a part of a cylinder. We have replaced it with the plane that passes through its intersections with the sides of the chamber. Second, we have translated the y coordinates, so that the approximate entry plane ($y = -102.6$ in standard PACKAGE coordinates) would become $y = 0.0$ above. This transformation explains the inclusion of insignificant digits in the constants of the entrance and exit planes. Without them, a reversion to standard coordinates would be inaccurate. All coordinates are given in centimeters.

The chamber boundaries above are the boundaries set by PACKAGE in its volume test. Tracks passing out of this volume will still be visible in some views, but then reconstruction will be less reliable. PACKAGE regards, therefore, any track that left the above volume as a leaving track (LSZ = 1) even if it stops in the remaining portion of the chamber. Our

preoccupation with stopping protons dictates the adoption of this volume as our acceptance region. Further, because most of our tracks are short compared to the chamber dimensions, we allow the full volume specified for the elastic-scattering interaction, even though a proton track starting just within this volume would be, with high probability, carried outside it before coming to rest.

We have found the path available inside the chamber for the neutron emitted at the specified THETA and azimuth from the specified point in the chamber. (For a two-body final state, such as ours, THETA determines the neutron momentum up to a possible ambiguity of root. At our momentum, one root gives a momentum that is of the order of 25 MeV/c, which implies that the other root is the interesting one.) We need only the mean free path for n-p scattering, which, in turn, requires only the n-p cross section. For our range of energies, the n-p cross section is given, in barns, reasonably well by (10/T) MeV. Thus, a 5-MeV neutron would have an approximate n-p cross section of 2 barns. At this point it is appropriate to point out that although our experiment has a low efficiency for detection, it involves reactions that have, for bubble chamber experiments, relatively high cross sections. The n-p scatterings we deal with have cross sections of substantial fractions of a barn. Charge exchange itself has a cross section that is substantial compared to most reactions studied in the chamber and is small compared only to elastic reactions (which are generally so copious as to be ignored or else more easily examined through other experimental means). This is important because it stresses how much weakening there is of our detection efficiency by the requirement of a secondary reaction, and because of its reflection on the possibilities of applying this or a similar technique to the study of a noncopious reaction.

By computing the mean free path for n-p scattering, λ_s, as above, the probability that a collision will take place in the available path, a, is $\exp(-a/\lambda_s)$. We must multiply this by a visibility or profile factor, discussed in a separate section, which is computed on the assumption that all recoils are reliably measurable and detectable by scanners if they are shallow with respect to, and project 0.7 cm on the plane of, the top glass. The physical condition involved should more properly relate to the sizes of images (on the planes of the cameras) of the views used to reconstruct the track, and the condition we have adopted must therefore be regarded as an

approximation. The accompanying graphs and tables give the numerical results of the calculations, as averaged over the sample of selected points for specific values of THETA and the corresponding values of $\cos \theta_n^{c.m.}$.

The results in Table VIII are quoted to approximately full computer accuracy and represent the exact results of the calculation described above. The calculation gives, as has been pointed out, only an approximation to the magnitude of the effect for which we are correcting. The results should be treated as a two-digit estimate of the effects approximated.

Note that the efficiency for detecting events is less strongly a function of angle when the 60-deg-dip restriction is applied. That restriction was invoked primarily for three reasons: First, to reduce the number of spurious recoils that might masquerade as real ones; second, to render our measurements of recoils reproducible within convenient limits; and third, to eliminate the possibility that the ends of a recoil might be mistakenly interchanged. It appears that this criterion has a fourth desirable property. The variation of detection efficiency with angle is smoother after the restriction is imposed than before. As a result, the fluctuations in our result due to large variations in correction are somewhat moderated. The price, in lessened efficiency of detection, of the imposition of the steepness criterion can be determined by comparison of the last two columns of Table IX.

Table IX. Efficiency for detecting neutrons (as given by program HOUND).

θ_n(lab) (deg)	p_n (MeV/c)	$\cos\theta^{c.m.}$	E(scatter...) (%)		Range (Proj.) ≥0.4 cm(110 MeV/c) E(... + visibility) (%)		E(... + steepness) (%)		Range (Proj.) ≥0.7 cm(130 MeV/c) E(visibility) (%)		E(... + steepness) (%)	
60	524.72	0.6114	5.81	02190	5.50	44757	4.76	57164	5.37	54468	4.66	87167
61	506.47	0.6363	6.14	40057	5.79	69913	5.01	33251	5.65	05590	4.90	34618
62	488.26	0.6606	6.51	46931	6.11	87180	5.28	58929	5.95	17381	5.16	09887
63	470.10	0.6840	6.92	69968	6.47	25757	5.58	62441	6.28	16132	5.44	25641
64	452.00	0.7067	7.38	60180	6.86	05124	5.91	62220	6.64	19156	5.75	08180
65	433.94	0.7286	7.90	04628	7.28	90983	6.28	17122	7.03	72012	6.08	99719
66	415.92	0.7498	8.47	88435	7.76	20187	6.68	71147	7.47	09772	6.46	20932
67	397.96	0.7701	9.12	59742	8.28	22046	7.13	10292	7.94	14325	6.86	56632
68	380.04	0.7896	9.85	91321	8.85	89263	7.62	40332	8.45	61933	7.30	82093
69	362.17	0.8083	10.69	4462	9.49	98103	8.17	27530	9.01	71798	7.79	37449
70	344.35	0.8261	11.64	7281	10.20	8952	8.77	93015	9.61	94067	8.32	29268
71	326.56	0.8431	12.74	3928	10.99	3993	9.45	20048	10.26	3082	8.89	72355
72	308.81	0.8593	14.01	4246	11.86	1725	10.10	7667	10.96	0031	9.51	69578
73	291.10	0.8746	15.49	5353	12.81	0681	11.02	3965	11.69	5584	10.17	2652
74	273.42	0.8891	17.23	4317	13.82	0887	11.92	7526	12.45	0135	10.84	8768
75	255.96	0.9027	19.29	1410	14.90	8985	12.90	0086	13.17	9446	11.50	1901
76	238.12	0.9155	21.74	4367	16.04	4609	18.91	6712	13.80	5904	12.07	2823
77	220.49	0.9274	24.69	4046	17.15	5456	14.91	3933	14.14	2827	12.43	3394
78	202.86	0.9384	23.27	1905	18.09	4396	15.76	4979	13.76	7190	12.42	2843
79	185.22	0.9485	32.64	8767	18.50	8257	16.20	5618	12.53	2136	11.70	6309
80	167.54	0.9578	38.04	3917	17.47	5241	15.81	6353	9.60	08573	9.48	61174
81	149.79	0.9662	44.72	8568	14.44	8140	13.79	2961	5.48	09423	5.48	09423
82	131.94	0.9738	53.00	7364	8.86	62360	8.86	62360	0.33	66554	0.33	66554
83	113.92	0.9804	63.12	9525	0.98	56135	0.98	56135	0		0	
84	95.58	0.9862	75.01	6147	0				0		0	
85	76.64	0.9911	87.54	3446	0				0		0	

K. Computation of the Average Visibility of Protons Recoiling from a Neutron of Given Momentum and Direction; FORTRAN Routine: PROFIL

Proton recoils are visible only if they project more than a certain minimal length, L_{min}, on the plane of the film. In general, then, we want to calculate the fraction of recoils that result from the elastic collision of a neutron of momentum $p_0\hat{n}_1$ with a proton target and that give final-state protons whose track projection on the film plane exceeds L_{min}. (We let the normal to the film plane be given by the vector $\hat{n}_2$.)

The following approximations are made.

(i) The n-p collision is nonrelativistic,

(ii) The n-p mass difference is zero,

and

(iii) The range-momentum relation for protons is given by range = constant $\times$ [(momentum) to the power (ALPHA)], where ALPHA is a constant (=0.278) for liquid H].

Approximations (i) and (ii) enable us to deduce that the surface of the sphere whose diameter is the initial momentum vector $P_0\hat{n}_1 = \overline{P_i}$ will contain all the termini of the final-state proton vectors, if the initial point of each of these vectors is set at the initial point of $\overline{P}_i$.

If $\hat{p}$ is a unit vector in the direction of the final-state proton momentum, then the magnitude of the latter is $(\hat{p}\cdot\hat{n}_1)p_0$. Since we have specified L_{min} to be the length of the shortest visible proton profile, $L_{min}/[(1-(\hat{p}\cdot\hat{n}_2)^2]^{1/2}$ is the minimal length for a visible proton emitted along the direction $\hat{p}$.

Then, since momentum = constant $\times$ (range)^a and since $p = p_1 \times (\text{range})^a$ for a minimally visible proton recoil,

$$p_{min} = p_1 \left\{ \frac{L_{min}}{[1-(p\cdot n_2)^2]^{1/2}} \right\}^a .$$

So, for a given $\hat{n}_1$, $\hat{n}_2$, p_0, L_{min}, and a, a recoil is visible if emitted along a direction $\hat{p}$ such that

$$(\hat{p}\cdot\hat{n}_1)\, p_0 \geq p_{min} = p_1\, L^a_{min}[1-(\hat{p}\cdot\hat{n}_2)^2]^{-a/2} ,$$

or

$$(\hat{p}\cdot\hat{n}_1)\, \frac{p_0}{p_1 L^{\hat{a}}_{min}} \geq [1-(\hat{p}\cdot\hat{n}_2)^2]^{-a/2} ,$$

or

$$R(\hat{p}\cdot\hat{n}_1) \geqslant [\,1-(\hat{p}\cdot\hat{n}_2)^2]^{-a/2}$$

where

$$R = (p_0/p_1\, L^a_{min})\,.$$

(Here, R is the ratio of the incident momentum p_0 of the neutron to the momentum $p_1\, L^a_{min}$ of the shortest possible visible recoil.)

Since both sides of the inequalities above are invariant under rotations, we may rotate the vectors rigidly so that $\hat{n}_1$ lies along the z axis, and so that $\hat{n}_2$ lies in the yz plane with azimuth between $\pi/2$ and $3\pi/2$. Writing down the inequality with this orientation of the system gives

$$R\cos\theta \geqslant [\,1-\cos^2\theta\cos^2 T\,(1-\tan\theta\tan T\sin\phi)^2]^{-a/2}\,.$$

For a fixed θ, there is a range (possibly vanishing) of values of $\sin\phi$ for which the inequality holds. We seek to know it. We restrict ourselves to positive values of $a = \tan\theta\tan T$ by the following argument.

First, since the n-p collision is elastic, the proton must scatter in the forward hemisphere relative to the neutron's original course. This implies that $\tan\theta$ is positive.

Second, if $\tan T$ were negative, the form of the inequality could be preserved by mapping ϕ into $-\phi$. In other words, if ϕ satisfied the inequality for positive $\tan T$, then $-\phi$ would satisfy it for negative $\tan T$, and the magnitude of the range of ϕ satisfying the inequality would remain unchanged. Physically, we reach the same conclusion by considering that the projection on a plane is the essential feature. Clearly, reflection in that plane (taking $\tan T$ to $-\tan T$) causes no change in the projection. We can therefore assume $\tan T$ to be positive.

It is also convenient to restrict our calculation for the range $-\pi/2 < \phi \leqslant \pi/2$. The inequality remains fixed under the reflection $\phi \rightarrow \pi-\phi$, so that the result in the range $\pi/2 \leqslant \phi \leqslant 3\pi/2$ is the same.

Consider the sphere S whose diameter, the vector $\overline{P}_i = p_0\, n$, lies along the z axis. With our approximations, the end points of all possible final-state proton momenta lie on the surface of this sphere.

We define a function $f(\theta, \phi) = (0, 1)$ if a proton emitted at the given angle θ with respect to the incident proton would, if its azimuth were ϕ, have (an invisible, a visible) profile.

Then, if each element of area on the sphere containing the termini of the final-state proton-momentum vectors is to be weighted by a weighting function $w(\theta, \phi)$, the fraction of visible final states is

$$\frac{\int_0^{\pi/2} d\theta \sin 2\theta \int_{-\pi/2}^{\pi/2} d\phi \, w(\theta, \phi) \, f(\theta, \phi)}{\int_0^{\pi/2} d\theta \sin 2\theta \int_{-\pi/2}^{\pi/2} d\phi \, w(\theta, \phi)} .$$

We are looking then for the fraction of the sphere corresponding to visible final-state protons (i. e., the fraction of the sphere for which our inequality is satisfied). We note that the inequality will surely fail if $R \cos \theta < 1$. (This means that the final-state proton momentum is less than the minimum needed for visibility.) Thus we need only examine values of θ from 0 to arc cos(1/R). For each fixed θ in this range, there is a minimum value (ϕ_-) and a maximum value (ϕ_+) of ϕ such that the inequality is satisfied. All values of ϕ between ϕ_- and ϕ_+ will also satisfy the inequality. (We are restricting ourselves all along to $-\pi/2 \leq \phi \leq \pi/2$.)

Then the element of visible solid angle is $\sin 2\theta \; 2\Delta\theta \; (\phi_+ - \phi_-)$, and the element of visible total solid angle is $\sin 2\theta \; 2\Delta\theta \; \pi$. The first term sums to the visible solid angle, and the second term sums to the total solid angle ($=2\pi$).

For convenience, we divide the upper integral by 2π and evaluate only

$$\sum_{J=1}^{N} \Delta\theta \sin (2J\Delta\theta) \, (\phi_+ - \phi_-)/\pi,$$ where N is the number of intervals

to be used in the numerical integration, $\Delta\theta = \text{arc cos } (1/R)/N$, and $\phi_\pm = \text{arc sin } \left\{ \cot \theta \cot T \pm \left[1-(R \cos \theta)^{-2/a} \right]^{1/2} / \sin \theta \sin T \right\}$.

If the argument of the arc sin above is ≥ 1 or ≤ -1, then $\phi_\pm$ is set equal to $+\pi/2$, $-\pi/2$, respectively.

FORTRAN Routine: PROFIL

The integrations above are performed numerically by FORTRAN routine PROFIL, whose calling sequence is

CALL PROFIL (R, T, ALPHA, N, KERR, DATA, EREWON, RESULT),

where

R = ratio of incident neutron momentum to momentum of minimally visible proton recoil,

T = angle between normal to the plane with respect to which projections are being taken and the direction of the incident neutron momentum (radians),

ALPHA = exponent in momentum-range relation [range = constant × (momentum) to the power (ALPHA)],

N = number of intervals to be employed in the numerical integration,

KERR = error array of length 70.

KERR (37) contains number of output tape onto which a dump would be written in case of error. (Integer.) KERR (35) contains the number of BCD characters in a computer word.

DATA is an arbitrary array containing data for use in computing $W(\theta, \phi)$. This is done in the SHAW subroutine.

EREWON is an array of (100, 5) locations containing intermediate results.

RESULT is an array of 12 locations containing the results of the calculation.

The FORTRAN listing of the program may be consulted for further details. A sample of its numerical results is plotted in Fig. 8.

L. Scanning-Table Measurements

Preliminary measurements on our events were made, not on the Franckenstein measuring projector, but on the scanning table with ruler and protractor. With one exception, the method is described completely by Dr. Gerald R. Lynch.[23] We measure three tracks at once (π^-, n, p), and it is desirable to make all measurements with the same setting of the projected images. We do this by superposing the three images of the initial point of the recoil proton. This defines the relative setting of the three images that holds for all measurements on the given event. The depth (beneath the top glass) of the starting point of the proton track is determined by the separation Δ_f of the top fiducials. With the auxiliary assumption that the beam track is flat in the chamber, all the momenta can be derived.

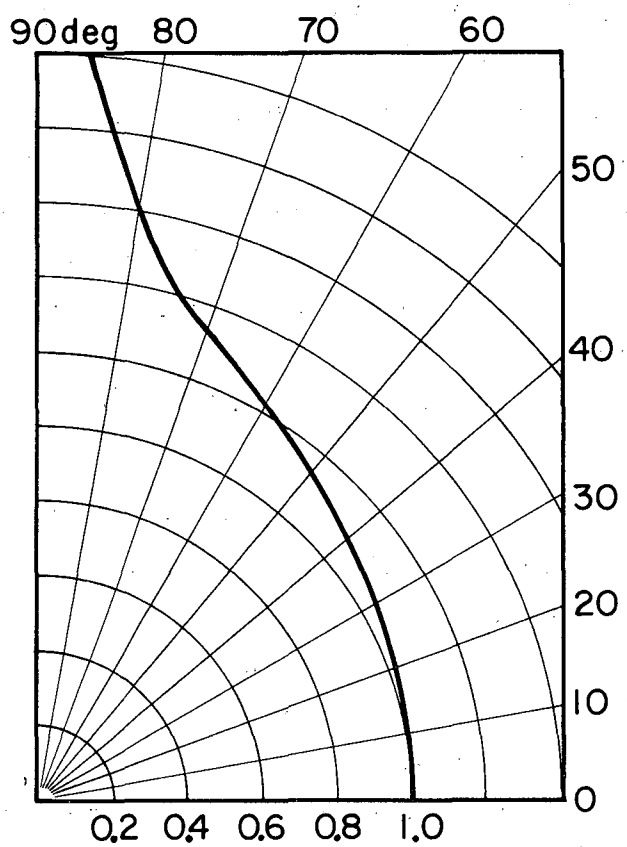

MU-32911

Fig. 8. Polar graph of normalized minimal visible momentum of proton vs angle of dip.

The momentum of the proton is determined from its range by $p = p_0 R^a$, where $a = 0.278$, and $p_0 = 140$ MeV/c. By knowing the beam momentum, we can calculate two values of the neutron momentum: the first from

(i) the beam momentum

and

(ii) the space angle $\theta_{n\pi}$ between the beam direction and the direction of the emitted neutron; and a second from knowing

(iii) the momentum of the recoil proton

and

(iv) the space angle θ_{np} between the direction of the neutron and that of the recoil proton track.

The kinematic relation is the same in each case and is derived in Appendix I.

The geometric quantities required are the cosines of the two spatial angles in (ii) and (iv); the formula is

$$\cos\theta_{ij} = \sin\lambda_i \sin\lambda_j + \cos\lambda_i \cos\lambda_j \cos\phi_{ij} ,$$

where λ_i is the dip of particle i, and ϕ_{ij} is the difference in azimuths of tracks i and j. We apply this formula twice to find $\cos\theta_{n\pi}$ and $\cos\theta_{np}$.

The angle $\phi_{n\pi}$ is measured directly (it is called ϕ_π for short). The angle λ_π is assumed to be zero (beam tracks are flat in the chamber to within the accuracy of scanning-table measurements).

We determine λ_n from the following equations (all equations given in this Appendix are taken directly from Reference 23), where

$$\tan\lambda_n = K\Delta_n/S_n ,$$

where Δ_n and S_n are measured directly. K is the stereo ratio, or

$$K = \frac{L'_f \; n_H + Z}{d} = \frac{(71.9)\,(1.09) + Z}{20.0} ,$$

in which

d = distance between cameras 1 and 2 (or 2 and 3) = 20.0 in.,

L'_f = effective distance from the lens to the top fiducial plane, or

$L'_f = L_f - L_g + L_g/1.5$ = (actual distance through air)/(index of refraction of air) + (actual distance through glass)/(index of refraction of glass)

$= (L_f - L_g)/1 + L_g/1.5 = L_f - 1/3\, L_g$

$= 74.1 - 6.7/3 = 71.9$ in.

We have n_H = index of refraction of liquid H_2 = 1.09,
and

Z = depth of event in chamber below the bottom of the top glass, or

$$\frac{\Delta_f K}{M_f}.$$

Thus we have $Z[1-(\Delta_f/M_f d)] = L_f' n_H/d$, which implies

$$Z = M_f d/(M_f d - \Delta_f) = L_f' n_H/d$$

$$= M_f L_f' n_H/(M_f d - \Delta_f),$$

where M_f equals magnification of the fiducial plane as measured on the scan table (= 0.69) and Δ_f equals separation (measured directly) of the fiducials. Thus we have determined $\tan \lambda_n$ by using Δ_n, S_n, and Δ_f.

Similarly, we can determine $\tan \lambda_p$ from Δ_p, S_p, and Δ_f. Strictly speaking, Δ_f should be measured when the middle of the track in question is superposed on all views. As an approximation, though, we use the separation Δ_f, measured when the images of the beginning of the proton track (or end of the neutron track) are superposed. For tracks that do not rise steeply, this approximation is good, and in fact, most of our neutrons and protons are of this kind.

Evaluating the errors in the measured quantities enables us to estimate the errors in the calculated quantities $\cos \theta_{\pi n}$ and $\cos \theta_{np}$. These errors can then be propagated straightforwardly to give the errors in the momentum determinations (by using the formulas in Appendix I). When the discrepancy between the two values calculated from the neutron momentum is compared with the joint experimental uncertainty, we have a way of deciding whether the supposed event is real or not. The SENTRY program performs all the calculations discussed above.

M. Scanning Efficiency

One of the greatest difficulties facing a scanner seeking our events is their topologic banality. They seem absolutely to lack any distinguishing, radical, and--more to the point--eye-catching features. A track that suddently ends in the chamber can very easily be missed if it is in the neighborhood of several other tracks. On experiments in the 10-inch Berkeley hydrogen bubble chamber, the expected scanning efficiency for zero-prongs was 0.60. This compared with nearly perfect efficiency for finding charged decays of strange particles or "vees." At an efficiency of 0.60, a double scan would miss $(1-0.6)\times(1-0.6)=0.16$ of all events. Further, we might expect the efficiency to vary strongly from scanner to scanner and from roll to roll depending on the number of tracks in each frame, the quality of the film, and the quality of the tracks in the chamber. Lastly, no two scanners can be expected to agree consistently on questions of film quality or event diagnosis. To meet such difficulties, we scanned each roll twice, insisted that all frames rejected be named, and set scanners to scanning for a set of configurations slightly larger than the one we wished to use. This last enabled us to confine disagreements to events that would never be used, while the similarity of events used to events scanned enabled us to assume the efficiencies to be the same for both. This point is discussed in the description of the scanning procedure.

The search for events is composed of a zero-prong search followed by a search for a recoil. We assumed these two efficiencies to be independent. In computing efficiencies we used only frames agreed to be good by both scanners, but we used as valid any zero-prong considered valid by either scanner. All scanners were instructed to note any questionable prongs and to ignore completely only the most obviously invalid. This slowed down scanning but was considered a necessary condition to the reliable estimation of scanning efficiency.

The recoil efficiencies were evaluated only on zero-prongs found and considered valid by both scanners. Recoils called valid by either scanner were treated as found by both for these purposes. The scanning efficiencies were thus compared only on areas of film that both had scanned, which permits us to call the scans comparable and renders the deduced efficiencies, presumably, approximately reproducible.

A good rate of scanning on good film over a long period is about 40 frames per hour. It should be noted, too, that a scanner who scans at 0.84 efficiency is worth two scanners scanning at 0.60 efficiency.

We derive total efficiencies E_T by assuming that the probability that either scanner finds any given recoil or zero-prong is a fixed constant for each roll. If on any roll, N_1 and N_2 zero-prongs are found on scan 1 and 2, respectively, and N_{12} are found on both scans, then $E_1 = N_{12}/N_2$, $E_2 = N_{12}/N_1$, and $E_T = 1-(1-E_1)(1-E_2)$.

Tables X, XI, and XII give the actual values of the efficiencies as computed from the formulas given above. The average efficiencies given for the whole experiment are the usual maximum-likelihood estimates

$$E^* = (\Sigma E_i/\sigma_i^2)/\Sigma\, 1/\sigma_i^2 ,$$

where each E_i is weighted by the inverse square of its error σ_i. The error, σ_i, is the maximum-likelihood estimate based on the multinomial distribution with four different possible cases. The cases are: event seen on neither scan, event seen only on scan 1, event seen only on scan 2, event seen on both scans; and their respective probabilities are: $1-E(1)-E(2)+E(1)E(2)$; $E(1)-E(1)E(2)$; $E(2)-E(1)E(2)$; and $E(1)E(2)$. The analysis of the resulting distribution gives the error in $E_1 = \sigma_1 = [E_1^2(1-E_1)/N_1]^{1/2}$. It is interesting to note that when E_1 is weighted by $1/\sigma_1^2$, it is thereby being weighted by N_1 (the number of events found on scan 1) and hence, essentially by the number of frames scanned on the ith roll. This is a reassuring point since we would expect an unbiased estimate to include such a factor.

The tables give the values of the efficiencies to four figures for purposes of calculation. Only the grand averages given below should be considered significant.

The quantity called the "ideal total efficiency" below is the efficiency that would obtain if each scanner scanned at his rated efficiency, under the following procedure:

Both scanners scan the roll for zero-prongs, and an overall list of zero-prongs is compiled. Then, both scanners scan all the zero-prongs for recoils. In this way, each scanner examines not only the zero-prongs he has found himself, but also those that are found by his partner. This "ideal" procedure is so-called because it gives the maximum possible overall efficiency for two scanners having fixed zero-prong and recoil efficiencies.

Table X. Scan comparisons: zero-prongs and recoils found on each scan.

Roll	No. of frames doubly scanned	By	Zero-prongs			Recoils		
			N(1)	N(2)	N(12)	N(1)	N(2)	N(12)
501	577	3,6	193	237	116	23	35	17
502	600	1,6	233	309	212	52	83	48
504	521	1,6	115	156	84	33	51	32
505	576	3,6	254	279	203	92	120	72
507	583	3,6	227	347	197	118	147	93
508	577	3,6	189	306	162	81	102	59
509	569	3,6	241	344	201	103	136	78
514	403	5,1	279	140	121	64	47	31
519	520	3,1	277	208	154	77	67	42
547	333	3,1	217	145	100	50	42	26
553	427	3,5	327	334	254	99	54	40
556	316	5,8	233	301	195	68	97	54
565	499	6,8	349	374	272	131	93	68

Table XI. Individual scanning efficiencies by roll.

Roll	Zero-prong (%)				Recoil (%)				Total (%)			
	$\overline{E}(1)$	$\delta E(1)$	$\overline{E}(2)$	$\delta E(2)$	$\overline{E}(1)$	$\delta E(1)$	$\overline{E}(2)$	$\delta E(2)$	$\overline{E}(1)$	$\delta E(1)$	$\overline{E}(2)$	$\delta E(2)$
501	48.95	2.517	60.10	2.466	48.57	7.263	73.91	6.381	23.77	3.759	44.42	4.246
502	68.61	2.518	90.99	1.554	57.83	5.208	92.31	2.810	39.68	3.858	83.99	2.932
504	53.85	3.411	73.04	3.036	62.74	6.667	96.97	2.364	33.79	4.179	30.83	3.413
505	72.76	2.383	79.92	2.144	60.00	3.956	78.26	3.331	43.66	3.214	62.55	3.147
507	56.77	2.477	86.78	1.694	63.27	3.530	78.81	2.992	35.92	2.544	68.40	2.920
508	52.94	2.642	85.71	1.852	57.84	4.173	72.84	3.759	30.62	2.686	62.43	3.493
509	58.43	2.427	83.40	1.832	57.35	3.690	75.73	3.199	33.51	2.567	63.16	3.007
514	86.43	1.906	43.37	2.758	65.96	4.810	48.44	5.073	57.01	4.344	21.01	2.574
519	74.04	2.267	55.60	2.569	62.69	4.364	54.54	4.493	46.41	3.530	30.32	2.864
547	68.97	2.608	46.08	2.810	61.90	5.403	52.00	5.559	42.69	4.061	23.96	2.949
553	76.05	2.058	77.68	2.008	74.07	3.791	40.40	4.245	56.33	3.261	31.38	3.395
556	64.78	2.519	83.69	1.948	55.67	4.495	79.41	3.659	36.07	3.232	66.46	3.430
565	72.73	2.033	77.94	1.893	73.11	3.312	51.91	3.733	53.18	2.831	40.46	3.071

Table XII. Joint scanning efficiencies by roll.

Roll	Zero-prong (%)		Recoil (%)		Whole events (%)	
	E(Z. P.)	δE(Z. P.)	E(R)	δE(R)	E(I)	δE(I)
501	79.63	1.611	86.58	3.789	68.95	3.324
502	97.17	0.538	96.76	1.251	94.02	1.322
504	87.56	1.676	98.87	0.903	86.57	1.836
505	94.53	0.755	91.30	1.586	86.31	1.650
507	94.29	0.802	92.22	1.329	86.95	1.455
508	93.28	0.950	88.55	1.948	82.60	2.002
509	93.10	0.862	89.65	1.632	83.46	1.705
514	92.31	1.143	82.45	3.022	76.11	2.945
519	88.47	1.207	83.04	2.597	73.47	2.507
547	83.27	1.655	81.71	3.348	68.04	3.099
553	94.65	0.665	84.55	2.513	80.03	2.444
556	94.26	0.800	90.87	1.867	85.65	1.904
565	93.98	0.684	87.07	1.883	81.83	1.867

The ideal procedure takes about twice as long as the standard one, in which each scanner seeks zero-prongs and recoil independently of his partner and, in succession, on a single scan.

Average of scanning efficiency for finding...		Extreme single-roll values Low	High	Grand average	Error
Zero-prongs	(indiv.)	0.43	0.91	-	-
	(joint)	0.83	0.97	0.937	0.002
Recoils	(indiv.)	0.40	0.97	-	-
	(joint)	0.82	0.99	0.926	0.005
Whole events	(exp., indiv.)	0.21	0.84	-	-
	(exp., joint)	0.56	0.90	0.758	0.007
	(ideal, joint)	0.68	0.94	0.845	0.005

We explicitly neglect deviations from our assumption that each recoil and each zero-prong are equally likely to be found by any single scanner. The effect of scanning efficiency on our experiment, then, is the factor 0.758 ± 0.007, which represents the fraction of events actually occurring that we estimate to have found in scanning. This compares with 0.845 ± 0.005 of events that could have been found, had the ideal (but slower) scanning method been used.

N. Imperfect Measurements and Their Reproducibility

All the information about each event we have analyzed has come, ultimately, from the careful tracing of the projected orbits of tracks by a measurer on the Franckenstein digitized measuring projector. If these tracing processes were unreliable (as we might expect them to be because of our short proton tracks), we could draw no conclusions from the computer programs that use them as a starting point. We estimate the reliability of measurements by examining a sample of twice-measured events. We observe the variation in appropriate physical quantities from one measurement to the next and deduce the magnitude of the natural fluctuations in measurement. Knowing the magnitude and character of these fluctuations, we can seek to reduce their influence on our final result.

The parameters we examine are the coordinates, angles, momenta, χ^2 and cos (center-of-mass angle). The (x, y, z) coordinates are reproducible, roughly speaking, to (1, 1, 4)mm, respectively. The z coordinate is less reproducible because the film planes of the cameras are almost parallel to the (xy) plane. The great bulk of events are reproduced to within about a factor of 4 of these values. Relatively few are reproduced to much better than (0.25, 0.25, 1.0)mm, and events that differ by more than (4, 4, 16) mm are more likely to be different events than separate measurements of the same event.

The coordinates are not as interesting as angles, however, and we find that measurements are very safely reproducible within the errors quoted by the PANG portion of PACKAGE for a single measurement. Momenta deduced from length are reproducible within a few MeV/c, as length measurements reproduce well.

Perhaps the most important quantity of all is χ^2, the goodness-of-fit parameter. It is important that our decision as to the validity of any given event be insensitive to the normal variations in measurement. This would be easy to achieve if the χ^2 parameter were reproducible within limits that are small compared with the acceptable range of χ^2 values. This is, unfortunately, not the case. An event that arose from our interesting sequence of events would, ideally, fit the hypothesis 90% of the time with a χ^2 value of 2.706 or better, and 95% of the time with a χ^2 value of 3.816 or better. The difference between χ^2 values for successive measurements of a single event often exceeds 6. Thus, if we measure each event only once, there is an excellent chance that events arising from our interesting sequence will be disregarded because their χ^2 values are too high owing to imperfect measurement.

We solve the problem by remeasurement of appropriate events. We assume that an event that fits with a low χ^2 does so because the tracks are really consistent with the hypothesis and not because an imperfect measurement makes them appear so. An event with high χ^2, on the other hand, may be--we assume--a good event that appeared poor because of imperfect measurement. We therefore remeasure every event that gave a χ^2 value between 2.706 and 15 on its first measurement, provided that the π^0 from the event was emitted at a forward angle in the c.m. ("forward" angles are those whose cosines exceed 0.7). Any event that fits our hypothesis with a

$\chi^2 < 2.706$ is considered valid and therefore need not be remeasured. (Note the assumption stated above.)

We evaluate the effectiveness of this procedure by dividing the χ^2 spectrum into five parts in order of decreasing significance: $\chi^2 \leq 2.706$; $2.706 < \chi^2 \leq 8.0$; $8 < \chi^2 \leq 15.0$; 0-c only (only the 0-c fit at recoil was successful); no fit.

On a sample of several hundred remeasurements, we found for only six events did the two measurements lie in parts of the spectrum that were not, at worst, adjacent. For the great majority of events (251/304), measurement and remeasurement lay in the very same part. For a somewhat smaller number (47/304), they lay in adjacent parts. The table below summarizes these results.

First/second measurement	$\chi^2 \leq 2.706$	$2.706 < \chi^2 \leq 8$	$8 < \chi^2 \leq 15$	0-c only	No fit
$\chi^2 \leq 2.706$	16	3	1	1	0
$2.706 < \chi^2 \leq 8$	5	3	4	2	0
$8 < \chi^2 \leq 15$	1	3	4	2	0
0-c only	0	1	3	130	5
No fit	0	0	0	22	98

The symmetry of the table above indicates that the value of χ^2 associated with any measurement of a given event is approximately independent of whether the measurement is the first or second measurement. It is conceivable that first measurements could give poorer χ^2 values because the measurers were getting used to measuring machines and the particular event types. Further, it might seem reasonable to suppose that when an event is given for remeasurement, greater care might be taken and a low χ^2 value might result. With one major exception, these effects introduce no significant asymmetry into the table.

An event that on first measurement gives no fit whatever (not even a 0-c fit of the elastic n-p recoil-forming scattering) is more likely to be remeasured than an event that gives only a 0-c fit. This is because the latter are expected to occur abundantly, whereas the former events are

often the result of imperfect measurement. Nearly all events seen as good candidates on the scanning table will give at least a 0-c fit to the elastic n-p scattering. Failure to achieve even this points to the conclusion that either the event was carelessly scanned or measured, or that the event was a questionable candidate that could not be eliminated on the scanning table.

The effect discussed explains the only large asymmetry in the table above; there were 22 events that gave no fit on measurement 1 and a 0-c fit on measurement 2, whereas only 5 had the converse history.

The six events that did not lie on or adjacent to the diagonal of the table are discussed in Appendix G. They fail to satisfy certain acceptance criteria imposed to achieve reproducibility. These events are therefore discarded and do not pollute the remainder of our sample.

The other aspect of measuring imperfection or nonreproducibility is the uncertainty as to which end of a short, stopping proton track is its beginning. Because our events have short proton tracks, it is difficult to be sure on the scanning table which way the track is curving. We expect, therefore, a certain fraction of events for which the proton was measured in the wrong direction, i.e., end-to-beginning. When the event is reconstructed, our information is more complete, but in most cases the error on the curvature is large enough to permit the curvature to change sign.

It is true that interchange of beginning and end of the proton track changes the direction of the neutron track, which would connect the zero-prong to the beginning of the proton recoil. Even this change, however, does not always render absurd the hypothesis that the ends of the proton track were interchanged.

We used two parameters to characterize the consistency of a measurement with the hypothesis of a mistaken exchange. The first was the consistency of the measured curvature with a negative value equal to absolute value of error in curvature divided by the curvature. (We always mean a positive curvature to correspond to the positive charge of the proton.) If this parameter is negative or greater than one-third, the measurement is said to be consistent with negative curvature. If it is positive and less than one-third, the curvature given is positive to within three standard deviations or better, and we reject the hypothesis of a mistaken exchange.

The second parameter we used needs a short introduction. Given the momentum of the proton (known from the accurate measurement of its range) and the coordinates of the measured end points of the proton and of the end of the beam track, it is possible to reconstruct the course of the neutron that is postulated to have originated at the zero-prong and caused the recoil. All this is done relative to the event as originally measured, and thus far no consideration has been given to the possibility of a mistaken interchange.

With the end points of the neutron, the momentum of the recoil proton and its initial direction, and the direction of the π meson when the charge exchange occurred, it is possible to make two independent calculations of the neutron momentum. The first is made by applying conservation laws at the charge-exchange vertex; the second by applying them at the recoil vertex. The single formula for both determinations is derived in Appendix I. The agreement of the two values for the neutron momentum is a direct measure of how consistent our unfitted measurement is with the hypothesis that the assumed neutron arose from the postulated elastic charge exchange, and then caused, by elastic scattering, the measured stopping proton. The discrepancy between these two computed values of neutron momentum is the parameter we use.

By examining the values of the discrepancy for different events, we find that it varied from less than 10 MeV/c to, on occasion, more than 200 MeV/c for events that fit the hypothesis with low χ^2. We assume that no valid event gives such a discrepancy of more than 500 MeV/c. We now have the second parameter with which to examine the hypothesis of mistaken exchange.

From the unfitted PANG data discussed above, we can construct the direction the assumed neutron would have in the case of exchanged proton end points, and we can then compute the discrepancy in values of neutron momentum as before. If this discrepancy exceeds 500 MeV/c, we assume the hypothesis of mistaken exchange to be false. We are left now with reversed events that have curvatures consistent with negative values within 3 standard deviations, whose neutron momentum values computed at production and recoil agree within 500 MeV/c. These events we treat with greater care.

Ideally, we should remeasure these doubtful events and verify that they do not indeed arise from the reaction chain in which we are interested. This is very time-consuming, of course, and, since we have measured all the tracks except the neutron for the reversed case, we use the original measurements to reconstruct the reversed proton and the appropriate neutron track. This neutron track always started at the end point of the beam track, but whereas--as originally measured--its end point was the first measured point of the proton track, now it is the last. From the end coordinates of the points of the neutron, we can compute its dip and azimuth and assume the errors in these to be unchanged from the first measurement.

The end points of the proton must be interchanged, π radians must be added to the azimuth to reverse the sense of the track, and the sign of the dip must be changed. These operations are performed by a special modification of the FAKE computer program discussed in the Section F.

The results of the calculation show that it is very unlikely that any events have been lost because of a mistaken interchange of ends of the recoil. The program reversed the sense of the proton on 538 events, which satisfy the criteria above. Of these, 33 events were able to produce a fit to our hypothesis with $\chi^2 < 15$. We discuss elsewhere the advantages of using the computed missing mass (a parameter that would equal, ideally, the mass of the π^0) and its error, calculated from unfitted data, in preference to the χ^2 parameter characterizing the fit to the hypothesis. In any case, no event having a $\chi^2 > 15$ gives a missing mass near the ideal value. We characterize the 33 fitted events according to missing mass and error and find that 17 events, for example, give imaginary missing masses (the missing momentum exceeds the missing energy), and only five events have errors in missing mass less than 30 MeV/c^2. In our analysis, we have insisted that an acceptable event have a missing mass within 1.65$\times$ (its missing-mass error) of the mass of the π^0, and that its error be no more than 16.0 MeV/c^2. Two of the five low-error events have recoil profiles less than 0.7 cm, which forces their immediate rejection. Of the remaining three, the first gave a missing mass equal to 320.2±23.84 MeV/c^2, which is strongly inconsistent with m_{π^0} = 135.00 MeV/c^2. A second of the three (serial 556-605) gave MM = 168.7 ± 9.43 MeV/c^2, inconsistent with m_{π^0}, but close enough to warrant a specific remeasurement. The latter, performed twice, gave χ^2 values of 7.99 and 4.24 compared with the FAKE-

calculated value of 8.34 and missing masses of 165.3 ± 9.04 and 158.7 ± 10.0 in each case. The actual remeasurements support the conclusion of inconsistency and give an index of the reliability of the computer-simulated reconstruction; in this case, the simulated reconstruction by the computer is within the limits of reproducibility of the physical measurements themselves. This reliability reassures us of the accuracy of the conclusions drawn from the computer results.

There remains one event unaccounted for (serial 565-430), whose calculated missing mass is 147.8 ± 14.2 MeV/c^2, a value consistent with m_{π^0} within an error less than our adopted standard of 16.0 MeV/c^2. (This is the only event of the 538 simulated that actually satisfies all the acceptance criteria.) We treat this event in the section on anomalous events and marginal interpretations. We conclude that the hypothesis of a mistaken exchange of ends of the recoil can be supported in, at most, one case in the entire experiment, and that no significant doubt is introduced into our result from that source.

In summarizing the conclusions and thesis of this section, we can say that the source of all our measuring difficulties is the exceptional shortness of our proton tracks. Because they stop, we can estimate their momentum well, and by judicious selection of criteria, we can achieve a reproducible sample. The χ^2 values are reproducible enough that the fraction of events lost owing to imperfect measurement is small and the fraction lost owing to interchange of end points on the proton, negligible.

ACKNOWLEDGMENTS

It is a pleasure to acknowledge my indebtedness to Professor Luis W. Alvarez for having been permitted to pursue research in his group. The experience of participating in the researches of a well-run group of helpful scientists devoted to their work in a milieu of frendliness and high morale is one that I value. It is a pleasure to thank him and them for their many kindnesses.

I would like to thank Professors Frank S. Crawford, Jr., and Bruce H. McCormick for having encouraged, directed, criticized, and discussed the research presented, throughout its span. Dr. Vo Xuan Bang of the Viet Namese Atomic Energy Commission Laboratory at Dalat participated in the work of the project, and I wish to thank him for his contributions and his kind cooperation. I am grateful to Fred Safier, Dr. Gerald Lynch and Dr. J. Peter Berge for having adapted the FAKE program for use on this experiment and for having endured patiently the dozens of disappointments and irritations that this entailed. I would like to thank Dr. Barrie Pardoe for his help in using the PACKAGE program and the members of the Associated Production Experiment Group for their many favors.

In particular, I wish to mention the burdens of librarianship and technical support borne by Colombe Langton and Albert Briggs, now of the Peace Corps. Without their splendid efforts and devotion to excellence, the course and duration of the experiment would have been vastly different.

This work has been supported by the United States Atomic Energy Commission.

REFERENCES

1. M. L. Goldberger, Phys. Rev. 99, 979 (1955); M. L. Goldberger, H. Miyazawa, and R. Oehme, Phys. Rev. 99, 986 (1955).
2. G. Puppi and A. Stanghellini, Nuovo Cimento 5, 1305 (1957); R. Cool, O. Piccioni, and D. Clark, Phys. Rev. 103, 1083 (1956).
3. A. Weinberg, A. E. Brenner, and K. Strauch, Phys. Rev. Letters 8, 70 (1962).
4. S. Wolf, N. Schmitz, L. Lloyd, W. Laskar, F. Crawford, Jr., J. Button, J. Anderson, and G. Alexander, Rev. Mod. Phys. 33, 439 (1961).
5. A. H. Rosenfeld, Current Performance of the Alvarez-Group Data-Processing System, Nucl. Instr. Methods 20, 1963 (to be published); M. Alston and H. Monteros, Data Analysis for the Associated-Production Experiment, Lawrence Radiation Laboratory Alvarez Group Memo No. 165, May 1, 1961 (unpublished).
6. Walter H. Barkas and Arthur H. Rosenfeld, Lawrence Radiation Laboratory Report UCRL-8030 Rev., April 1963 Edition (unpublished).
7. Arthur H. Rosenfeld (Ed.), Reference Manual for KICK IBM Program, Lawrence Radiation Laboratory Report UCRL-9099, May 1961 (unpublished).
8. G. Hahler and G. Ebel, The Complex Diagram of the Pion-Nucleon Forward-Scattering Amplitude, Report of the Institut fuer Theoretische Kernphysik, Technische Hochschule, Karlsruhe, Germany, July 1963 (unpublished); V. S. Barashenkov, Fortschr. Physik 10, 205 (1962).
9. J. W. Cronin, Phys. Rev. 118, 824 (1960).
10. Stanley Mandelstam (in a talk before the Physics Department) University of California, Berkeley, November 1963 (unpublished).
11. Gerald Lynch, Program FAKE: Monte Carlo Simulation of Bubble Chamber Events, Lawrence Radiation Laboratory Report UCRL-10335, July 10, 1962 (unpublished).
12. W. V. Quine, Am. Math. Month. 59, 521 (1952).
13. R. H. Urbano, and R. K. Mueller, IRE Trans. EC-5, 126 (1956).
14. E. J. McCluskey, Jr., Bell System Tech. J. 35, 1417 (1956).

15. Ronald E. Prather, The Simplification of Logical Truth Functions (M. S. Thesis), University of California, Berkeley, September 1958 (unpublished).

16. Ronald E. Prather, Journal of American Computing Machinery 7, 299 (1960).

17. Alan Natapoff, The Reduction of Boolean Truth Functions to Minimal Form, Lawrence Radiation Laboratory Report UCRL-9227, May 20, 1960 (unpublished).

18. T. J. Fletcher, The Solution of Inferential Problems by Boole Algebra, Math. Gaz. 35, 183 (1952).

19. A. D. Johnson, The EXAMIN System, Lawrence Radiation Laboratory Alvarez Group Memo No. 331, September 5, 1961 (unpublished).

20. Ronald A. Grossman, Gerald W. Meisner, and LeRoy Price (Lawrence Radiation Laboratory), private communication.

21. Alan Natapoff, FORTRAN Program HOUND: Calculating a General Beam Average or Geometric Correction for Secondaries Escaping from a Rectangular Chamber, Lawrence Radiation Laboratory Report UCRL-9871, October 4, 1961 (unpublished).

22. Robert J. Harvey, Some Subroutines Added to PACKAGE, Lawrence Radiation Laboratory Alvarez Group Programmers' Note P-12, October 1962 (unpublished).

23. Gerald Lynch, 72-inch Scanning Table Measurements, Lawrence Radiation Laboratory Alvarez Group Memo 135, December 1959 (unpublished).

This report was prepared as an account of Government sponsored work. Neither the United States, nor the Commission, nor any person acting on behalf of the Commission:

A. Makes any warranty or representation, expressed or implied, with respect to the accuracy, completeness, or usefulness of the information contained in this report, or that the use of any information, apparatus, method, or process disclosed in this report may not infringe privately owned rights; or

B. Assumes any liabilities with respect to the use of, or for damages resulting from the use of any information, apparatus, method, or process disclosed in this report.

As used in the above, "person acting on behalf of the Commission" includes any employee or contractor of the Commission, or employee of such contractor, to the extent that such employee or contractor of the Commission, or employee of such contractor prepares, disseminates, or provides access to, any information pursuant to his employment or contract with the Commission, or his employment with such contractor.